Thesis dissertation for the PhD course in neuroscience, curriculum Neuroscience and Neurotechnology cycle XXIV

Neural Control and biomechanics of the octopus arm muscular hydrostat

PhD Candidate:
Alessio Di Clemente

Supervisor:
Letizia Zullo

1 Table of Contents

Abstract

Octopus vulgaris is a cephalopod mollusk with outstanding motor capabilities, built upon the action of eight soft and exceptionally flexible appendages. In the absence of any rigid skeletal-like support, the octopus arm works as a “muscular hydrostat” and movement is generated from the antagonistic action of two main muscle groups (longitudinal, L, and transverse, T, muscles) under an isovolumetric constrain. This peculiar anatomical organization evolved along with novel morphological arrangements, biomechanical properties, and motor control strategies aimed at reducing the computational burden of controlling unconstrained appendages endowed with virtually infinite degrees of freedom of motion.

Hence, the octopus offers the unique opportunity to study a motor system, different from those of skeletal animals, and capable of controlling complex and precise motor tasks of eight arms with theoretically infinite degrees of freedom.

Here, we investigated the octopus arm motor system employing a bottom-up approach. We began by identifying the motor neuron population and characterizing their organization in the arm nervous system. We next performed an extensive biomechanical characterization of the arm muscles focusing on the morphofunctional properties that are likely to facilitate the dynamic deformations occurring during arm movement.

We show that motor neurons cluster in specific regions of the arm ganglia following a topographical organization. In addition, T muscles exhibit biomechanical properties resembling those of vertebrate slow muscles whereas L muscles are closer to those of vertebrate fast muscles. This difference is enhanced by the hydrostatic pressure inherently present in the arm, which causes the two muscles to operate under different conditions. Interestingly, these features underlie the different use of arm muscles during specific tasks

Thus, the octopus evolved several arm-embedded adaptations to reduce the motor control complexity and increase the energetic efficiency of arm motion.

This study find relevance also in the blooming field of soft-robotics. Indeed, an increasing number of researchers are currently aiming to design and construct bio-inspired soft-

robotic manipulators, more flexible and versatile than their “hard” counterparts and more suited to perform gentle tasks and to interact with biological tissues. In this context, the octopus emerged as a pivotal source of inspiration for motor control principles underlying motion in soft-bodied limbs.

1 Introduction

1.1 General introduction

Octopus vulgaris is a cephalopod mollusk belonging to the Cephalopod class. It is characterized by sophisticated motor, sensory and cognitive capabilities, making it a fascinating model in several disciplines.

Cephalopods have by far the most complex nervous (NS) system of all invertebrates. *Octopus vulgaris* NS has roughly half a billion neurons, a number comparable to that of the brains of small mammals such as cats and dogs. It is also the most behaviourally complex among cephalopods and is known to use a variety of different hunting and defensive strategies, and even shows tool use by employing rocks and empty shells as shields or hide outs.

From a motor perspective this behavioural complexity is supported by a highly developed, hyperredundant motor system.

Octopus body has a bilateral symmetry and comprises a “mantle” which encloses a cavity (the “mantle cavity”) hosting all the internal organs, and eight arms lined up with double rows of suckers. It is a continuously growing animal and can reach 25 cm in mantle length with arms up to 1 m long (Fig. 1). It lacks any kind of rigid endo- or exoskeleton, which means that its body is completely soft and can easily change shape or go through tight and narrow cracks. Moreover, it can use its eight arms to perform tasks where a fine motor coordination is needed. This is achieved with a motor system organized differently from the vertebrates’ one. Vertebrates’, but also arthropods, motor systems strongly rely on the presence of a rigid skeleton with fixed joints positions. The rigid skeletal elements hold muscles in place and provide the support against which they can work to generate movement. Joints also allow reciprocal movement of adjacent skeletal elements and limit the degrees of freedom of the system, thus reducing the computational burden on the NS. A few exceptions to this paradigm are vertebrates’ structures like the elephant trunk,

or the tongue where, due to the lack of any rigid support, movement is generated through the antagonistic action of different muscles under an isovolumetric constraint. Being constant the volume, here muscle contraction causes a redistribution of the internal hydrostatic pressures resulting in limb movement and/or shape changes. These organs are usually referred to as “muscular hydrostats” (KIER & SMITH, 1985) and present several advantages in terms of flexibility and movement capabilities. However, they also pose a number of problems regarding the biomechanics of movements and the computational cost of their control. The octopus has a completely flexible body, lacks any rigid skeletal elements and relies completely on hydrostatic muscles and organs for support and movement.

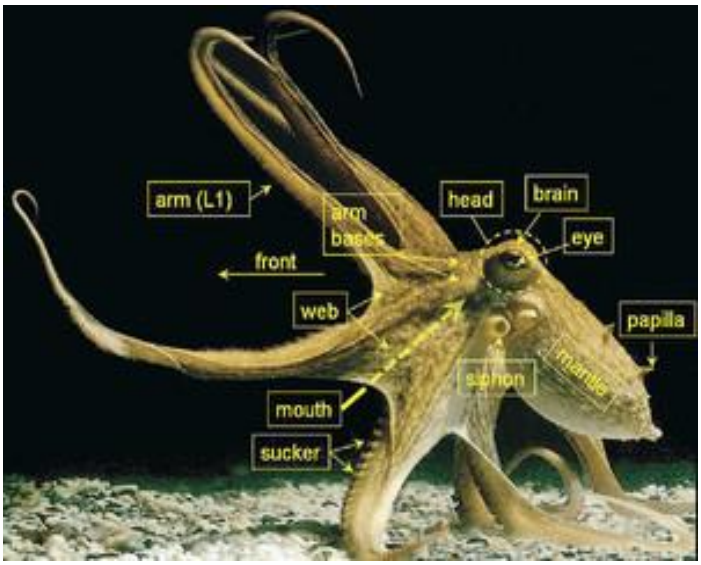

Figure 1 ***Morphology and body parts of the octopus.*** *The [front] side is shown by an arrow. The first left [arm (L1)] is labelled. Two [suckers] on one of the arms are shown by arrows. Part of the interbrachial [web] that runs between the proximal parts of the arms is labelled with arrows. The [head] that sits above the [arm bases] is labelled along with the left [eye], and the location of the [brain] (between the two eyes) is also labelled. The [mantle] is labelled along with the [siphon] and one of the skin [papillae] is also labelled. An arrow points to the location of the [mouth] right below the head (surrounded by the arms bases). Picture adapted from Levy et al., 2017*

Muscular hydrostats are also of great interest for engineers working on soft robotics implementations, a field of robotics that emerged in the last 15 years and is rapidly developing. The main focus of this field is to build soft-bodied robotic actuators, more flexible and versatile than their “hard” counterparts and suited to perform tricky tasks like moving in narrow and unconstrained environment and interact with biological tissue (Kim et al., 2013; Cecilia Laschi & Cianchetti, 2014). Nevertheless, as mentioned above, working with soft-bodied structures faces a series of problematic issues relative to motor planning and execution.

In this perspective, the octopus represents an ideal model to investigate biomechanics and motor control principles implemented during evolution to overcome the problems associated with motion in soft-bodied limbs (Guglielmino et al., 2012; C. Laschi et al., 2009; Mazzolai & Laschi, 2015).

The next chapters will summarize the current knowledge on motor control principles in vertebrates and octopus highlighting the differences and similarities between the two systems and the control strategies implemented by the octopus to cope with hyperreduntant limbs.

1.2 Vertebrates Motor Systems

Motion is a defining feature of animal life and a large portion of the vertebrate's NS is devoted to control and coordinate muscle activity, integrating sensory inputs and issuing commands for purposeful movements. Motor systems are hierarchically organized and often redundant such that the nervous system can trigger different actions by activating overlapping groups of muscles and the same group of muscles can be controlled voluntarily, rhythmically or reflexively (Kandel et al., 2013).

We are hardly ever aware of the complexity of common motor acts. Simply standing upright requires the sensorimotor transformation of vestibular signals evoked by microscopic swaying into continual adjustments of a large number of postural muscles (Deprá et al., 2019; Forget & Lamarre, 1990; Massion, 2017). Walking, running and other forms of locomotion need the integrated activity of higher motor centers in the brain, central pattern generators in the spinal cord (CPGs) and gated sensory information from the moving body (Marder E. & Bucher D., 2001; Prochazka et al., 2017). Other movements, such as catching a ball or avoiding obstacles while running, happens simply too fast to allow for sensory feedback integration. Hence, specialized motor centers, like the cerebellum, use predictive models to simulate the outcome of the ongoing movements and correct them with much shorter latency (Kandel et al., 2013).

Vertebrates Motor Control Networks Organization

Motor control networks in vertebrates are hierarchically organized. Higher level motor centers plan more general goals, whereas lower centers implement the command actions based on several internal and external parameters. The hierarchy of the motor control networks also means that even if some movements, like locomotion or spinal reflexes, can be executed by lower motor centers alone, they can still be controlled and/or modulated by the higher motor centers (Grilliner & El Manira, 2020; Hsu et al., 2017; Kandel et al., 2013; Pearson, 1993).

Motor neurons (MNs), responsible for the direct activation of muscles, are localized in the motor nuclei at the level of spinal cord and brainstem. They are topographically organized so that MNs innervating muscles close to one another are usually located in neighbouring regions within the spinal cord. A typical vertebrate muscle is innervated by a few hundred MNs clustered together. The axon of each MN exits the spinal cord through a ventral root (or a cranial nerve in the brain stem), reaches the muscle and then branches to innervate from a few to several hundred muscle fibers (Fig. 2) thus making up what is known as ‘motor unit’. The number of muscle fibers in a single motor unit indicates the finesse of control of the muscle. In vertebrates, this value is highly variable spanning from an average of 5 for an eye muscle (*rectus lateralis*) to 1800 for a leg muscle (gastrocnemius medial) (Enoka, 2008).

The collective population of MNs makes up the spinal cord grey matter, which also host populations of interneurons responsible for a large part of motor commands and sensory input processing. Here, information from sensory receptors, nociceptors and muscle proprioceptors, entering the spinal cord through the dorsal root, can trigger motor reflexes without the involvement of higher motor centers (Chandar et al., 2014; Guertin, 2013).

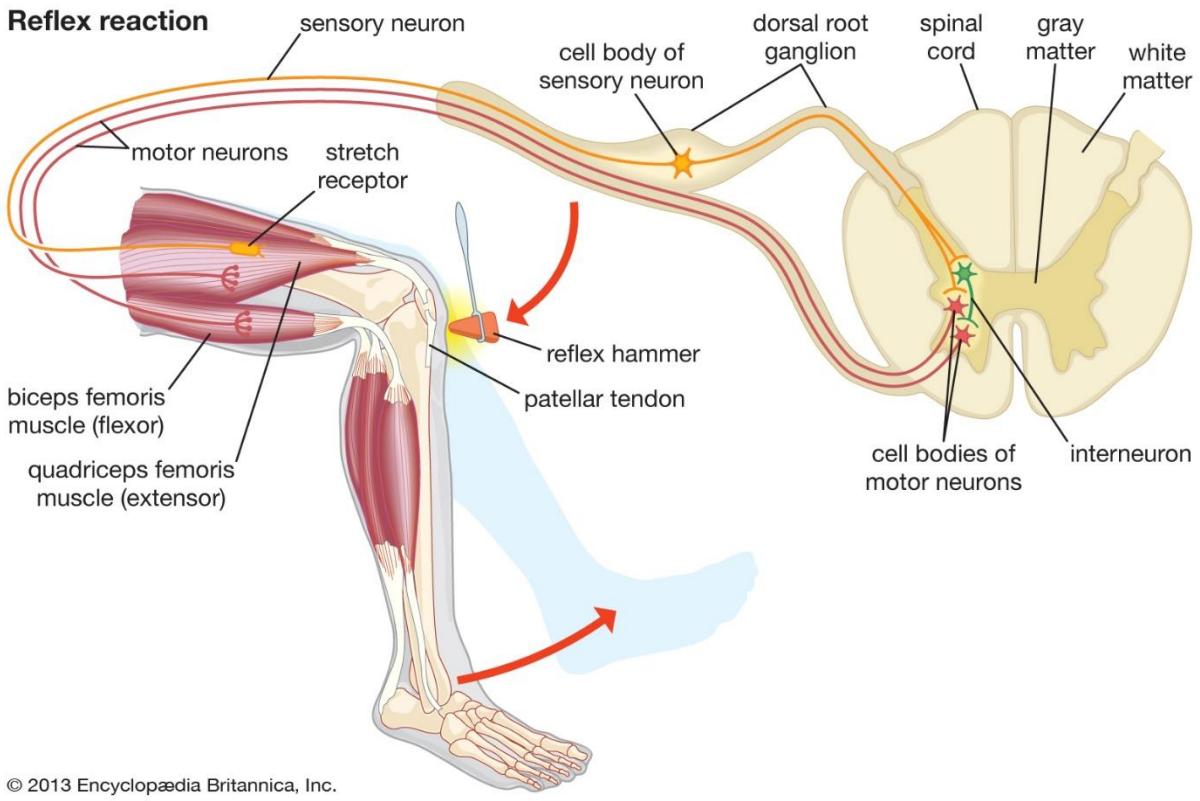

Figure 2. Schematic representation of spinal cord-muscles connections and the classical knee-jerk reflex. *Grey matter in the spinal cord is organized in a butterfly-like shape with two dorsal and two ventral horns surrounded by the white matter hosting all the fibers to and from the brain. In the classical knee-jerk reflex, percussion of the patellar tendon causes a sudden stretch of the quadriceps femoris. This sudden stretch is perceived by the stretch receptors (muscle spindles) in the muscles causing the activation of the sensory neurons which, in turn, directly activate the motor neurons, resulting in muscle contraction and knee extension.*

These stereotyped motor responses are called spinal reflexes, and the most classical example is the knee-jerk reflex, depicted in Fig. 2. Specialized spinal circuits, the so-called central pattern generators (CPGs), are also able to initiate and sustain rhythmic motor activities, like those involved in locomotion (Guertin, 2013; Prochazka et al., 2017; Puhl et al., 2018). Even during complex and purposeful motor actions, neuronal spinal networks carry out most of the computational work needed to refine and adjust motion. Hence, the spinal cord can be considered as a first station of sensorimotor integration. Higher level sensorimotor transformations occur in large brain cortical areas (parietal, premotor, prefrontal and primary motor cortices, Fig. 3A), deep nuclei (basal ganglia) and cerebellum.

Parietal, premotor and prefrontal cortices are part of a distributed network that receives and integrates multimodal sensory information into sensory representations defining the framework for motor actions. Together with the basal ganglia, they host higher order cognitive and motor functions associated with action selection and planning (Kandel et al., 2013).

The primary motor cortex represents the main output of the motor system and converts general motor plans and intentions into motor commands delivered to the spinal cord.

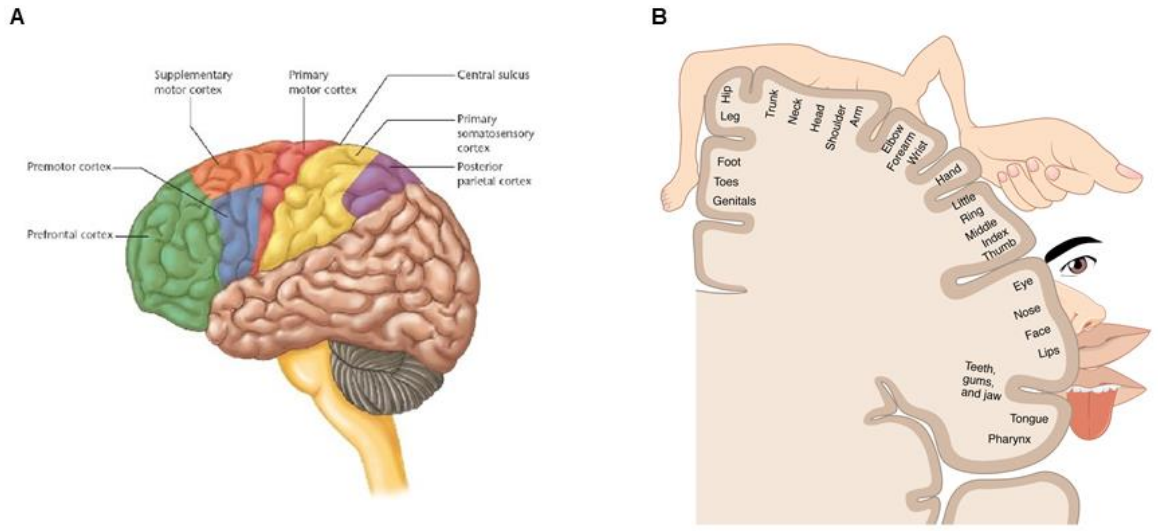

Figure 3. (A) *Cortical areas involved in motor processing.* ***(B)*** *Somatotopic map in the primary motor cortex. Finely controlled body parts take up disproportionally large areas. Adapted from Kandel et al., 2013*

The topographic organization found in the spinal cord, is maintained at the level of the primary motor cortex, where it gives rise to a somatotopic motor map of the body mirrored, in the somatosensory cortex, by a somatotopic sensory map (Kandel et al., 2013; Penfield & Rasmussen, 1950). These central representations of the body are usually referred as "*homunculi*", and are thought to play a pivotal role in interfacing motor and sensory systems to allow sensorimotor transformation. However, this organization masks a deeper complexity. It is known that, at least in the motor map of the arm and hand, there is a consistent overlap of areas controlling muscles across different joints, and that a single muscle can be activated by stimulating different spatially segregated sites. In addition, local horizontal axonal connections, link distant cortical areas allowing neuronal

activity at multiple sites to be coordinated during motor command processing (Novojilova & Babmindra, 1978; Park et al., 2001; Rathelot & Strick, 2006).

Finally, the cerebellum plays a major role in motion by modifying the motor commands of the descending pathways. It is involved in important functions such as the maintenance of balance and posture, coordination of voluntary movements, and motor learning.

Principles of motor control in vertebrates

As previously mentioned, motor commands that act on muscles are directly related to sensory inputs reaching the NS. Sensory inputs can be either intrinsic or extrinsic. Extrinsic information can be provided by visual and auditory systems and concerns the location and properties of objects in the space around us. Intrinsic information is mostly produced by visual and proprioceptive systems and concerns kinetic and kinematic information about the body.

Kinematic information includes the parameters of motion itself (position, velocity and acceleration of body and limbs, joint angles, and lengths of muscles) without any reference to the forces causing them. Kinetic information, instead, are about the forces generated and experienced by the body. Interestingly, these two types of information usually comes from different set of receptors. In muscles, for example, information about length and its rate of change is provided mainly by muscle spindles, while Golgi tendon organs provide information about the force the muscle is exerting on the bone.

In vertebrates, the primary motor cortex encodes kinetic and kinematic parameters of motion as a population code. This was elegantly shown by Georgopoulos and colleagues (Georgopoulos et al., 1983; Georgopoulos, 1988), who recorded from the primary motor cortex of a monkey reaching in different directions toward targets arrayed on a circle in the horizontal plane. They observed that single neurons fired during different movements and not just a single one. Interestingly, their activity was maximal for a preferred direction and decreased gradually, reaching its minimum when the movement was in the opposite direction. The global pattern of population activity, expressed as a population vector, corresponded closely to the actual movement direction (a kinematic parameter) (Fig. 4).

Further studies confirmed these results and showed also that loads applied to the limb (a kinetic parameter) changed the activity of many primary motor cortex neurons (Evarts et al., 1983). This result suggests that the primary motor cortex should not be considered as a point-to-point map of the body, where the activation of one or a few neurons selectively activates specific muscles, but rather as a dynamic computational map whose internal organization and spinal connections convert motor intentions and sensory representation into motor commands.

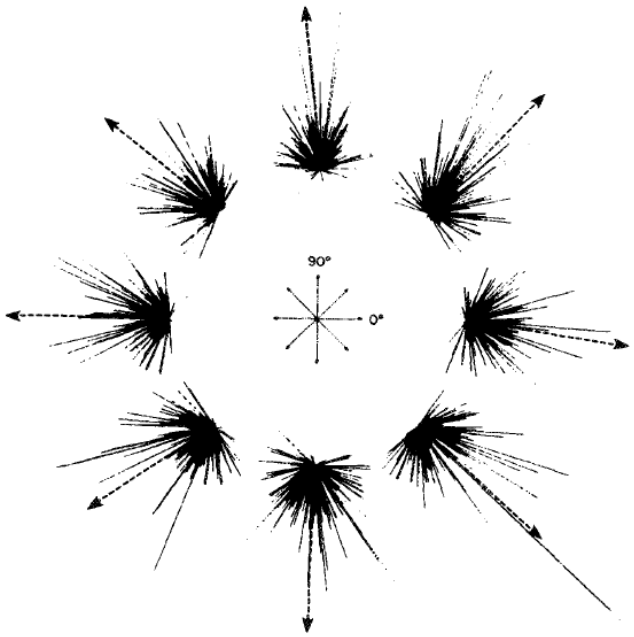

Figure 4. Results of the population analysis applied to eight movement directions studied in 2-D space. The movement directions are shown in the diagram at the center. The population vector (broken arrow) points approximately in the direction of the movement. (From Georgopoulos et al., 1988.)

In order to achieve a simple reaching movement the NS needs to calculate the position of the object (the target) and the initial location of the hand or the tip of the tool we wish to place on the target (the end-effector) and perform a kinematic computation to reach the goal. The target position can be calculated in the egocentric space (the space centered on ourselves) based on visual information (where do the object falls in each retina) and proprioceptive information (the head position and direction of gaze). Visual information can also be used to calculate the initial location of the end-effector. However, in this case the computation can also be carried on using proprioceptive information on muscle lengths and joint angles alone (Kandel et al., 2013; Shadmehr & Wise, 2005).

To understand how kinematic computational problems can be solved, we need first to introduce a concept called degrees of freedom. A degree of freedom is simply one

dimension along which the joint, and hence the limb, ca be moved (Shadmehr & Wise, 2005). Vertebrate's motor system relies on limbs with fixed-lengths segments interconnected by joints with limited degrees of freedom. If we do not consider the wrist, for example, our upper limb has five degrees of freedom: three at the level of the shoulder and two at the elbow. The shoulder is a ball-and-socket joint. A structure like that can be rotated inward (supination) or outward (pronation), abducted or adducted (to move the arm closer or further from the body laterally) and flexed or extended (to move the arm closer or further from the body frontally) (Fig. 5) (Narayan et al., 2021). Given the fixed length of the arm segments and the limited degrees of freedom of the joints, there is a defined mathematical relationship between joints configuration and position of the end-effector which allows to compute the latter based on the former (Shadmehr & Wise, 2005). Changes in joints configuration are achieved through the torques produced by the muscles. In contrast to torque motors, that can produce both positive and negative torques, muscles can only pull. This means that a pair of muscles pulling in opposite direction (antagonistic muscles) is required to operate a single joint. When the torques

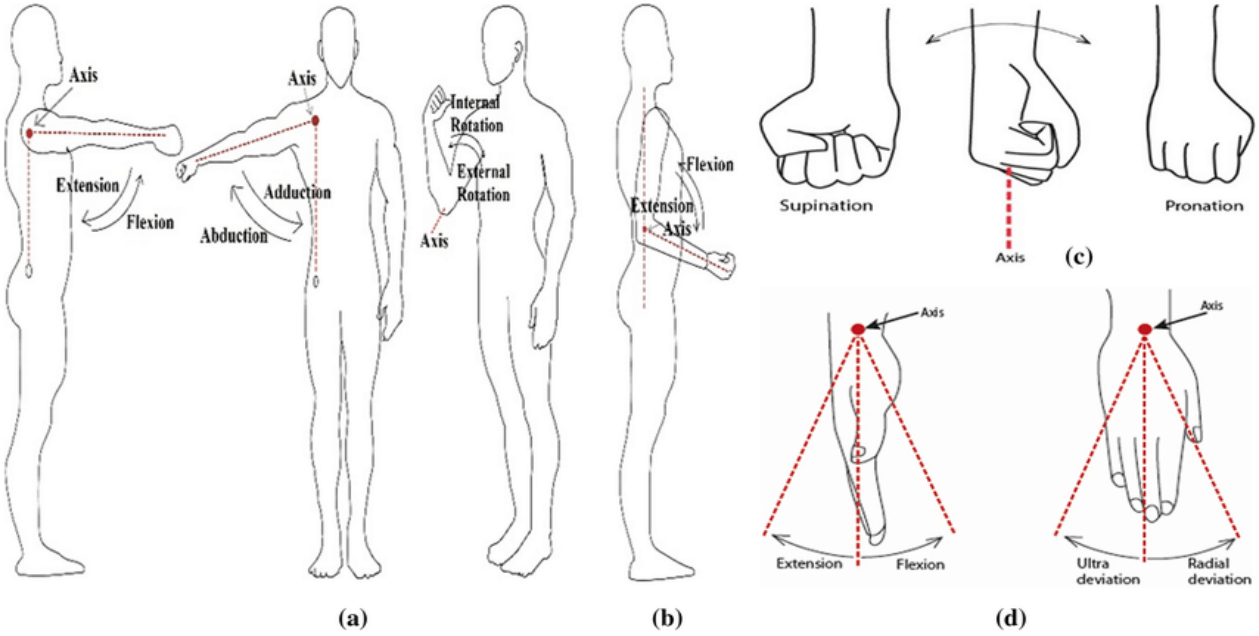

Figure 5. (a) *Schematic diagram of a shoulder flexion/extension, abduction/adduction, and internal/external rotation,* ***(b)*** *elbow flexion/extension,* ***(c)*** *forearm supination/pronation,* ***(d)*** *wrist flexion/extension and ulnar/radial deviation. From Narayan et al., 2021.*

produced by the two muscles are equal, the net torque will be zero and the joint will be at

its equilibrium point. When one of the two muscles produces more force, the joint will be moved into a new configuration, which is a new equilibrium point. This has relevant consequences for motor planning and execution (Polit & Bizzi, 1979).

Once the CNS has obtained an estimate of the end-effector and target locations, neural networks will subtract the former from the latter resulting in a difference vector for the end-effector. This will be translated into a trajectory that brings the end-effector on the target. Moreover, each point along the chosen trajectory can be reached by a great number of combinations of joint angles and muscle activation, meaning that the inverse kinematics cannot be uniquely specified. The ability to perform the same motor task in many ways is called motor redundancy and is typical of every motor system (Kandel et al., 2013).

Several studies have shown that many aspects of movement are stereotypical and invariant (motor invariance). In the reaching movement, for example, the end-effector tends to follow a roughly straight trajectory from the initial position to the target. Motor invariance has also been observed in more complex movements. One well-established theory states that the NS plans and performs complex motor tasks using simple, stereotyped movements as building blocks. These simple stereotyped movements are named motor primitives and can be scaled in size and time (Bizzi et al., 2008; Flash & Hochner, 2005; Giszter, 2015; Polit & Bizzi, 1979).

Finally, the NS converts kinematic parameters into movement dynamics by adjusting the muscle torques and joint rotations to those required to keep the end-effector along the desired trajectory. This means that the torques applied to a given joint is dependent on the level of activation of the muscles working on that particular joint, which adds a further layer of complexity.

Vertebrate muscle physiology

Movement is always accomplished through the interaction of NS and muscles. The role of the NS is to selectively activate those muscles that will produce the force needed to perform the desired task. Because motion requires a controlled variation of the muscle

force, the NS must be able to predict the outcome of the contraction in terms of force production, acceleration and displacement of the limb.

Muscles convert patterns of motoneuronal stimulation into the mechanical force and the torque needed to generate the movement, serving the same role as torque motors in robotics. In muscles, this is done through the ATP-dependent formation of cross-bridges between the myosins, forming the thick filaments, and the surrounding actin filaments forming the thin filaments. After the establishment of the cross-bridge a conformational change in the myosin, the power stroke, “pull” the thin filament, resulting in force production and/or reciprocal sliding of thick and thin filaments. In striated muscles, thin and thick filaments are organized in repetitive units called sarcomeres. Cross-bridge cycling is triggered by calcium and causes sarcomere shortening and, hence, the contraction of the muscle fiber (AL-Khayat, 2013). The relationship between the intensity of the stimulation and the force produced is not linear and it is influenced by several parameters.

Muscle response to a single pulse of stimulation consists in a single, relatively small and fast peak force known as twitch contraction.

The twitch contraction kinetics depends upon a complex series of events involving calcium dynamics, sarcomere accessory regulatory proteins and myosin isoforms

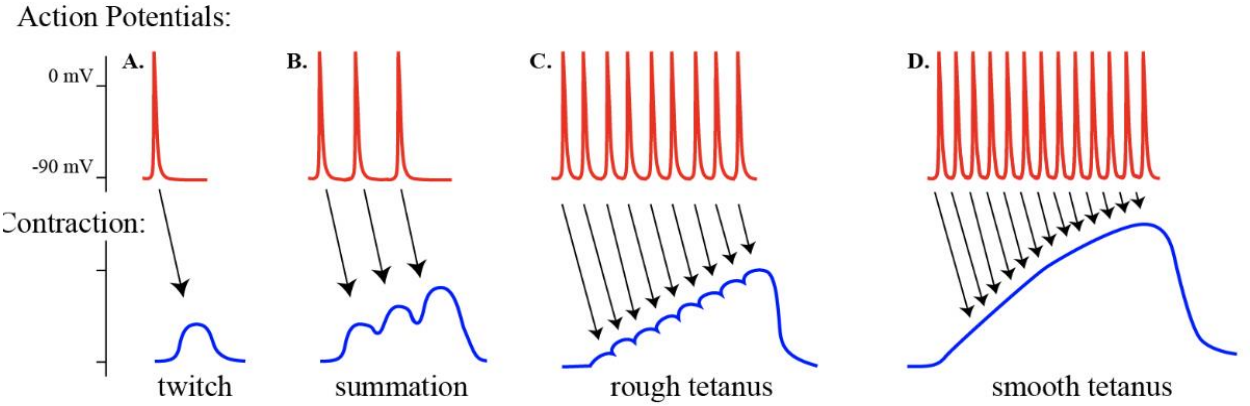

Figure 6. Twitch and tetanic contractions. *A single pulse of stimulation causes a twitch contraction. Increasing the frequency of stimulation lead to twitch summation into rough (unfused) and smooth (fused) tetanic contractions.*

composition. Different muscle types can exhibit very different twitch contraction kinetics

(Ferrantini et al., 2014; Mijailovich et al., 2021). Vertebrate's muscles, for example, can be classified in slow- and fast-twitch muscles. Slow-twitch muscles require a longer time to reach their peak force (time to peak, TTP) and have longer relaxation kinetics, making them more suited for the prolonged contractions, needed, for example, in postural muscles (Schiaffino & Reggiani, 2011). A rapid series of presynaptic inputs causes the twitches to sum-up until they are completely fused in a smooth tetanus (Fig. 6). The force generated by a tetanic contraction is strictly dependent on the frequency of stimulation and is described by the force-frequency relationship (Fig. 7). Slow muscles tend to reach the fusion frequency and to exert higher fractions of their maximal force at lower stimulation frequencies than fast muscles (Fig. 7) (Botterman et al., 1986; Fuglevand et al., 1999).

The amount of force produced by muscle contraction ultimately depends on the force exerted by a single cross-bridge and the number of cross-bridges formed (Fitts et al., 1991).

The force produced by a single cross-bridge depends on the myosin isoform as well as several physicochemical parameters including temperature and calcium concentration

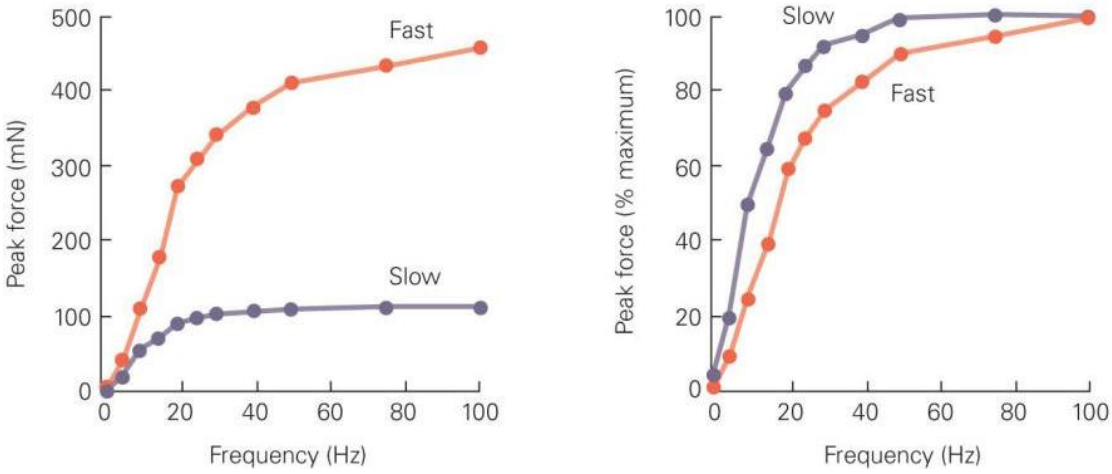

Figure 7. Typical force-frequency relationship of fast and slow twitching muscles. *Slower muscles tend to exert higher fractions of their maximal force at lower frequencies of stimulation*

(Bottinelli & Reggiani, 1995; Kandel et al., 2013). Myosin molecules comprise two heavy chains (myosin heavy chain, MHC) and four light chains (myosin light chains, MLC). The C-terminal tail domains of the MHCs twist together to form a long coiled-coil rod-shaped structure. The N-terminal of each MHC forms a globular domain, referred to as the head

domain, which hosts the ATPase activity and the actin binding site. One essential MLC and one regulatory MLC interact with each MHC head, influencing the protein function (AL-Khayat, 2013; Sweeney & Houdusse, 2010). Several studies have shown that the specific MHC and MLC isoform composition can impact not only the force produced by a single cross-bridge but also the cross-bridges cycling rate and, therefore, the number of cross-bridges formed (Bottinelli et al., 1991, 1994, 1996; Bottinelli & Reggiani, 1995; Canepari et al., 2000).

In addition to myosin isoform composition, stimulation frequency and calcium dynamics, the number of cross-bridges formed depends on the degree of superposition between thick and thin filaments, i.e. the sarcomere length, and on the velocity of their reciprocal sliding, i.e. the sarcomere shortening velocity.

The length dependence of the force production gives rise to the force-length relationship, which is usually a bell-shaped curve. This relationship indicates that muscles generate the greatest force at values around their optimal length, often corresponding to the resting length in skeletal muscles, and decreasing forces at both longer and shorter lengths. Skeletal muscles manifest a small range of length variation due to their attachment to rigid structures (the bones) through tendons (for a review see Burkholder & Lieber, 2001).

It is also worth mentioning that, while the active contractile tension generated by the muscle follows the relationship just described, lengthening the muscles produce a passive tension which increase exponentially with muscle length. This passive component allows the total tension generated by a muscle to increase even beyond the range of its active contractile tension (Fig. 8) (Aljure & Borrero, 1968; Crocini & Gotthardt, 2021).

The relationship between shortening velocity and the force production, (the force-velocity relationship) follows a hyperbolic function and is well described by Hill's equation. The force is maximal in isometric condition (which means without shortening) and falls as the velocity increases. The maximum shortening velocity corresponds to zero force production and can be extrapolated using Hill's equation as the intercept on the velocity axis (Hill, 1938).

Besides muscle contractile properties, force production and the final torque exerted by the muscle are strongly affected by the structural properties of the tissue. Forces generated by muscles have also to be considered relative to the resistive forces arising from tissue stiffness and viscosity and to the tissue elasticity. Stiffness quantifies muscle resistance to length changes and is dependent on the structure of the muscle fiber itself and that of the surrounding extracellular matrix. Muscles may manifest important

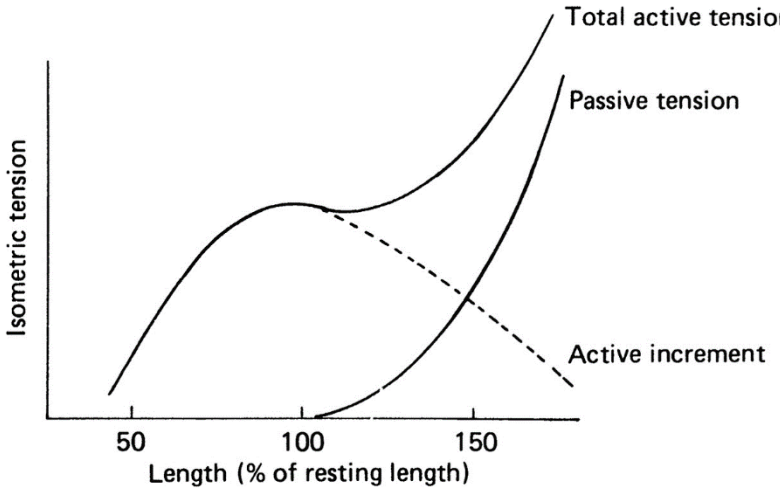

***Figure 8. Typical force-length relationship of skeletal muscles**. Active tension its maximal around the resting length of the muscle and decreases with muscle lengthening. Passive tension, instead, starts to be relevant at longer lengths and increases exponentially causing the total tension even beyond the contractile range of the muscle. From Aljure & Borrero, 1968*

differences in stiffness and this is reflected in their functional specialization. For example, a higher stiffness might help keeping the length fixed during prolonged isometric contractions at a reduced energetic cost and can be useful to counteract sudden length changes (Shadmehr & Wise, 2005; Winter et al., 2022). Viscosity and elasticity also play crucial roles in shaping the outcome of muscle contraction. An example is provided by the insect flight muscles that can efficiently store and release elastic energy, thus working like springs and reducing the energy consumption of motion (Full & Meijer, 2010). Higher elastic energy dissipation through heat (due to material internal friction), on the contrary, has been shown to play a role in reducing oscillation and increase motion stability through

damping effect in various type of striated muscles (Franklin et al., 2004). Altogether, muscles work as complex viscoelastic systems in which the outcome of sarcomeres contraction is strongly influenced by the mechanical and dynamical properties of the tissue.

Another critical aspect in determining the contraction outcome is muscle architecture (Alexander & Ker, 1990). The force a muscle can produce is directly proportional to the number of sarcomeres working in parallel, which in turn depends on the muscle's cross-sectional area (CSA). The range of motion and velocity of shortening, on the other hand, are strongly influenced by the number of sarcomeres working in series and, hence, by the length of the muscle. In addition, musculoskeletal geometry and fibers arrangement determine the muscles resting state and affect their functional attributes. Most vertebrate

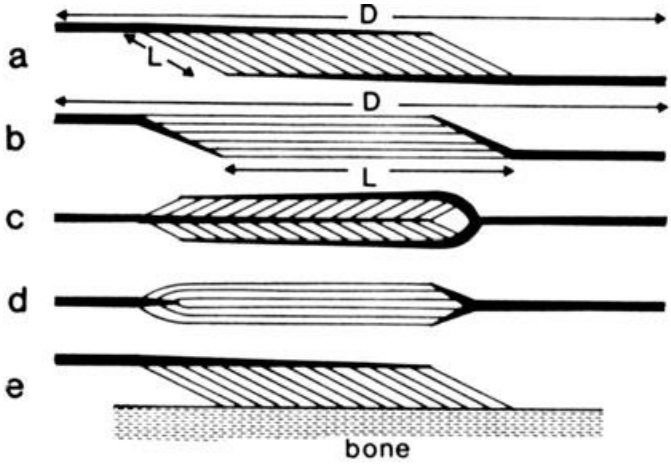

Figure 9. Five common arrangements of tendons and muscles. *In (b) and (d) fibers are organized in parallel to the line of pull so the muscle has wider range of motion and higher shortening velocity. In (a), (c) and (e) the pennation angle allow for the increase in CSA and, hence, in force per unit of volume. From Alexander & Ker, 1990*

muscles, for example, are kept at lengths close to their L_0 with fascicles not parallel to the line of pull but arranged in a feather-like (pennate) configuration (Fig. 9). The angle between the direction of the muscle fibers and the line of pull, the so-called pennation angle, obviously influences the torque exerted by the muscle on the bone. Furthermore, because more fibers can fit into a given volume as the pennation angle increases, muscles with large pennation angles typically have myofibrils in parallel and, hence, a larger CSA. However, fibers in pennate muscles are usually shorter and have lesser maximal shortening velocity and range of motion.

1.3 Octopus motor system

Octopus vulgaris displays one of the richest motor repertoires in the animal kingdom. It can swim by either using arms and web to row or by using the siphon to propel the body with a jet of water. Octopuses also show a surprising adaptability to different situations, being able to use the same organ and/or the same motor action in multiple tasks. For example, the same jet of water, produced through the siphon can be used as a defensive mechanism against intruders (mixing it with ink), to clean the den, throw small object or even remove sand from a shell to ease carrying it (Finn et al., 2009). The octopus arms are multitasking organs that can be used to open large clams and jar plungers, walk over the sea floor, 'taste' potential food and explore the environment (Anderson & Mather, 1996; G. Fiorito & Gherardi, 1999). Relative to motion, they can manifest several patterns of locomotion, such as walking, crawling, and climbing. In some octopus species, arms can even be used for mimicry by shaping them into algae-like branches (Huffard et al., 2005; Norman et al., 2001).

How can an octopus control this large repertoire of arm movements and behaviors? Skeletal animals' motor systems strongly rely on the fixed dimensions of their body parts and the limited degrees of freedom of their joints to plan and execute movements (see chapter 1.2). In contrast, the unconstrained nature of the octopus body and the need to coordinate eight exceptionally flexible appendages means that the octopus must have developed unique motor control strategies.

Octopus motor control network organization

Octopus vulgaris NS is divided into three main parts: a central brain surrounded by a cartilaginous capsule, two large optic lobes connected to the retinae of the highly developed camera-like eyes; and the peripheral nervous system of the arms (Fig 10) (Levy et al., 2017).

Much like the vertebrates one, octopus motor system is hierarchically organized. Sensorimotor processing involves large areas of the CNS as well as the highly developed

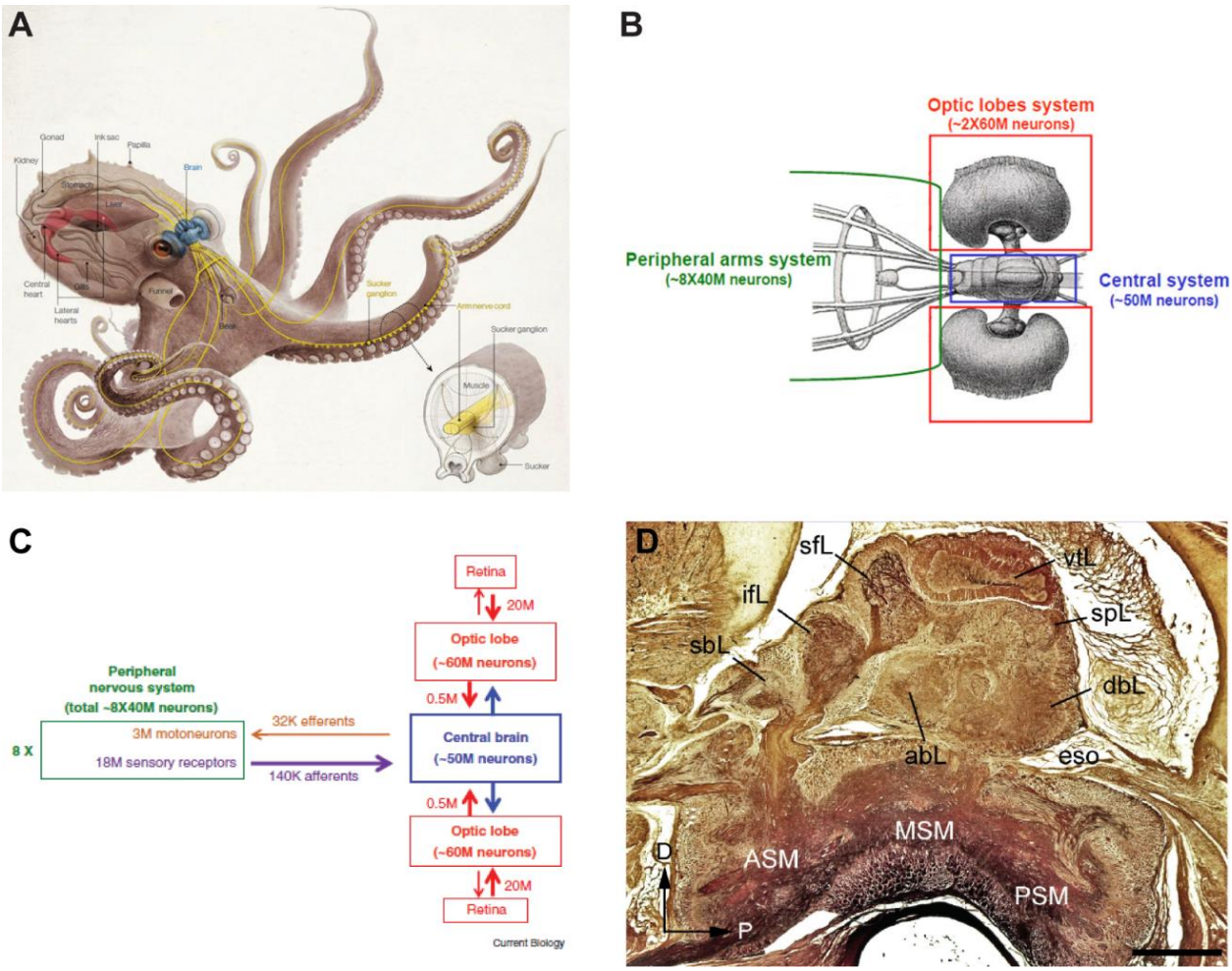

Figure 10. Octopus nervous system. (A) *Schematic outline of the octopus CNS (in blue) and PNS (in yellow).* ***(B)*** *The octopus NS is divided into three main part: the optic lobes (red), the CNS (blue) and the PNS (green). Only bracial nerves and interbrachial commissures, and not the ANCs, are showed in this image.* ***(C) S****chematic of the three parts of the octopus NS and the relative connections.* ***(D)*** *Longitudinal section of the supra- and sub-esophageal mass of O. vulgaris (parasagittal plane). Sections of stained with the Cajal silver method. abL, anterior basal lobe; ASM, anterior subesophageal mass; dbL, dorsal basal lobe; eso, esophagus; ifL, inferior frontal lobe; MSM, middle subesophageal mass; PSM, posterior subesophageal mass; sbL, superior buccal lobe; sfL, superior frontal lobe; spL, subpedunculate lobe; svtL, subvertical lobe; vtL, vertical lobe. Scale bars: 500 mm. Adapted from Hochner, 2012 and Shigeno et al., 2018.*

PNS. Nevertheless, the specific contribution of peripheral and central nervous systems to motor planning and execution is still under investigation.

The exceptionally large central brain includes more than 30 interconnected lobes. As for other cephalopod species, octopus' brain is assembled through a series of ganglia to form

lobes that are fused together and connected to the periphery by many nerve trunks. It is organized around the esophagus which divides it into two major masses: the supra-esophageal mass (SEM) and the sub-esophageal mass (SUB) (Fig. 7) (Shigeno et al., 2018; Young, 1971).

The SEM is involved in higher cognitive and motor functions. Higher motor centers are localized in the so called 'basal lobes' of the SEM and they receive inputs from optic lobe, pedunculated lobe and receptor organs (Shomrat et al., 2008; Turchetti-Maia et al., 2019). They are assumed to work hierarchically through intermediate and lower motor centers to produce a wide variety of movements and behaviors from different body parts, like fin, arm or mantle (Messenger, 1983).

Lower and Intermediate motor centers lie in the SUB and send their commands both directly (lower) and indirectly (intermediate) to the motor effectors (Robertson et al., 1993; Shigeno et al., 2018). They are controlled by the higher motor centers and receive input from various receptors. They host neurons that innervate the funnel, arms, retractor muscles of the head, eyes, chromatophores and the frontal part of the body (Young, 1971).

The SUB provides the major direct connection between CNS and peripheral nervous system of the arms. Eight nerve bundles, the brachial nerves, exist anteriorly and project to the arms. Before reaching the elaborate peripheral nervous system of the arms, these nerve bundles are joined together by a circumbrachial commissure, which is considered to have an important function in multiple arm coordination (Budelmann & Young, 1985; Shigeno et al., 2018; Young, 1971).

Octopus motor control

Motor control system must integrate extrinsic and intrinsic sensory information with experience (memory) to allow motor action selection, planning and execution. It is generally accepted that this complex integration occurs by interfacing some sort of central representation of the two systems. As described in chapter 1.2, sensory and motor representations of the body can be found in vertebrates cortices where they give rise to

somatotopic maps, the "*homunculi*" first described by Penfield (Penfield & Rasmussen, 1950).

In vivo brain recording and stimulation experiments in freely behaving animals demonstrated that a similar organization does not exist in the higher motor centers of an octopus (i.e., the basal lobes)(Zullo et al., 2009). Recordings from this area showed that sensory inputs from various body regions do not localize in discrete areas topographically arranged, as in vertebrates. In addition, most areas appeared to respond to multimodal sensory inputs such as visual and tactile stimulation (Zullo, 2004).

Relative to the motor response, local electrical stimulations over different regions of the octopus' higher motor centers resulted in complex motor behaviors (like arm extension, crawling and jetting) involving the use of several arms and body portions. Each of these motor behaviors was built up from combinations of discrete motor elements recruited alongside with stimulation (Zullo et al., 2009). These results suggest that motor programs, rather than body parts, are represented in the higher motor centers. They also indirectly suggested that these motor programs may be represented in the form of 'overlapping circuits', where groups of cells can be alternatively recruited in different pathways to generate a variety of motor behaviors. Interestingly, this kind of representation is consistent with the representation of movements in the form of motor primitives, which would not require the representation of actions in terms of body coordinates (Flash & Hochner, 2005).

It is also worth noting that these results were comparable in nature to those obtained by stimulating higher order multisensory integrative areas in vertebrates. Microstimulation of the ventral intraparietal area of the macaque brain, for example, resulted in complex movements of hand and shoulder as well as facial grimacing, eye closure and head withdrawal (Cooke et al., 2003). This might indicate that the basal lobes system should be seen more as an integrative area. If that is the case, it might well be possible that somatotopic-like representations are present at lower levels, namely the SUB and the arms nervous system. Several studies, for example, suggested the existence of a topographical representation of arm and chromatophore motor neurons in the SUB of octopus, cuttlefish and squid (Budelmann & Young, 1985; Dubas et al., 1986; Gaston & Tublitz, 2004, 2006; Saidel, 1981).

No evidence has been reported so far about the organization of motor neurons in the nervous system of the arms. This, in particular, may represent a major gap in our knowledge since roughly two-thirds of the octopus' neurons are located inside the arms, suggesting a major involvement of this compartment in processing sensory information and possibly motor commands.

However, even if somatotopic-like representations are present in the octopus motor system, the existence of sensory and motor representations in terms of body coordinates, in a way comparable to the vertebrate one, is very unlikely. The flexibility and unusual morphology of the octopus body pose several major difficulties for accomplishing motor control based on precise body representation. Octopus arms are unsegmented, slender, and long, and can perform many types of active arm deformations at any point along their length. It is therefore difficult to envisage a control system capable of coping with the huge computational burden arising from the need to handle the virtually infinite degrees of freedom in a deterministic manner.

In 1978, Wells even went so far as to say that "octopuses are not aware of their arms" (Wells, 1978). It is currently know that tactile stimulations of the arms result in strong activity at the CNS brain level, so that's likely not true. However, it may not be entirely false.

One intriguing possibility is that the octopus evolved unique motor control strategies based on motor programs embedded in the PNS, taking advantage of the high flexibility of the arm to simplify motor programs and computational processes. This is usually referred to as the "embodied solution". The term embodiment (also referred to as "intelligent embodiment") comes from robotics and refers to the design of autonomous robots whose behavior arises from the local dynamic interplay between their morphology, the mechanical properties of their materials, the sensory feedbacks from the environment and the central controlling system (Pfeifer et al., 2007). The proper adjustment of such interactions simplifies motor control, as it leaves it to deal mainly with perturbations (Hochner, 2012; Kang et al., 2016). Several evidence supports this theory, suggesting that a large part of the computational work associated with motor processing is carried out at the arm level and further simplified by the arm-embedded morphofunctional properties.

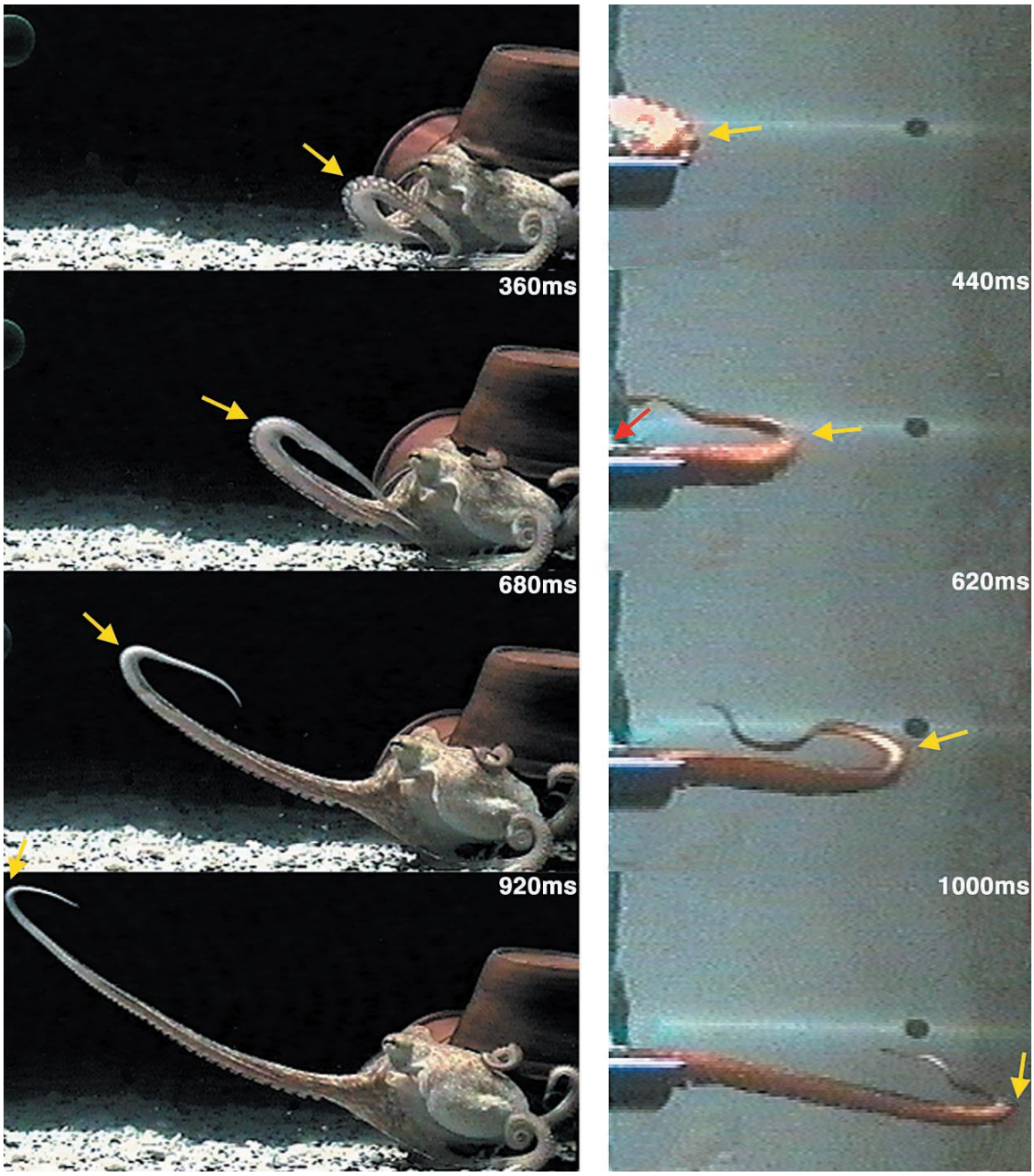

Figure 11. *A freely behaving octopus reaching toward a target (left) and the electrically evoked bend propagation in the denervated arm of a decerebrated animal (yellow arrows indicate the bend point). From Sumbre et al., 2001*

Like vertebrates, the octopus employs stereotyped motor schemas to reduce the degree of freedom of motion. One example is the reaching movement, where one or more arms are extended towards a target (Fig.11). This goal-directed arm extension is performed by propagating a bend from the base to the tip of the arm over a planar direction, thus reducing the virtually infinite degrees of freedom to three: two for the direction of the base

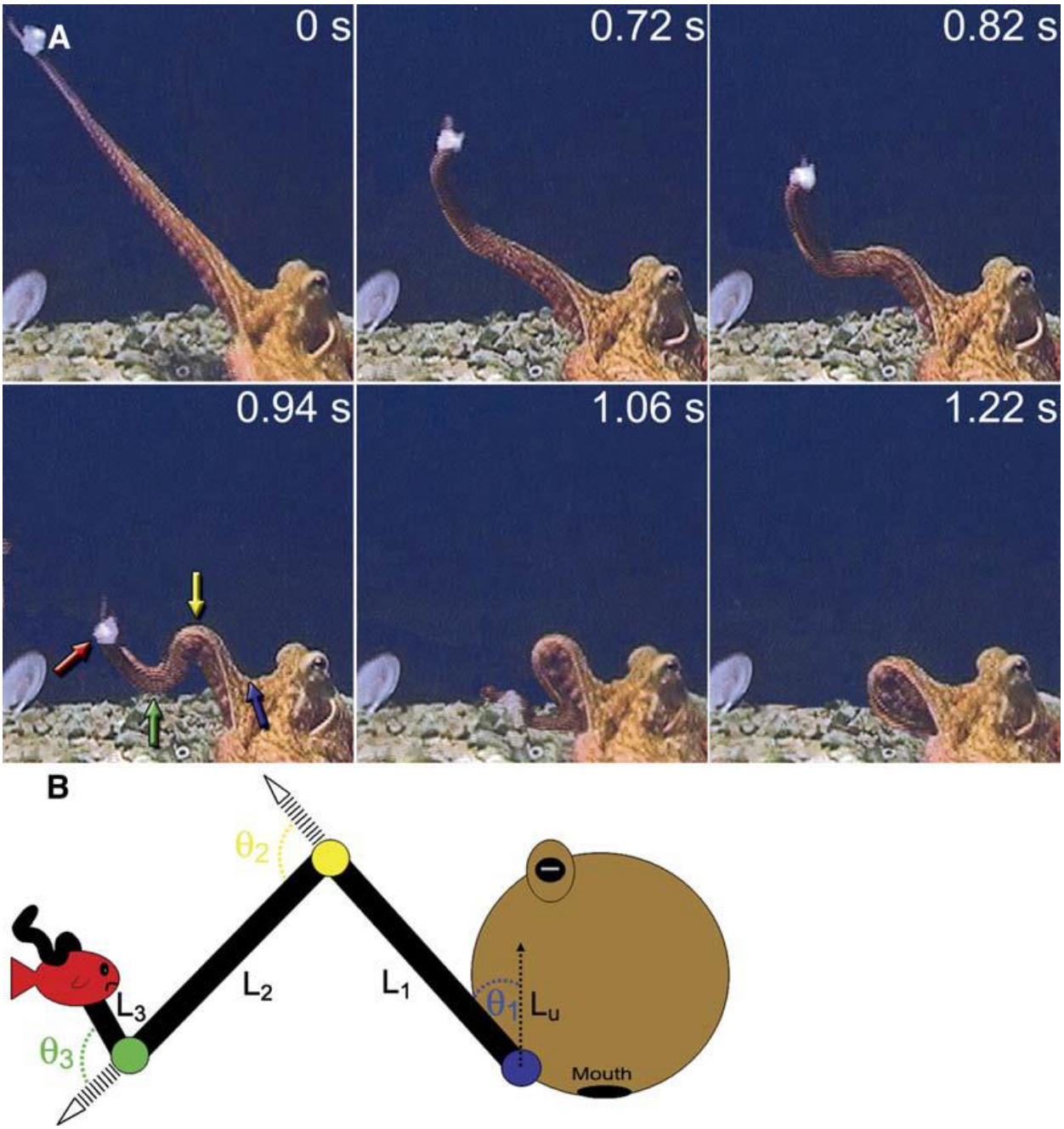

Figure 12. Octopus Fetching Movements Involve a Quasi-Articulated Structure of the Arm. (A) *Sequence of six video images at times indicated during a fetching movement. Red arrow marks location of the food. Green, yellow, and blue arrows, respectively, mark the distal, medial, and proximal bends.* ***(B)*** *Schema of the quasi-articulated structure with the nomenclature for the joints and segments used in the text. From Sumbre et al., 2006*

and one for the velocity of the bend propagation. More importantly, the bend propagation is controlled by a local motor program embedded in the arm neuromuscular system, and

requires minimal computational intervention from the higher centers (Yekutieli et al., 2005).

This also was confirmed by Sumbre and collaborators, who demonstrated that arm extension and other stereotyped motions with natural kinematic characteristics can be elicited in amputated arms by electrical stimulation of the ANC (German Sumbre et al., 2001).

Another striking example of the octopus unique motor strategies comes from the kinematic analysis of the fetching behavior, the motion used by the animal to bring food to the mouth after catching it (Fig. 12). In this movements, the arm is reshaped in a quasi-articulated structure in which three linear segments can be distinguished: a distal segment grasping the object and working like a 'hand', a proximal and a medial segment serving as 'upper' and 'forearm'. Once the object is grasped, it is brought to the mouth mainly by rotating the medial joint following a stereotyped movement with only three degrees of freedom (Fig. 12 B). Interestingly, the point where the medial joint will be formed is not fixed, as it is determined by the position of the object. The sensory inputs associated with the grasped object elicit two ways of muscle activation: one starting from the base of the arm and the other from the grasping position. The medial joint is formed where the two waves meet and provides a simple and elegant way to reshape the arm in a quasi-articulated structure (Germán Sumbre et al., 2006).

Therefore, peripheral sensory inputs from arm sensory receptors and local motor processing in the arm nervous system are likely to play a crucial role in the establishment of peripheral motor programs in the octopus arm.

Octopus Arm Nervous System

The arm nervous system comprises a main axial nerve cord (ANC) in the center of the arm, five peripheral intramuscular nerve cords and the suckers' ganglia (subacetabular ganglia) (BOYLE, 1986)(Fig. 13).

The ANC runs throughout the entire length of the arm in its central portion, surrounded by a layer of fibrous connective tissue. It is composed by two dorsal axonal tracts, the cerebrobrachial tracts (CBTs), and one ventral cord, the medullary cord (MC) (Fig. 9).

The MC is composed by a cellular cortex of unipolar nerve cell bodies surrounding an inner neuropil with interconnecting fibers that expands in a local swelling (the arm ganglia) opposite to each sucker (Zullo et al., 2019a).

The organization of the ganglia is that of a typical invertebrate ganglion with cell bodies densely packed in an external "cell layer" surrounding a neuropil hosting fibers and connections. Based on their size, at least two different groups of cells have been described: one composed by a low number of very large cells clustered in the dorsal part of the ganglion and the second by a large number of small cells throughout the ganglion (Young, 1971). However, the identity of these cells remains to be investigated. A series of nerve roots emerge from each ganglion, carrying afferent information from skin, suckers and muscles and efferent motor commands to the intrinsic muscles of arm and suckers. The ventral roots connect the ganglion with the sucker, whereas the dorsal and lateral roots innervate small areas of the arm intrinsic musculature (Fig. 14C) (Rowell, 1963; Young, 1971).

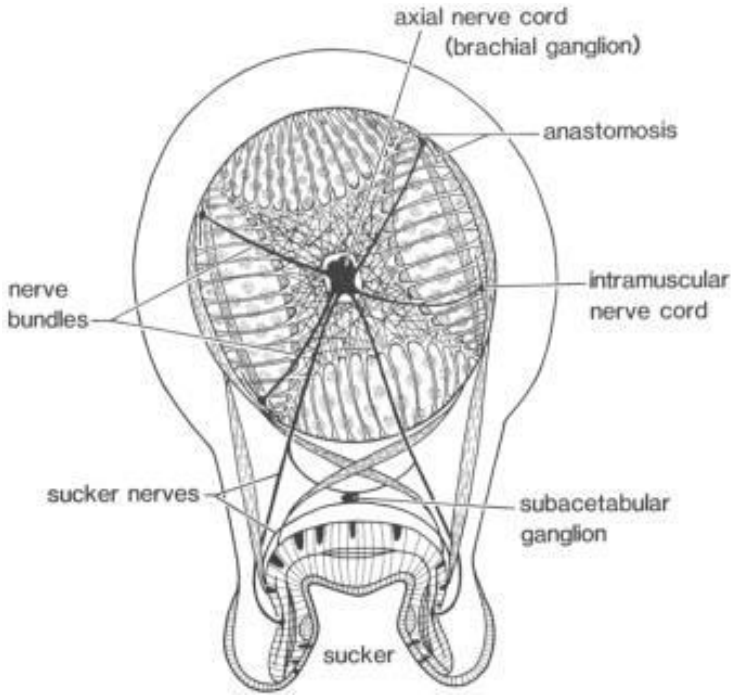

Figure 13. *Arm transverse section showing the different compartments of the arm nervous system. From Boyle, 1986*

The CBTs contain axons carrying information to and from the brain. The motor command neurons of the central brain do not directly innervate the arm muscles but send projections to the MC where motor neurons lay. Here, the motor command can be further processed and transmitted to the musculature of arms and suckers (Gutfreund et al., 2006). Along the pathway connecting the ANC ganglia to the intrinsic musculature of the sucker, there is a further processing station, the sucker ganglion. Suckers' ganglia are located right above each sucker and are supposed to be the first integration point of the sucker sensory information (Fig. 13) (Rowell, 1963).

Octopus Arm Musculature

The intrinsic musculature of the arm is organized around the axial nerve cord. It is composed by three differently oriented muscle groups. The Transverse (T) muscles occupy the inner layer, surrounding the axial nerve cord. T muscle fibers are oriented in planes perpendicular to the arm longitudinal axis, originate from the external connective tissue layer and pass through longitudinal muscles as trabeculae between longitudinal

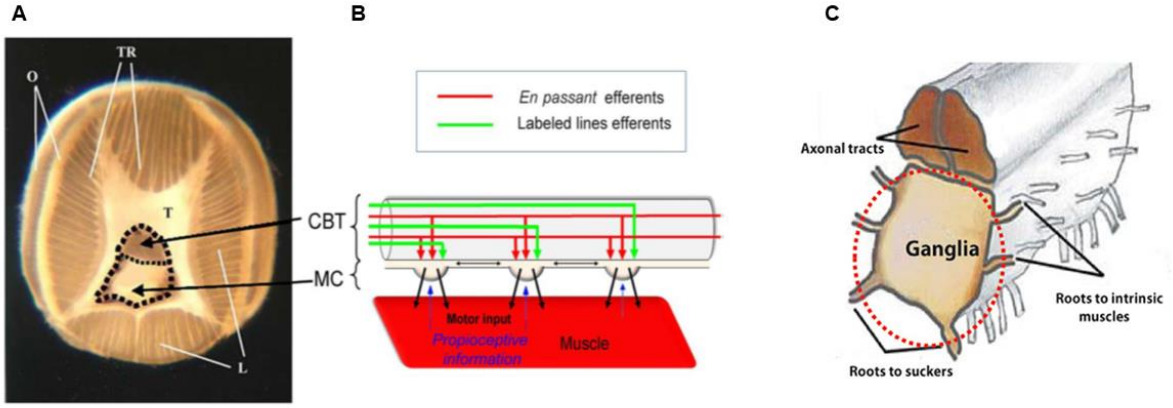

Figure 14. (A) *octopus arm transverse section: O = oblique muscles, L = longitudinal muscles, T = transverse muscles, TR = transverse muscles trabeculae, CBT = cerebrobrachial tracts, MC = medullary cord.* ***(B)*** *schematic representation of octopus arm nervous system.* ***(C)*** *schematic representation of an ANC ganglion. Nerve roots to suckers and intrinsic muscles are indicated.*

muscle bundles (Fig. 14 and 15). Longitudinal (L) muscles occupy an outer layer and are organized in bundles separated by the T trabeculae and running parallel to the main axis of the arm (Fig. 14 and 15). Three sets of oblique muscle fibers are present on each side of the arm. The external oblique muscles enclose the intrinsic musculature of the arm and are the most superficial. The median oblique muscles are separated from the external oblique muscles by longitudinal muscle fibers. The internal oblique muscles are the most central, located on each side of the core of transverse muscles (Fig. 14 and 15). The

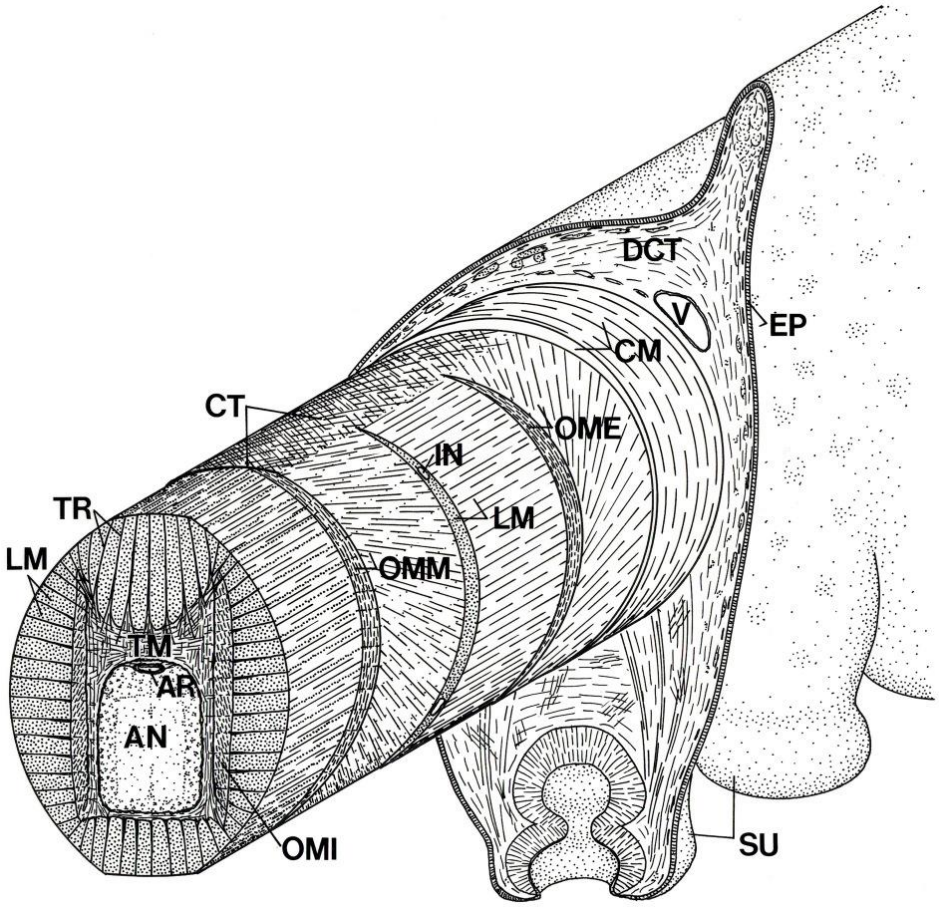

***Figure 15**. Schematic diagram of the arm of Octopus showing the three-dimensional arrangement of muscle fibers and connective tissue fibers. AN, axial nerve cord; AR, artery; CM, circumferential muscle layer; CT, connective tissue; DCT, dermal connective tissue; EP, epidermis; IN, intramuscular nerve; LM, longitudinal muscle fibers; OME, external oblique muscle layer; OMI, internal oblique muscle layer; OMM, median oblique muscle layer; SU, sucker; TM, transverse muscle fibers; TR; trabeculae; V, vein. From Kier, 1988.*

handedness of a given oblique muscle is opposite to that of the other member of the pair on the opposite side of the arm. Surrounding the intrinsic muscle of the arm there is a thin

layer of circular muscle with fibers arranged circumferentially around the arm (Kier & Stella, 2007). A layer of connective tissue packs the three muscle groups together imposing a constant volume to the whole system, which works as a muscular hydrostat (for a review see also Kier, 2016).

As mentioned in the beginning of this manuscript, muscular hydrostats are structures where muscles evolved to produce both mechanical force and structural reinforcement (Kier, 2012; KIER & SMITH, 1985). In the octopus arm, this is achieved through the action of antagonistic muscles, arranged in different orientations, under the constant volume constraint. This configuration can generate a variety of motion through some combination of four basic deformations: elongation, shortening, torsion and bending (Kennedy et al., 2020). Torsion movements are elicited by the contraction of the oblique muscles (Fig. 16). All other basic deformations arise from combinations of T and L antagonistic action. Given the constant volume constraint, a contraction of T muscles will cause a decrease in cross-section and, hence, an increase in length. Conversely, contraction of L muscles will cause the arm to shorten, increasing its cross section. Arm bending requires selective contraction of longitudinal muscle bundles along the side of the arm that represents the inside radius of the bend. The support required to resist the longitudinal compressional force that would otherwise simply shorten the arm is provided by the T muscles (Fig. 17). Active bending movements thus require simultaneous contraction of the transverse and longitudinal muscles. Bending may also occur if the transverse muscle decreases the

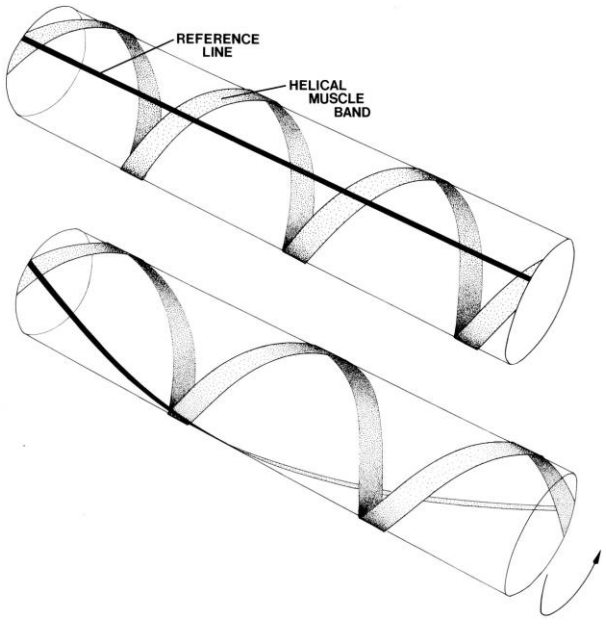

Figure 16 Schematic diagram of the torsion movement. *The image shows a single left-handed helix of oblique muscles and a black reference line in the center. Upon muscle contraction the arm twists. The direction of torsion depends on the handedness of the helical muscle band. From Kier & Smith, 1985.*

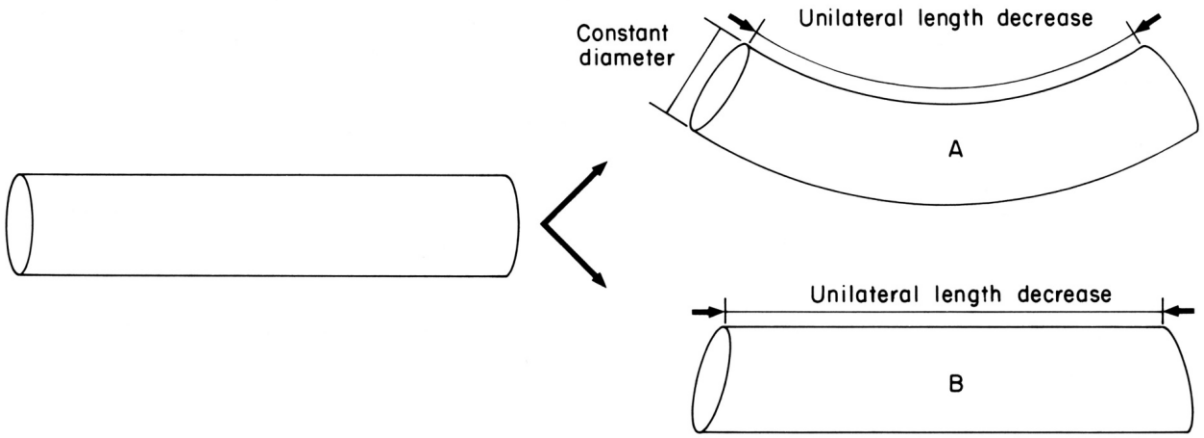

Figure 17. Schematic diagram of the bending movement (first case). *L muscles contraction on one side causes an unilateral length decrease. In case A, constant diameter is maintained by providing resistance to longitudinal compression and causing bending. Incase B, constant diameter is not maintained and without resistance to longitudinal compression the structure is shortened but not bent. Constant diameter can be maintained by contractile activity of the transverse muscle. From Kier & Smith, 1985*

cross-section while the longitudinal muscle on one side of the arm (again, the inside radius of the bend) maintains a constant length (Fig. 18). In addition to arm bending, co-contraction of T and L muscles can also induce arm stiffening, resulting in semi-rigid skeletal-like arm segments. This last pattern of muscle activity has been shown to be a component of several arm motor tasks including arm extension and bending as well as more complex tasks like bipedal walking (Kier, 1982, 1985, 2016a; Kier & Stella, 2007).

Hydrostatic muscles can undergo dramatic changes in shape without any loss of functionality. This requires mechanical and structural adaptations. One of the most

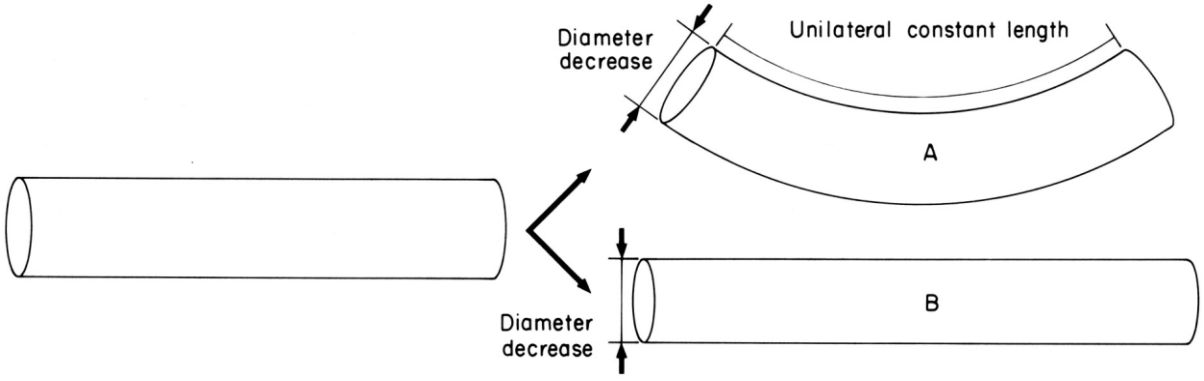

Figure 18. Schematic diagram of the bend movement (second case). *T muscles contraction causes a decrease in diameter. In case A unilateral constant length is maintained through the activity of L muscles thereby causing bending. In case B unilateral constant length is not maintained and T contraction results in arm elongation. From Kier & Smith 1985.*

important concerns the length-tension relationship. Each muscle is designed to work over a determined range of lengths, and different kinds of muscles show different length-tension relationships. Hydrostatic muscles usually show a very wide length-tension relationship, which enables them to exert forces over a broad range of lengths (Full & Meijer, 2010). The spatial organization of the muscles is also very important since the strain rate will be different in different positions. It has been shown that muscles in hydrostatic structures have different architectures based on their spatial location and accordingly to their functional use in motion (Thompson et al., 2014). Finally, the structural and mechanical properties of the connective matrix play a fundamental role in the functionality of hydrostatic muscles and, in octopus, they have been shown to vary in relation with muscle type and localization within the arm section (Di Clemente et al., 2021).

At the cellular level, the three muscles present no differences. In contrast with vertebrate muscle fibers, cephalopod muscle fibers are uninucleated cells generally not exceeding 8-20 μm in diameter and 1 mm in length. The central region of the cells is filled with mitochondria, while the cortical zone is occupied by the contractile apparatus, which gives rise to an obliquely arranged striation that is uniform and continuous among neighboring cells. Within the sarcomere, all but the M line components are present, and the oblique striation arises from a slight dealignment of the contractile filaments rather than a different orientation of them (Feinstein et al., 2011). The molecular composition of the contractile machinery and the contraction mechanism are supposed to be similar to those typical of vertebrate skeletal muscles, although no evidence of the mechanics of the contractile machinery have been produced so far. Interestingly, while proteins involved in the contraction mechanisms show high level of homology with those of vertebrate and others invertebrate, regulatory proteins, such as tropomyosin, seem to be highly cephalopod specific (Motoyama et al., 2006; Nödl et al., 2016; Zullo et al., 2017). This might imply that, being equal the general mechanisms, cephalopod muscles might possess a different regulatory system, calcium sensibility and different kinetics of the cross-bridge cycle. Another relevant morphological difference between vertebrate and cephalopod muscle cells is the organization of the sarcoplasmic reticulum. The plasma membrane T-tubule system and the triads are completely absent in the latter, suggesting a completely

different excitation-contraction (EC) coupling, probably relying more on extracellular calcium. However, at the level of the z lines, specialized sarcoplasmic structures called terminal *cisternae* are present and seem to be in thigh contact with plasma membrane invaginations, forming what has been termed dyads in analogy with the vertebrate triads. Several different functions have been proposed for such complexes, including fostering calcium release from internal stores by bringing membrane depolarization closer to the SR. Moreover, electron microscopy experiments pointed out that, at the level of the dyads, plasma membrane forms finger like processes seemingly connecting muscle cells to the collagen matrix. However, no functional assessment of their role has been performed thus far (Fig.19) (Zullo et al., 2017).

The electrical properties of the cephalopod muscle cells have been extensively characterized through patch clamp and sharp recordings in both, dissociated cultures and tissue preparations. Such cells are electrotonically compact, show mainly linear membrane properties and can generate several types of regenerative responses ranging from neuronal-like spikes to voltage oscillations. Spike initiation seems to rely only on the activation of L-Type Ca^{2+} channels, which are thought to provide also the $[Ca^{2+}]_{in}$ increase needed to trigger contraction. The extent to which the calcium released from the internal stores participate to the contraction mechanism remains matter of debate. Recent studies pointed out that intracellular calcium may play a major role lowering the threshold for contraction activation, possibly via Calcium Induced Calcium Release (CICR) (Nesher et al., 2019).

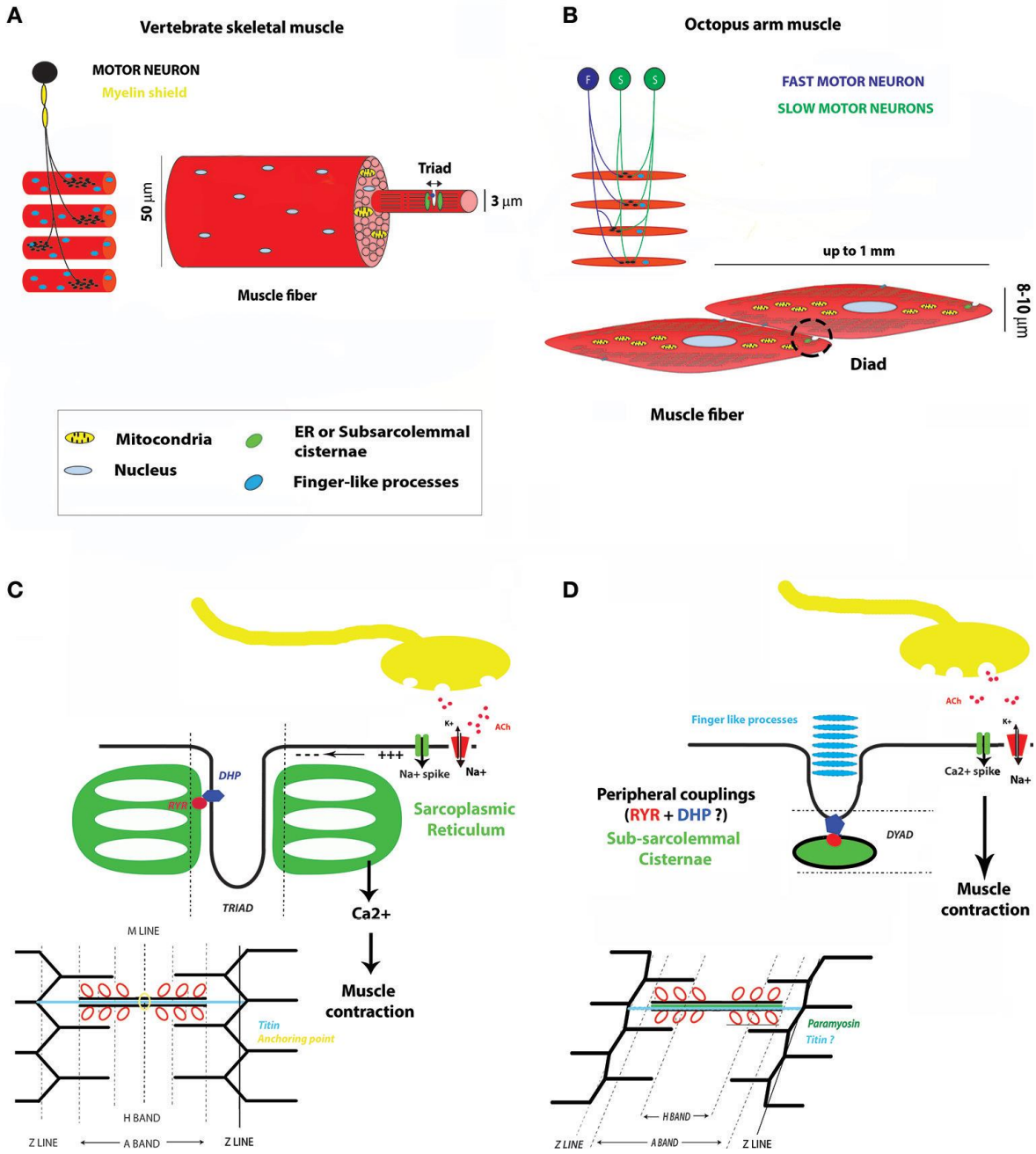

Figure 19. Main similarities and differences between a vertebrate skeletal muscle and a typical cephalopod arm striated muscle. ***(A)*** *Vertebrate skeletal motor unit and myofibril.* ***(B)*** *Motor unit and muscle fiber in the octopus arm.* ***(C)*** *Vertebrate skeletal muscle at NMJ and main steps of E-C coupling.* ***(D)*** *Octopus muscle at NMJ and main steps of E-C coupling. For a better comprehension of the illustration the sarcomere was not represented at a striation angle typical to the muscle at rest (between 6◦ and 12◦). These drawings mean to be representative of the general arrangement of muscle compartments but their single elements are not scaled on real dimensions. DHP, dihydropyridine channel; RYR, Ryanodine receptor; ACh, Acetylcholine.*

Interestingly, each muscle cell receives three different types of cholinergic excitatory

inputs. One has fast kinetics and a large quantal amplitude (fast PSP), the other two have slower kinetics and a small quantal amplitude (medium and slow PSPs). One single fast PSP synaptic input appears to be enough to trigger a regenerative response, whereas the other two, due to their longer kinetics and lower amplitude, seem to be more dependent on temporal summation. None of the three showed a strong activity-dependent plasticity. This, together with the linear membrane properties, suggests a simple and direct transformation of neural activity into muscle contraction (Matzner et al., 2000).

Morphological studies also suggested that a single motor neuron innervates ~3300 muscle cells occupying an area of approximately 0.2 mm^2 (Feinstein et al., 2011; Hochner, 2012; Young, 1971). If this is indeed the case, the small dimensions of the motor unit should allow a fine spatial regulation of muscle contraction. However, we currently have no direct evidence on the motoneuronal innervation pathway at a reduced scale (meaning from a single to a very small number of motoneurons).

2 Aims

Octopus vulgaris offers the unique opportunity to study a complex motor system, different from those of vertebrates, but showing sophisticated performances.

The octopus motor system is hierarchically organized into a higher central nervous system (CNS) and a peripheral nervous system (PNS). Complex motions in the octopus are executed not only through the activation of the sensorimotor areas of the CNS, but also through the rather autonomous PNS of the arms. Here, reflex motor responses and some stereotyped motions can occur rather independently form CNS control.

Moreover, the existence and specific contribution of 'arm-embedded' determinants of motion execution are still at the beginning of its understanding. Similar to other hydrostatic organs, several features of the arm might contribute to the type of motion produced following a certain motor input. These include the biomechanics of different arm muscles, their morphological organization within the arm, and the topographical arrangement of their motor neurons at the level of the arm PNS.

Here, we investigated the octopus arm 'design constraints', meaning the set of architectural and biomechanical features of the arm muscles that collectively contribute to the arm motion. These features are exploited in a highly coordinated manner to perform a rich behavioral repertoire while leveraging the needs of a complex computational load.

We first depicted the organization of the PNS motor neurons innervating the arm muscles and receiving their input from the decision-making center of the higher motor control areas of the CNS. We then addressed the morphofunctional relationship of the two main muscles composing the arm bulk by studying their passive strain, activation, contractile properties, and morphological arrangement within the arm. This, especially in soft limbs, can strongly affect the mechanical output of a muscle and, eventually, the type of limb deformation produced.

This study will lead to uncover the motor control strategies for soft limbs developed by a highly intelligent animal. The results provided here may be applicable in the field of soft-

robotics as an increasing number of researchers are currently aiming at designing and constructing bio-inspired, soft-robotic manipulators capable of semi-autonomous functions. These may find several uses in fields spanning from human surgery, to industrial applications and autonomous environmental exploration.

3 Materials and methods

3.1 Animal treatment

Animals of both sexes (weight range, 200–300 g) were collected from October to May from local anglers of the Ligurian coast of Italy. All our research conformed to the ethical principles of the three Rs (replacement, reduction and refinement) and of minimizing animal suffering, following the Directive 2010/63/EU (Italian D. Lgs. n. 26/2014) and the guidelines from Fiorito *et al* (Graziano Fiorito et al., 2014, 2015). All experimental procedures were approved by the Institutional Board and by the Italian Ministry of Health (authorizations n. 465/2017-PR).

After the capture, animals were placed in 80x50x45 cm aquarium tanks filled with artificial sea water (SW, Tropic Marine) and enriched with sand substrate and clay pot dens. The temperature was maintained constant at 17°C, corresponding to the average temperature at the collection site, and continuously circulated through a biological filters system. Oxygenation was ensured by a dedicated aeration system and all relevant water chemo/physical parameters were checked daily. Animals were left to adapt for at least 5 days before experiments. They were inspected daily and fed three times a week with shrimps.

Before experiments, animals were anaesthetized in 3.5% $MgCl_2$ SW. A short segment was then cut from the medial portion of one arm (either L2, L3 or R2) and kept in oxygenated SW at 4°C for further procedures.

3.2 Histology

Neuronal tract tracing

Neuronal tract tracing of motor neurons innervating the arm muscles, was performed with both *in vivo* and *in vitro* methodologies to identify the best-suited strategy and we injected alternatively T or L muscles to label retrogradely innervating motor neurons.

For the *in vivo* methodologies, we performed a series of microinjection with dextran fluorescent conjugate diluted in ipotonic solution (5% in MilliQ) (dextran, Alexa Fluor®568; 10,000MW, anionic, fixable, Termofisher scientific). Each injection was performed on a different animal. A total number of 13 animals were employed.

To perform the injections, animals were anaesthetized with 3.5% $MgCl_2$ and a medial-distal portion of one arm was cut to expose the area to inject. A small volume of Dextran was manually injected with a Hamilton syringe in the arm muscles (T or L). The animal was then returned to its home tank and allowed to recover from anaesthesia.

Based on literature (Fritzsch, 1993; Lanciego & Wouterlood, 2020; Vercelli et al., 2000) we tested five different incubation time: 4 h, 24 h, 72 h, 7 days and 10 days. Each incubation time was tested on two different animals with two different volumes of injection: 1 µl and 0.5 µl. Three additional microinjections were performed with 4h incubation with a volume injection of 0.2 µl.

After the incubation time, animals were euthanized with terminal anaesthesia and the arm samples at the injection sites were collected. Arm samples were fixed overnight (O/N) in 4% Paraformaldehyde (PFA) in artificial sea water (ASW: NaCl 460 mM, KCl 10 mM, $MgCl_2$ 55 mM, $CaCl_2$ 11 mM, Hepes 10 mM, glucose 10 mM; pH 7.6), cryopreserved O/N in 30% sucrose, embedded in O.C.T. compound (Electron Microscopy Sciences) and sectioned in 40 µm transverse slices with a cryostat microtome (MC5050 Cryostat Microtome). Slices were then further treated for immunofluorescence to stain nuclei (Hoechst, 1:1000) and neuronal cells (anti-acetylated tubulin monoclonal antibody, 1:500, Sigma-Aldrich). Images were acquired either with a confocal microscope (Leica SP8) or with an epifluorescence microscope (nikon Eclipse N*i*) and analysed offline with ImageJ software to identify and analyse dextran positive (dxt^+) cells.

For the *in vitro* methodologies, we performed a series of DiI (1,1'-Dioctadecyl-3,3,3',3'-Tetramethylindocarbocyanine Perchlorate, TermoFisher Scientific D3911) microinjections on fixed samples.

Samples were collected as described in chapter 2.1, fixed O/N in PFA 4% in ASW, thoroughly washed in PBS (3 washes, 15 minutes each) and injected manually with small volumes of DiI (suspended in DMSO 1 µg/µl) into T or L muscles using a Hamilton syringe. After the injection, samples were kept in PBS at 4 °C to allow for the dye to diffuse.

Different incubation times and volumes of injection selected on the basis of the literature (Vercelli et al., 2000) were tested on samples from two different animals. Three samples were injected with 0.5 µl and incubated for 2 weeks, three samples were injected with 0.5 µl and incubated for 4 weeks and two samples were injected with 0.2 µl and incubated for 8 weeks.

After incubation, samples were sectioned with a vibratome (Leica VT1000) in 200 µm transverse slices. Slices were then counterstained with Hoechst (1:1000 in PBS, 2 h incubation at RT), mounted on microscope slides and visualized with a confocal microscope (Leica SP8).

Immunohistochemistry

Immunohistochemistry was employed to stain ANC ganglia neurons on 40 µm arm transverse sections.

Sections were rinsed with phosphate buffered saline solution with 0.1% triton (PBS-T) two times for five minutes to eliminate the residual O.C.T. compound and then permeabilized for 30 minutes with the same solution. After permeabilization, sections were incubated for 1 hour in blocking solution (PBS-T + 1% BSA + 10% goat serum) at RT and then O/N with primary antibody in blocking solution at 4°C. Secondary antibody was applied in blocking solution during two-hour incubation at RT.

Ex-vivo morphometric measurements

Twenty-one whole arm samples (5-10 mm length) from four different animals were hand-cut with a scalpel from the middle portion of eleven arms. Skin and suckers were rapidly removed and L or T aboral proximo-distal (P-D), latero-lateral (L-L), oral-aboral (O-A) dimensions were measured with a caliber under a dissection microscope in the whole arm configuration (Fig. 20). Each measurement was taken three times from two independent experimenters to account for individual variability. In details, L muscle P-D was measured as the end to end distance of the whole arm segment, O-A as the maximum height of L aboral muscle (from derma on the aboral side to the upper edge of transverse aboral muscles), and L-L as the side to side maximum width of L aboral muscles (see black solid arrows in Fig. 20). In T muscles, P-D was considered as the end to end distance of the whole arm segment, O-A as the minimum height of T aboral muscles (from the ANC on the oral side to the lower edge of L aboral muscles) and L-L as the side to side width of T aboral muscles (see red dashed arrows in Fig. 20).

Next, the entire L or T aboral muscle strips were dissected from the whole arm segment.

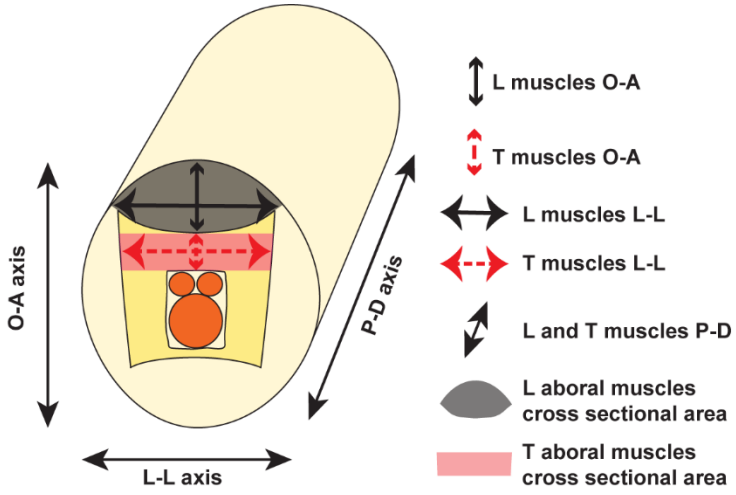

Figure 20. *In the whole arm configuration, the length along the P-D axis was obtained measuring the length of the whole segment cut out from the arm. Red, dashed arrows in figure indicate how was measured the length of T muscles along O-A and L-L axes. Black solid arrows indicate how was measured the length of L muscles along O-A and L-L axes. Grey and red shadings indicate, respectively, the cross sectional area of L and T muscle dissected from the arm to measure the change in their dimension once all the other tissues were removed*

The dimensions of dissected L and T muscle strips were then measured with a caliber under a dissection microscope.

The length of the dissected muscle was considered as muscle resting length (L_R) and used as a reference to calculate T and L muscles length in whole arm configuration (L_{in}) as a % of L_R.

3.3 Muscle biomechanics

General procedure

For biomechanical procedures, small strips of muscles (length: ~3-6 mm, width: ~1-3 mm, height: ~0.5-1.5 mm) were dissected by hands from the aboral portion of longitudinal or transverse arm muscles (Fig. 21).

For simplicity we will hereafter refer to them as T (transverse) and L (longitudinal) muscles. To dissect L muscles, first, epidermis and dermal connective tissue were removed together with circumferential and oblique muscle layers. Then, a strip of L muscles was cut out from the arm following a proximo-distal axis. We thus obtained a bundle of L muscles containing thin sheets of transverse fibers perpendicular to the main muscle force vector (the so-called trabeculae, ((Kier, 2016b; Young, 1971)). To dissect T muscles, a thin transverse arm slice was cut and a rectangular strip of solely T muscles was removed from its central portion following a latero-lateral axis. It should be noted that, given the intrinsic organization of the transverse muscle fibers, the T muscle bundle we obtained is composed by fibers oriented in multiple planes including planes perpendicular to the main muscle force vector.

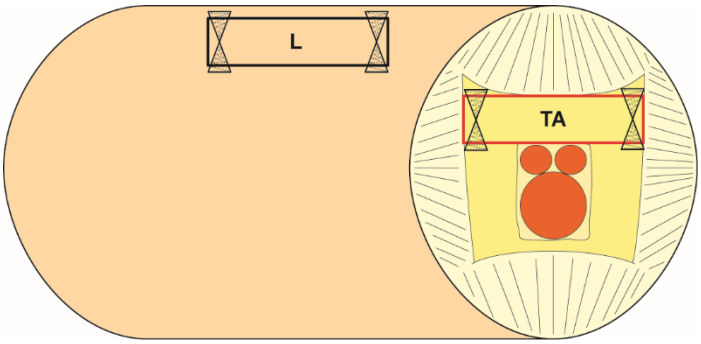

***Figure 21. Schematic of the arm muscle dissection methodology employed for biomechanics and histology**. Transverse aboral (TA, red box), longitudinal muscle (L, black box) and the position of the knots used to tighten the muscle strips to the dual model lever arm system are represented.*

After the dissection, muscle strips were immediately mounted in the recording chamber of a Dual Mode Lever Arm System (ASI 300C-LR, Aurora Scientific Instruments). Samples were attached to a micrometer block on one end and to a lever arm on the other using suture threads (silk suture threads 5/0, Ethicon Inc, code: K880H) tighten with double square knots. Muscle strip resting length (L_R) was adjusted by slowly increasing it until a small transient passive force was apparent and it was measured with an electronic calliper as the distance between the knots. The recording chamber was continuously perfused with oxygenated ASW at 16°C using a peristaltic pump (SJ-1220, Atto Co.). Particular attention was paid to avoid perfusion flux to induce noise in the force recordings. Recordings were digitized and analysed using a LabVIEW based data acquisition and analysis system (ASI 604A and 605A, Aurora Scientific Instruments). Data were acquired at 10 kHz sampling frequency and filtered with a lowpass filter at 3.3 kHz. Stimulus strength-twitch response was determined for each muscle strip (10 ms stimuli, 60 s interval between successive stimulations). It is worth noticing that, similarly to what observed by Thompson and collaborators, supramaximal stimulation consistently caused a decrease in the force response and therefore, at the end of the test, we adjusted the stimulus strength at the level employed to reach the maximum force (Thompson et al., 2014). In our experiments, this corresponded most of the time to a value ~900 mAmp (Fig. 22). Preparation not reaching the maximal stimulation were discarded.

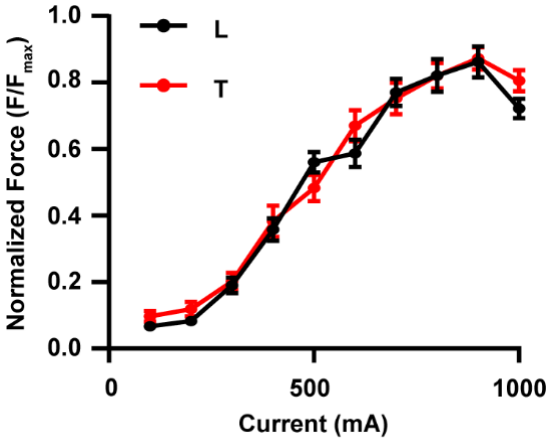

***Figure 22. Stimulus Current-twitch response relationship**. Force is expressed relative to the maximum twitch force produced by the preparation. Data are presented as mean ± SEM N = 16 for both experimental groups*

Muscle L_0, defined as the length at which the muscles strip exerts its maximal isometric force (F_0), was then found for each sample using brief tetanic stimulations (50 Hz, 100 ms, 10 ms pulse width). Occasional control isometric stimulations where delivered during each experimental session to monitor the force decline. The experiment was terminated and the data discarded if the force decreased more than 10%.

At the end of the experiment the height (*h*) and width (*w*) of T and L muscle strips were measured at rest with an electronic calliper under a dissection microscope.

Cross-Sectional area calculation

In order to identify the best strategy to calculate the cross-sectional area (CSA) of our samples, we compared three different methods on 8 different T and L muscle strips.

The first one was to calculate the fresh sample wet volume, and measure its length using an electronic calliper under a dissection microscope. The fresh sample wet volume was calculated by placing the sample in a volumetric cylinder previously filled with ASW and measuring the volume displacement (Archimedes' principle). The average CSA was then calculated following the simple relation $CSA = v/l$. The second method was to measure the fresh samples height (h), width (w), length (l) and radius (r) under a dissection microscope with an electronic calliper. CSA was then calculated assuming the muscle strips to hold either a parallelepiped ($CSA = h \cdot w$) or a cylindrical ($CSA = \pi r^2$).

The third method was performed on fixed samples. Muscle strips were fixed O/N in 4% PFA in ASW, cryopreserved O/N in 30% sucrose, embedded in O.C.T. compound (Electron Microscopy Sciences) and sectioned to obtain 80 µm transverse slices with a cryostat microtome (MC5050 Cryostat Microtome). Micrographs of the transverse slice were acquired with a microscope (Nikon Eclipse N*i*) and their area was measured using ImageJ software. The CSA of each sample was calculated as the average area from ten transverse slices.

Each method was tested on 8 samples and no significant differences were observed among the different methodologies (Fig. 23, RM one-way ANOVA, $P > 0.05$). However, measurements from the micrographs (MICRO) showed a tendency to underestimate CSA of both T and L when compared with V/l measures. Cylinder assumption (CYL) calculations of L CSA had the largest variability, while worked pretty well for T muscles, and parallel assumption (PAR) worked well with both muscles.

CSA calculated from V/l may give the most realistic values as it returns the CSA average based on the fresh sample length and volume and therefore it is not influenced by the

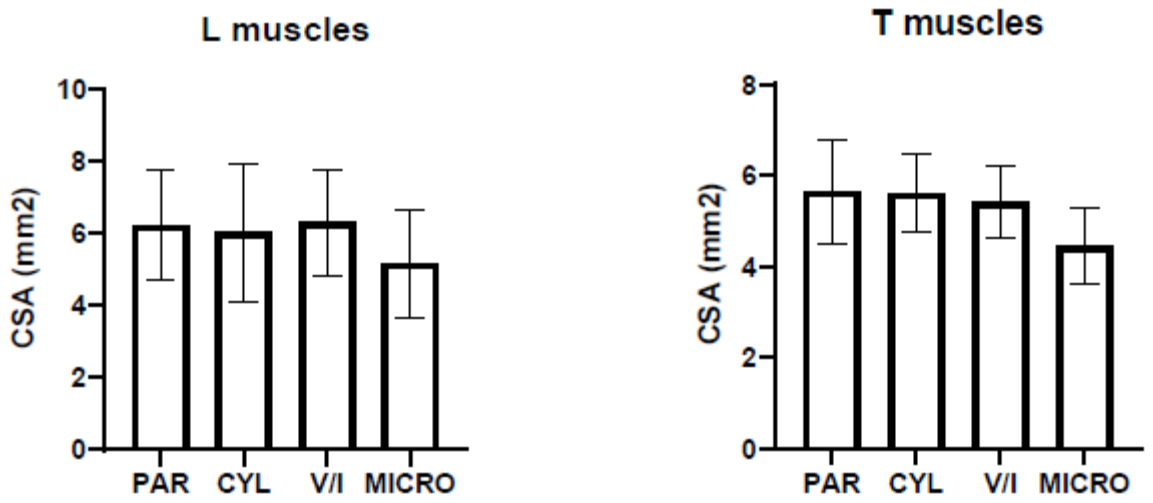

Figure 23. Calculation of muscle strips' CSA. *Comparison of four different methodologies employed to estimate sample CSA (see text for details). No significant differences were observed between the different methods of measurements (RM one way ANOVA, P > 0.05, N = 4 for each experimental group). PAR = calculation based on parallelepiped shape assumption, CYL = calculation based on cylindrical shape assumption, V/I = CSA calculated dividing samples' volume for its length, MICRO = measurements from micrographs.*

tissue irregularity. However, this methodology involve a certain amount of sample handling and therefore it is not suitable for further biomechanical investigations.

We thus calculated the CSA of the experimental samples assuming a parallelepiped shape.

It is worth noticing that, as mentioned above in this chapter, both T and L preparation incorporate fibers orthogonal to the muscle main force vector. Moreover, especially in T muscles, the rather chaotic arrangement of the fibers poses serious problems to the quantification of these orthogonal fibers. Consequently, the values of CSA presented in this manuscript cannot be directly correlated with the number of fibers participating to the force generation.

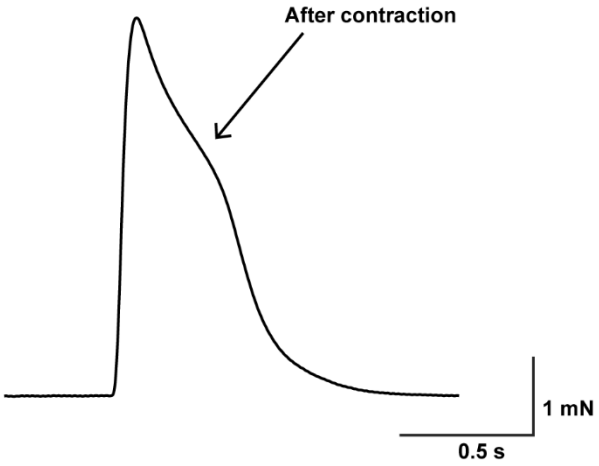

***Figure 24. Representative force-time trace for isometric twitch contraction**. After-contraction during the relaxation phase is indicated by the arrow.*

Isometric Twitch dynamics

To characterize T and L twitch contraction dynamics, 10 muscle strips from 4 different animals were employed. Muscle strips were stimulated with a single squared current pulse (10 ms) with the length fixed at L_0. The force-time traces were analyzed offline with MATLAB to obtain the time to peak tension and the half relaxation time of each sample. Interestingly, in some samples we observed the occurrence of an after-contraction early during the muscle relaxation phase (see Fig. 24 for an exemplary trace). This phenomenon can significantly alter the relaxation kinetics parameters here considered and therefore these traces were excluded from this analysis.

Force frequency

The force-frequency relationship was investigated in isometric condition keeping muscle length fixed at its L_0. Ten muscle strips from 4 different animals, were tested with 1 s train stimulation (from 1 to 50 Hz , 10 ms pulse duration, 300 s intervals between successive stimulations) as in most of the cases shorter duration did not allowed samples to reach the max plateau force. The peak force generated at each tested frequency of stimulation was measured offline with MATLAB and used to establish the force-frequency curve. To allow comparison between different samples data were normalized for the maximal isometric tension developed by each muscle strip.

Force velocity

Force-velocity relationship was investigated by means of an isotonic protocol on 10 muscle strips from three different animals. The F_0 of each sample was first determined in isometric condition with brief tetanic stimulations (50 Hz, 100 ms, 10 ms pulse width) with the length fixed at L_0. The lever arm was then switched to force-clamp mode with imposed

loads ranging from 10% to 90% of the sample F_0. A brief tetanic stimulation (same as above) was delivered at each load with 30 s intervals between different trials. The resulting isotonic shortening (see exemplary traces in Fig. 25) was analyzed offline with a custom made MATLAB algorithm to obtain shortening velocity and normalized for the sample L_0.

Force velocity curves were fitted using Hill's equation in the form expressed in Eqn 1:

$$V = V_{max} \cdot F_{max} \frac{F_{max} - F}{G \cdot F + 1} \qquad (1)$$

Where V is the velocity of shortening (L_0/s), F is the force during shortening normalized for the max isometric force, V_{max} is the intercept on the velocity axis, F_{max} is the intercept

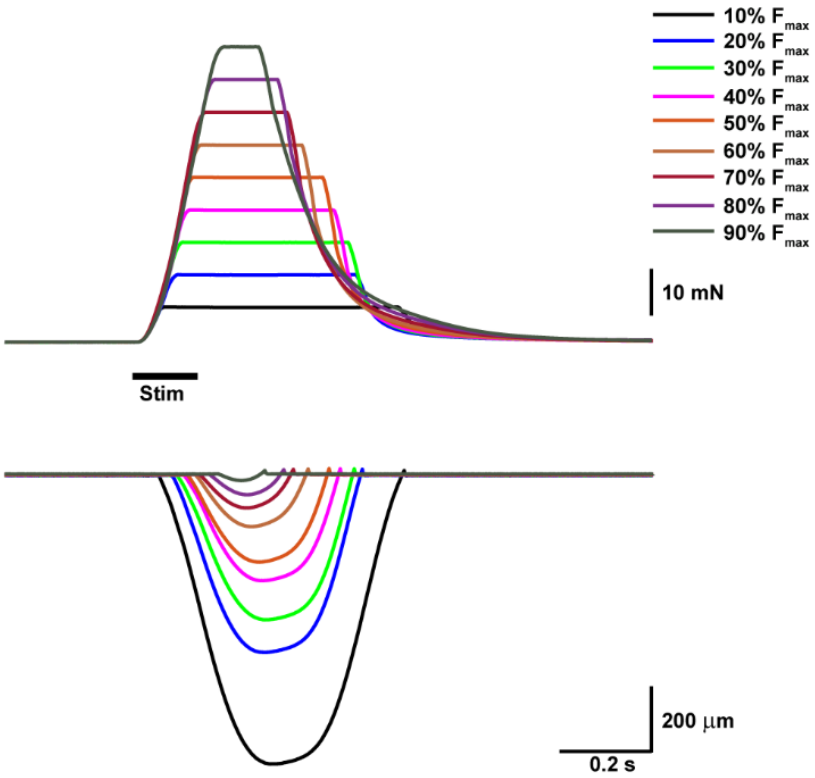

Figure 25. Force-velocity protocol and representative traces. *Upper panel: force-time representative traces. Train stimulation is showed by the black bar below the traces.Lower panel: position-time traces*

on the force axis and G is a constant expressing curvature. The fitting was performed using the ordinary least squares method and constrained to have F_{max} = 1.

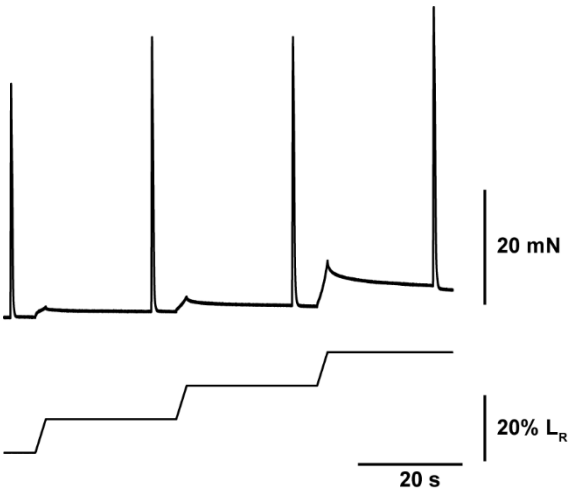

Figure 26. Force-time trace (upper trace) and corresponding position-time trace (lower trace) with length ramp protocols at increasing amplitudes (expressed as percentage of L_R).

Force length

10 muscle strips from 4 different animals were employed for this experiment. Force-length relationship was investigated using brief tetanic stimulations (50 Hz, 100 ms, 10 ms pulse duration) under static strain condition. Sequential mechanical strain ranging from 1% to 70% of muscle L_R were tested. Muscle strips were lengthened to the desired length using a 2 s long ramp. They were allowed to rest for 20 s and then stimulated (Fig. 26). The resulting force-time traces were analyzed offline using a custom made MATLAB algorithm to obtain passive and active components of the force generated by the muscle. Length data were normalized to the optimal length of the muscle (L_0), and both, passive and active components were normalized to the sample F_0.

Stress-strain relationship

Stress-strain relationship was tested using a step-stretch, stress-strain protocol. Mechanical strain (ε) ranging from 1% to 60% of L_R was sequentially applied to the dissected muscle strips with 5% incremental steps (Fig. 27). Each strain step was maintained for 10 s and the resulting force-time trace was recorded and analysed offline with a custom made MATLAB algorithm.

Soft tissue response to mechanical strain is often characterized by an early peak force followed by an exponential decline and a late steady state force (Fig. 27A). According to the Hill model, passive forces in skeletal muscles can be described by the interplay between two elastic components: one organized in series (SE) to the contractile element (CE) and the other organized in parallel (PE) (Fig. 27B). Following this model, SE characterizes the early peak force (F_{SE}, Fig. 27A) while the PE characterizes the steady-state force, reached upon stabilization (F_{PE}, Fig. 27A). We calculated F_{PE} by averaging 0.5 s of the steady state force at the end of each length step. F_{SE} was measured as the difference between the early peak force of each step and the F_{PE} of the step before (Fig. 27A). We next calculated the corresponding stress (σ) as a way to correct for differences in preparation size. Stress was calculated dividing F_{SE} and F_{PE} forces for the CSA of the muscle strip (Eqn 2 and 3).

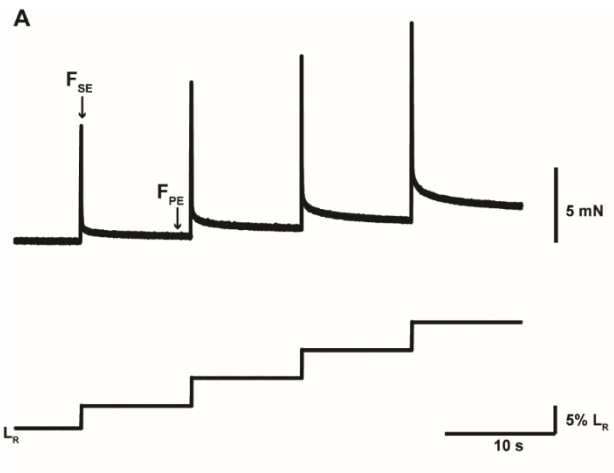

Figure 27. Elastic and contractile elements of muscle forces. (A) *Representative trace of the step-stretch protocol. Series elastic force (F_{SE}) and the parallel elastic force (F_{PE}) are indicated.* ***(B)*** *Hill model/diagram showing contractile element (CE), parallel elastic element (PE) and series elastic element (SE).*

$$\sigma_{SE} = \frac{F_{SE}}{CSA} \quad (2)$$

$$\sigma_{PE} = \frac{F_{PE}}{CSA} \quad (3)$$

Eventually, we used the obtained stress-strain relationship to calculate Young's Modulus for SE (E_{SE}) and PE (E_{PE}) components (Eqn 4 and 5) at low (0-15%), medium-low (15-30%), medium-high (30-45%) and high (45-60%) levels of strain for each preparation

$$E_{SE} = \frac{\Delta\sigma_{SE}}{\Delta\varepsilon} \quad (4)$$

$$E_{PE} = \frac{\Delta\sigma_{PE}}{\Delta\varepsilon} \quad (5)$$

3.4 Proteomics

Six small arm samples were collected from 6 different animals (one for each animal). From each arm sample, one small strip of T or L muscles were dissected, following the procedures described in chapter 1.3.1, and immediately frozen in dry ice. A total of N = 3 samples for each muscle type were analyzed.

Tissue samples (30-60 mg) were kept at -80 °C prior to use. For protein extraction, frozen samples were triturated using a tissue mortar, re-suspended in 1.5 ml of RIPA buffer supplemented with phosphatase and protease inhibitor cocktails (phosphatase inhibitor cocktails 2 and 3, Sigma-Aldrich P5726 and P0044, respectively, and protease inhibitor cocktail, Sigma-Aldrich P2714) and moved to 4 °C. Tissues were further homogenized with Tissue Lyser, sonicated and then centrifuged for 15 minutes at 4 °C to remove cell debris. The supernatant was collected and used for protein content determination *via* BCA assay.

Further proteomic analysis was outsourced to the proteomic core facility of the Gaslini hospital in Genoa (group of dott. Andrea Petretto). 50 ug of sample lysed in RIPA buffer were reduced and alkylated in 10 mM TCEP and 40 mM CAA. Then proteins were isolated by PAC method (Batth et al., 2019) with minor modifications. Briefly, proteins aggregation

was induced by addition of 70% ACN and 200 ug of magnetic beads were added to capture aggregated proteins. Magnetic beads were retained by magnet and the supernatant was removed. Beads were washed one time with acetonitrile, followed by one wash with 70% ethanol and one wash with isopropanol. Washed beads were resuspended in 100 µl TRIS 25 mM pH 8 and captured proteins were digested O.N. at 37°C with 0.7 µg Trypsin and 0.3 µg LysC. Obtained peptides were analyzed by nano-UHPLC-MS/MS using an Ultimate3000 RSLC with a 200 cm uPAC C18 column (PharmaFluidics) mounted in the thermostated column compartment maintained at 50°C. At first was applied a concentration gradient from 5% to 10% buffer B (80% ACN and 20% H2O, 5% DMSO, 0.1% FA) coupled with a flow gradient from 750 nl/min to 350 nl/min for 15 min. Then peptides were eluted with a 178 min non-linear gradient from 10% to 55% of buffer B at a constant flow rate of 350 nl/min. Eluting peptides were analyzed using an Orbitrap Fusion Tribrid mass spectrometer (Thermo Scientific Instruments) in data dependent acquisition mode.

MaxQuant software (Cox & Mann, 2008), version 1.6.17.0, was used to process the raw data. The false discovery rate (FDR) for the identification of proteins, peptides and PSM (peptide-spectrum match) was set to 0.01. A minimum length of 6 amino acids was required for peptide identification. Andromeda engine, incorporated into MaxQuant software, was used to search MS/MS spectra against Uniprot octopus database. In the processing the variable modifications were Acetyl (Protein N-Term), Oxidation (M) and Deamidation (NQ). Carbamidomethyl (C) was selected as fixed modification. Algorithm MaxLFQ was chosen for the protein quantification with the activated option ‘match between runs’ to reduce the number of the missing proteins. The intensity values were extracted and statistically evaluated using the ProteinGroup Table from MaxQuant, the global.modsummary table from FragPipe and Perseus software (Tyanova et al., 2016) version 1.6.15.0. GO enrichment analysis was performed with the app ClueGO of Cytoscape software (Paul Shannon et al., 1971).

3.5 Statistical analysis

Statistical analysis was carried out using Prism 9 software (Graphpad Software Inc.), unless otherwise indicated. Datasets normality was assessed with Shapiro-Wilk normality test. Two-tailed Student's *t* test or Mann-Whitney test were used to compare two experimental groups with, respectively, parametric and non-parametric distributions. Comparisons among three or more groups were performed with ordinary one-way ANOVA and Kruskal-Wallis test for parametric and non-parametric datasets, respectively. In both cases, the analysis of variance was followed by Tukey's post-hoc test.

Repeated measures (RM) two-way ANOVA followed by Tukey's post-hoc test was used to compare force-frequency and force-velocity curves, stress-strain relationships and Young's Modulus.

4 Results

4.1 Arm's motor control network organization

In vivo dextran injections

First, we performed pilot experiments to determine the best incubation time and volume of injection. We tested five different incubation times: 4 h, 24 h, 72 h, 7 days and 10 days, with volumes of injection of 1 µl and 0.5 µl (dextran 5% in milliQ water).

Only 4 h incubation gave consistent results. After 4 h of incubation, dextran (dxt) injections into T and L muscles resulted in the selective staining of specific neuronal cells (dextran positive, dxt^+ cells) mostly localized in the dorsal part of the ganglion, close to the dorsal nerve roots (Fig. 28A), which is supposed to host the fibers innervating T and L muscles (Young, 1971; Zullo et al., 2019b). However, sign of lateral diffusion of the dye in neighboring tissues were present with all the volume tested.

We next performed another series of injections with 4 h incubation, reducing the volume of injection to 0.2 µl to reduce lateral diffusion. We performed three different injections: one in the L-aboral muscles (dorsal to the ANC ganglion), one in T-aboral muscles (dorsal and slightly lateral to the ANC ganglion) and one on L-lateral muscles (lateral to the ANC ganglion). Again, these injection resulted in clear staining of few, very large cells in the dorsal part of the ganglion.

To understand if dxt^+ cells belong to a morphologically distinct subpopulation, we measured their soma size comparing it with the average soma size of ganglion neurons measured on $AcTub^+$ cells (Fig. 28B). The $AcTub^+$ cells soma size showed the expected distribution (median = 79.64 μm^2, interquartile range = 52.25-161.5 μm^2) with a large number of small cells localized throughout the ganglion and few very large cells in the dorsal part. Dxt^+ cells soma size were on average very large (median = 513.7 μm^2, interquartile range = 243.2- 1025 μm^2, Fig. 28C and D, Mann-Whitney test, ***P<0.001) and comparable with the large $AcTub^+$ cells and localized in the dorsal ganglion area.

Hence, in our samples, dxt+ cells belong to a distinct neuronal subpopulation spatially and morphologically segregated from other ganglion cells and most likely corresponding to motor neurons population.

We also found an interesting topographic organization of the motor neurons within the arm ganglion. We performed three different dxt injections in three different samples. When the injection site was on lateral muscles, dxt^{+} cells were localized mostly on the

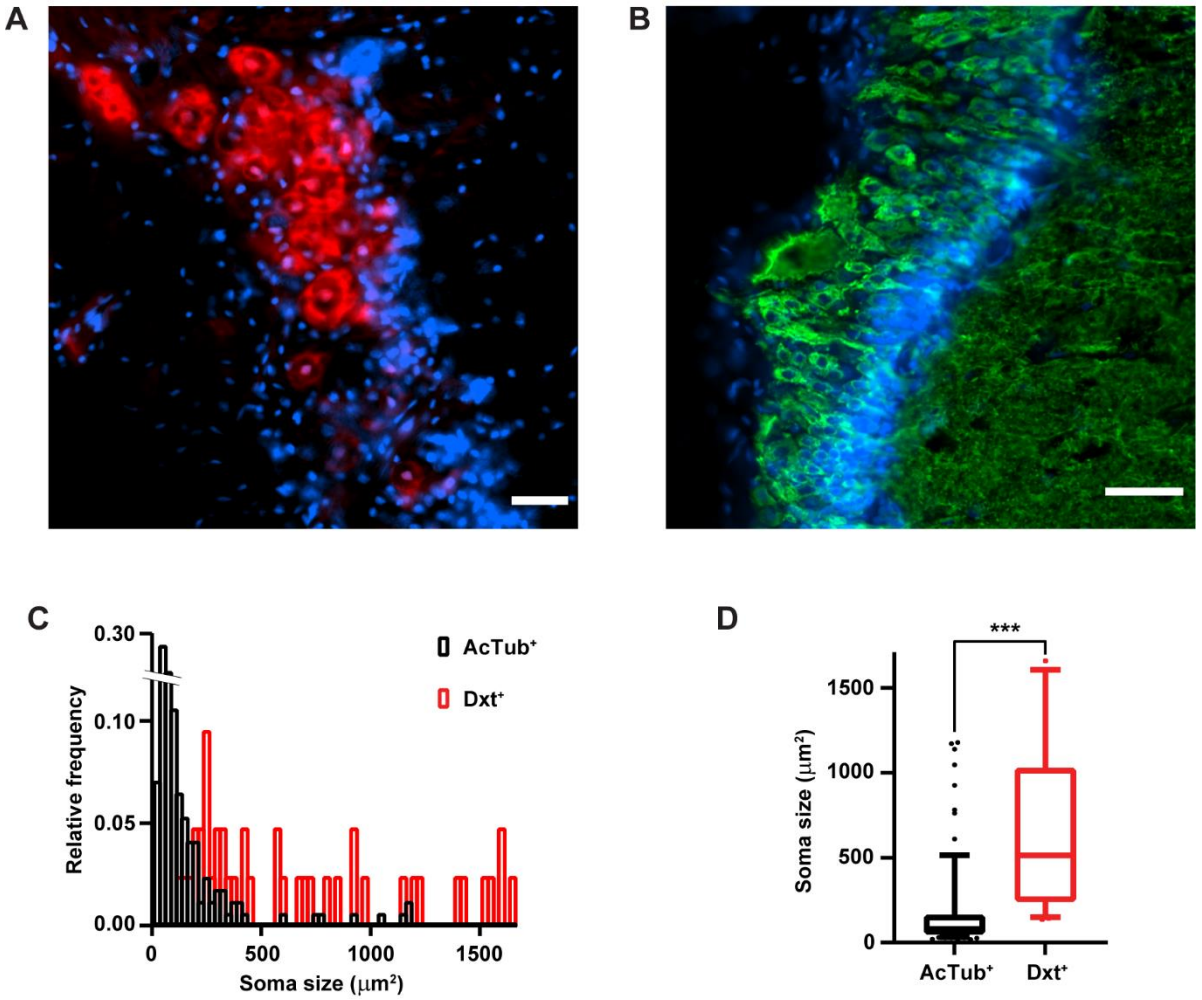

Figure 28. (A) *Representative image of dxt+ cells (red) in the dorsal part of the ganglion. Nuclei are stained with Hoechst (blue). Scale bar: 50 µm.* ***(B)*** *Representative image of ANC ganglion neurons stained with anti-acetylated tubulin antibody (green) and Hoechst (blue). Scale bar: 50 µm* ***(C)*** *Soma size distribution for AcTub+ and dxt+ cells* ***(D)*** *Soma size comparison between AcTub+ and dxt+ cells. Bar and box show median and interquartile range, respectively. Whiskers show 5-95 % range. Dxt+ cells represent a small popupation of very large ganglionic cells compared to the total population (Mann-Whitney test, ***P<0.001, n = 217 from 6 samples (3 different animals)).*

ipsilateral side of the ganglion. Conversely, when the injection was in the aboral muscles, dorsal to the ganglion, dxt^+ cells were found on both sides of the ganglion. When the injection was in the aboral muscle but slightly lateral to the ganglion, eventually, dxt+ cells were found on both sides of the ganglion with a little prevalence on the ipsilateral side (table 1 and Fig 29). However, further experiments are needed to fully characterize the spatial organization of the motor neurons innervating T and L muscles in different regions of the arm.

Injection site	**Number of dextran positive cells**	
	Ipsilateral side	Contralateral side
Lateral	14	1
Latero-medial	25	11
Dorsal	7	5

Table 1. Number of dxt^+ cells found ipsi- and contralateral sides of the ganglion after injections in different region of the arm

Altogether, our data suggest that motor neurons segregate in the dorsal part of the ganglion, close to the dorsal nerve root, and possibly correspond to the previously identified large dorsal neurons (Young, 1971). Moreover, the connections between muscles and motor neurons seems to hold a topographic-like organization with motor neurons on one side of the ganglion innervating mostly the ipsilateral muscles and aboral muscles receiving fibers from both sides of the ganglion.

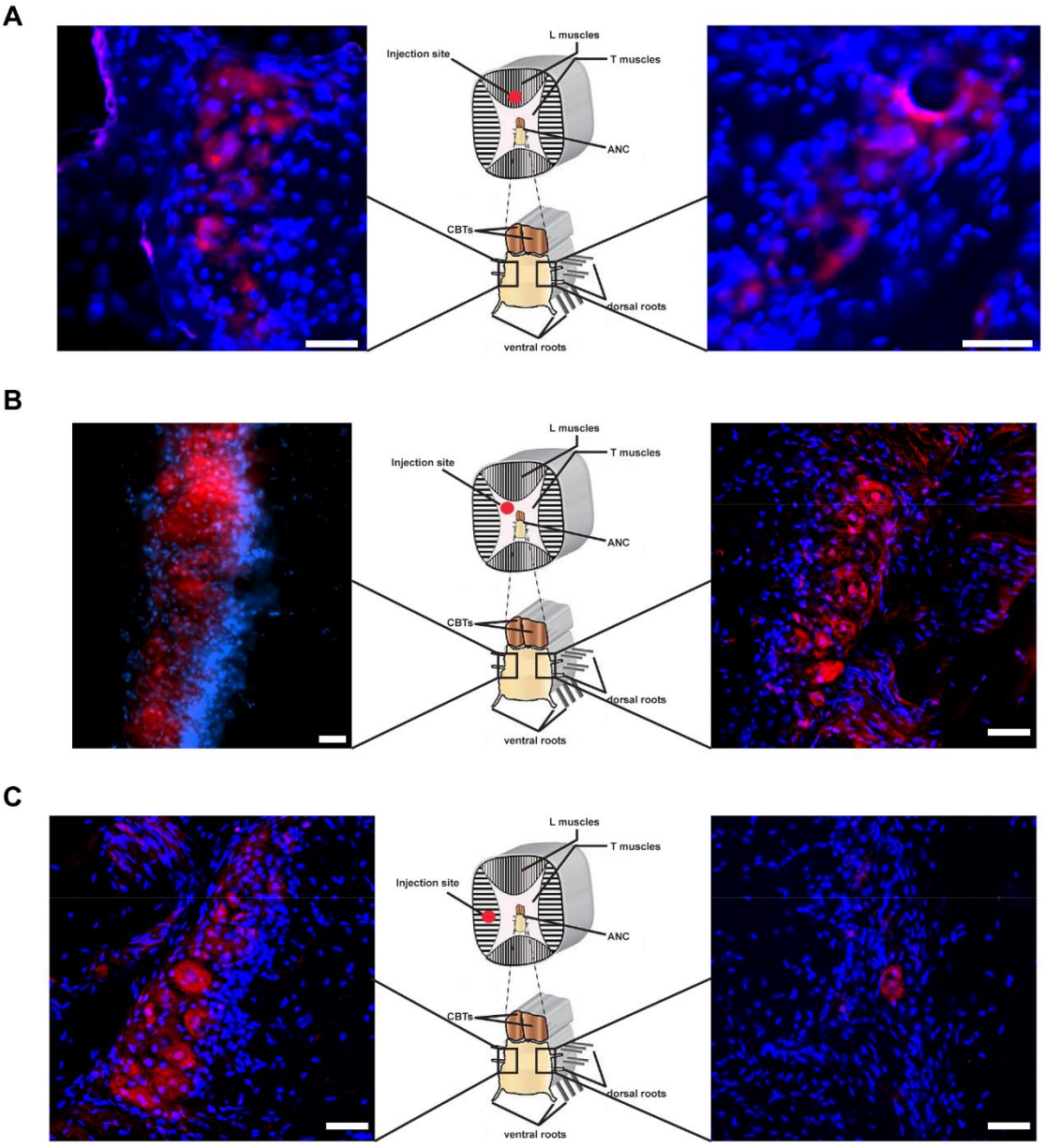

Figure 29. Distribution of motor neurons in the ganglion after injections in different regions of the arm. (A) *Dxt was injected in L-aboral muscles, dorsal to the ANC ganglion. Dxt+ cells were found on both sides of the ganglion. Scale bars: 50 µm.* ***(B)*** *Dxt was injected in T-aboral muscles, dorsal and slightly lateral to the ganglion. Dxt+ cells were found on both sides of the ganglion but in higher number on the ipsilateral side. Scale bars: 50 µm.* ***(C)*** *Dxt was injected on L-lateral muscles, lateral to the ganglion. Dxt+ cells were found almost exclusively on the ipsilateral side. Scale bars: 50 µm*

DiI injections on fixed samples

DiI is a lipophilic fluorescent dye that gets incorporated in the cell membrane and diffuses passively along it, staining the entire cell. It offers two major advantages. The first is that allows the identification of both the cell bodies and fibers. The second is that it works well in fixed samples thus simplifying the injection procedure and allowing to reach areas not accessible in the living animal. The major drawback concerns the time required for the staining. Passive diffusion is slower than axonal transport. Furthermore, velocity of diffusion of the dye in fixed samples is few orders of magnitude lower than in fresh samples. This results in longer incubation times compared to other dyes like, for example, the dextran (see table 2 for a direct comparison of the two methods).

We tested three different incubation times: 2 weeks, 4 weeks and 8 weeks, injecting either 0.5 µl or 0.2 µl of DiI.

While the 2 weeks injections showed little diffusion of the dye along the fibers (Fig. 30A), in both, 4 weeks and 8 weeks injections, stained fibers departing from the injection site were clearly distinguishable with eight weeks injections resulting in a major number of clearly stained fibers (Fig. 30C to D). The nerve path of the injected cells was clearly stained until the exit of the nerve from the muscle bulk, then the diffusion stop abruptly without reaching the ganglion (Fig. 30E and F). This is possibly due not to a lack in diffusion of the dye but to a damage of the tiny process of the motor neurons leaving the muscles to reach the ANC (white arrows in Fig. 30C and D).

Although motor neuron cell body in the ganglia was not reached, we could map the end projection of the fibers. Similarly to what observed in dextran injection, when the injection was on lateral muscles, the projection area was ipsilateral to the injection site with few fibers that seemed to divert from the main path (Fig. 30B and C). If the injection site was located in dorsal muscles, fibers split to reach the ganglion from both sides (Fig. 30D).

Results of this set of experiments confirmed the topographic organization found with dextran staining.

	Dxt (*in vivo*)	DiI (*in vivo*)	DiI (fixed samples)
Incubation time	Short	Long	Very long
Injection procedure	Complex	Complex	Relatively easy
N° of animals required	High (one animal for each injection)	High (one animal for each injection)	Low (several samples can be collected from the same animal)
Extracellular diffusion in the tissue	High, but different dxt conjugates have different diffusion constants	Low	Very low
Retrograde labeling	Yes	Yes	Yes
Anterograde labeling	Yes	Yes	Yes
Cell compartment labeled	Only the soma (retrogradely) or the processes (anterogradely)	Cell membrane. Allows to visualize the entire cell but the staining is lost if membrane integrity is disrupted	Cell membrane. Allows to visualize the entire cell but the staining is lost if membrane integrity is disrupted

Table 2 Comparison between Dextran and DiI microinjections in fixed tissues and live animals

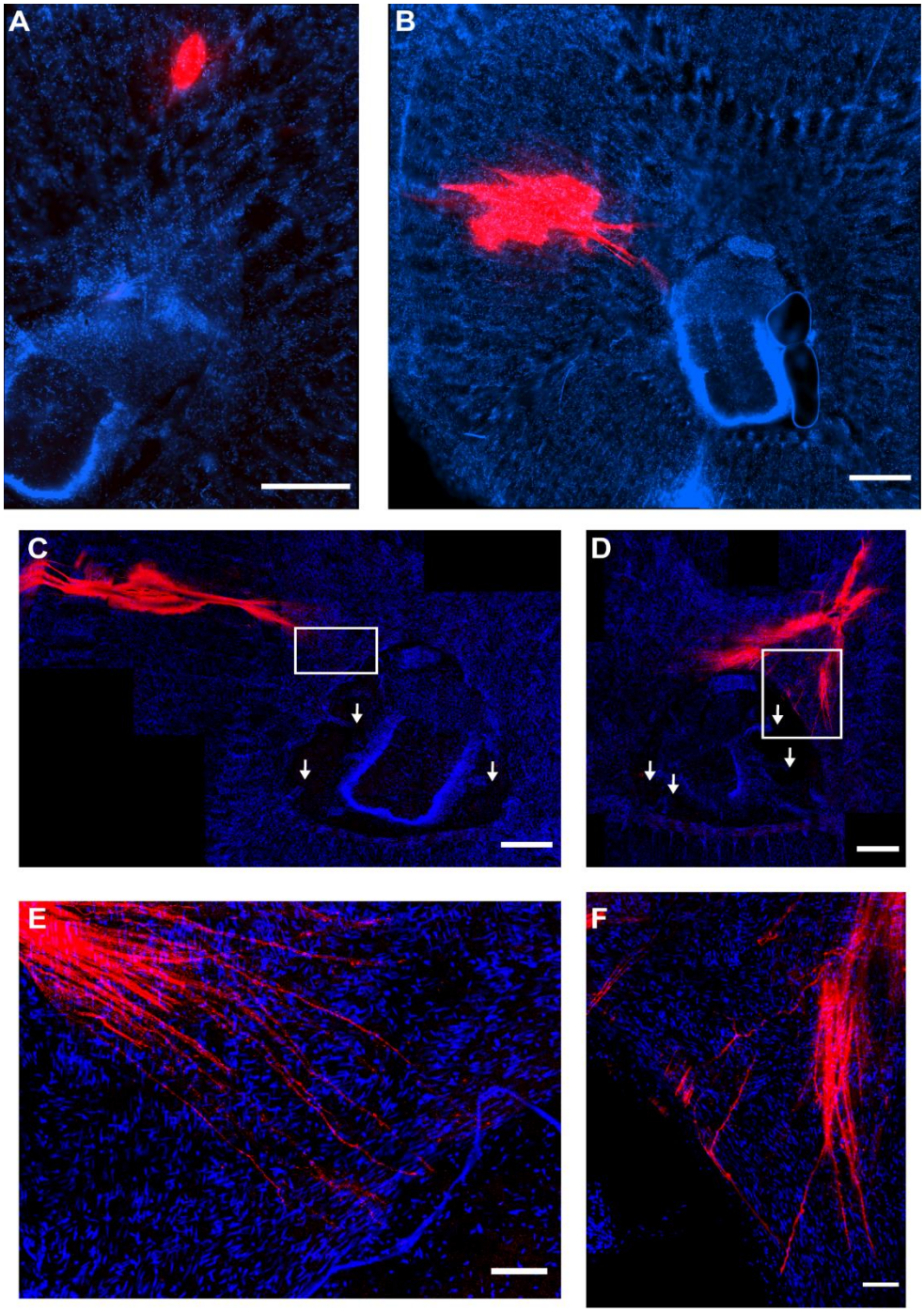

Figure 30. *Representative images from 2 weeks (A), 4 weeks (B) and 8 weeks (C and D) DiI Injections. Both 4 and 8 weeks gave good results in terms of fibers staining, but at 8 weeks the number of clearly stained fibers leaving the injection area was higher. However, in both cases fibers stopped at the level of the connective tissue surrounding the ANC cavity. Scale bars: 500 µm. Images (E) and (F) are enlargements of white rectangles in Fig. C and D, respectively. Scale bars: 100 µm. It is worth notice that the nerve roots seems to be damaged thus ending in the empty space between the musculature and the ANC (white arrows in C and D).*

4.2 Muscle contractile properties

Isometric twitch dynamics

To investigate twitch contraction dynamics of T and L muscles we analyzed muscles' responses to single pulses of stimulation in isometric condition with muscle strips' length fixed at their L_0. In particular, we compared time to peak tension and half relaxation time of T and L muscles.

Time to peak tension was significantly different between the two muscles. Average values were 59 ± 15 ms for L muscles and 107 ± 42 s for T muscles (Fig. 31A, unpaired t-test, *P<0.05). Half relaxation time was also significantly different with values of 54 ± 12 ms for L muscles and 165 ± 39 s for T muscles (Fig. 31B, Mann-Whitney test, *P<0.05).

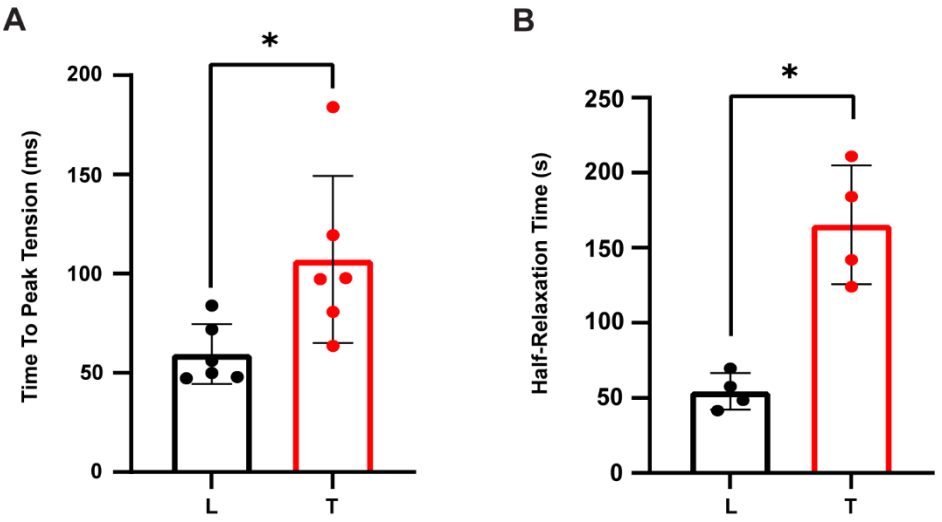

Figure 31. Twitch contraction dynamics. ***(A)*** *Time to peak tension (unpaired t-test, *P<0.05 n = 6 for both experimental groups).* ***(B)*** *Half-relaxation time (Mann-Whitney test, *P<0.05, n = 4 for both experimental groups)*

Force frequency

Here we characterized the force-frequency relationship of T and L muscles by stimulating isolated muscle strips in isometric conditions at their L_0. Representative traces for L and T are reported in figure 32A; both muscles reached the fusion frequency between 25 and 50 Hz. Force-frequency relationship of T and L was found to be significantly different (Fig. 32B, RM two way ANOVA, *P<0.05). In details, T muscles force rose more steeply between 1 and 10 Hz and resulted significantly different from L muscles at 10 Hz (RM two

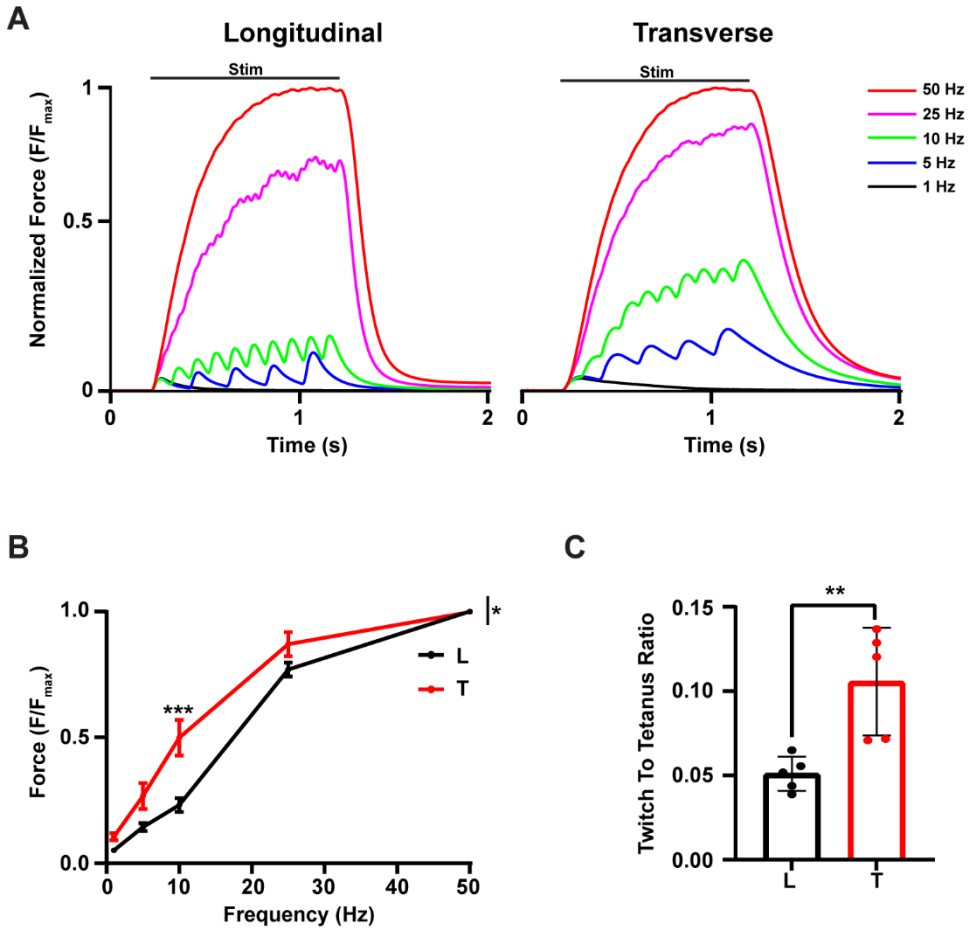

***Figure 32**. **Force-frequency relationship. (A)** Representative force-time traces from one L (left) and one T (right) samples normalized for their maximal isometric force. The different increase in relative force between the two muscles can be appreciated and is particularly evident at 10 Hz stimulation. Stimulus duration is indicated. **(B)** Average force-frequency curve of T and L muscles. Data are represented as mean ± SEM. T muscles were able to exert higher fractions of their maximal forces at lower frequency of stimulation (RM two way ANOVA, *P<0.05, n = 5 for both experimental groups). **(C)** Twitch to tetanus ratio was shown to be significantly higher in T muscles (unpaired t-test, **P<0.01, n = 5 for both experimental groups). Rectangular bar shows the mean values.*

way ANOVA with Sidak's post-hoc test, ***P<0.001). This might underlie a difference in the physiology of muscles occupying inner to outer portion of the arm diameter, with T manifesting slower characteristics. As expected, also the twitch to tetanus ratio was, significantly higher in T muscles (Fig. 32C, t-test, **P<0.01).

Maximal tetanic tension

The maximal tetanic tension generated by the two muscles was measured as the 50 Hz force peak from the force frequency protocol normalized for the sample CSA. The average value was significantly different between the two muscles (106.9 ± 22.69 $mNmm^{-2}$ for L muscles and 56.77 ± 23.22 $mNmm^{-2}$ for T muscles, unpaired *t*-test, **P < 0.01, N = 6 for each experimental group, Fig. 33). It is worth noticing that these values are likely to be an underestimation of the actual values. As mentioned above in this manuscript, our preparations incorporate fibers oriented perpendicularly to the main force vector that do not contribute to the measured tension. Hence, these force values have to be taken cautiously and different types of experiments are needed to have a more realistic estimation of the arm muscle fibers maximal forces.

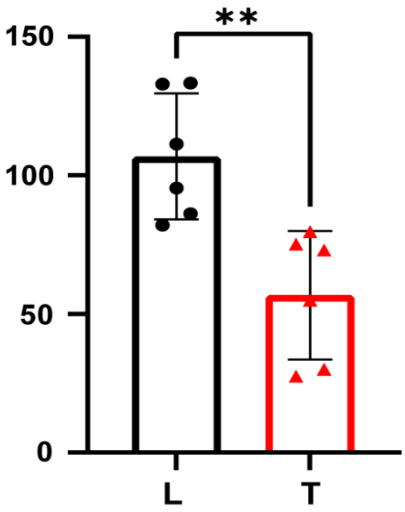

Figure 33. *The maximal tetanic tension was significantly higher in L muscles (unpaired t-test, **P < 0.01, N = 6 for each experimental group).*

Force velocity

Force-velocity relationship of T and L muscles were investigated under isotonic conditions imposing loads ranging from 10 to 90% of the maximal isometric force (F_0) of the sample (see methods).

Data were normalized for samples L_0, averaged, plotted and fitted with Hill's equation to extrapolate V_{max} (Fig. 34). The two curves proved to be significantly different with L muscles showing higher shortening velocities (Fig. 34, RM two-way ANOVA, **P<0.01).

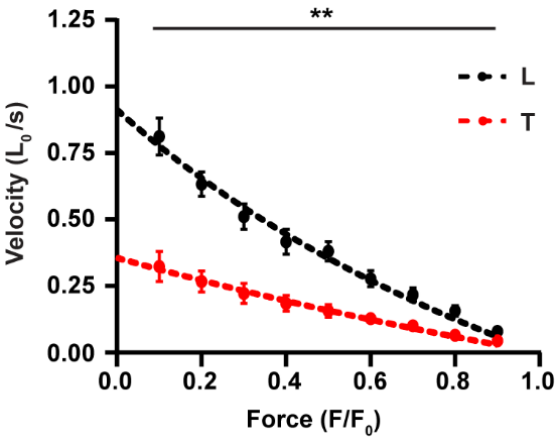

Figure 34. Force velocity relationship. (A) *. Force and velocity were normalized for F_0 and L_0 respectively. Data are represented as mean ± SEM. Dashed lines represent the Hill's fitting of the curves. L muscles showed significantly higher shortening velocities than T muscles (RM two-way ANOVA, **P<0.01).*

The extrapolated V_{max} was also significantly different in the two muscle types (Extra sum-of-square F test, ***P<0.001) with a best-fit values of 0.913 L_0s^{-1} for L muscles (95% confidence intervals: 0.804 to 1.043 L_0s^{-1}) and 0.3560 L_0s^{-1} for T muscles (95% confidence intervals: 0.2908 to 0.4414 L_0s^{-1}).

Overall, these data show that T muscles have lower contraction and shortening velocities; this, consistently with the isometric contraction dynamics and force-frequency relationship results, suggests that they behave as 'slow' muscles compared to L.

Myosin isoforms composition

Proteomic analysis revealed several myosin related genes (such as troponin, tropomyosin, paramyosin, etc.) including three myosin heavy chain genes (MHC) and eight myosin light chains related genes.

In details, one gene (LOC115219750) codes for seven unconventional myosin-Va isoforms, one gene (LOC115222368) codes for six non-muscle MHC isoform and one gene (LOC115225111) codes for a single striated muscle MHC (see table 3).

The myosin-related genes identified were: four myosin regulatory light chains, two myosin essential light chains, one myosin catalytic light chain and one myosin light chain kinase (see table 3).

We further analyzed the MHC protein A0A6P7TRC4 specifically expressed in muscles. For simplicity, we hereafter refer to it as muscle MHC. Octopus muscle MHC was aligned to the MHC isoforms of sepia (ISO A, ISO B1, ISO B2, ISO C, ISO D and ISO E) to look

	Gene name	Protein IDs	Protein names
1	LOC115219750	A0A7E6FCU8	unconventional myosin-Va isoform X1
2		A0A7E6FCV1	unconventional myosin-Va isoform X2
3		A0A7E6FCV6	unconventional myosin-Va isoform X3
4		A0A7E6FDE7	unconventional myosin-Va isoform X4
5		A0A7E6FDF1	unconventional myosin-Va isoform X5
6		A0A7E6FE23	unconventional myosin-Va isoform X6
7		A0A7E6FFB5	unconventional myosin-Va isoform X7
8	LOC115222368	A0A6P7TBL9	myosin heavy chain, non-muscle isoform X1
9		A0A6P7TBM5	myosin heavy chain, non-muscle isoform X2
10		A0A6P7TBP7	myosin heavy chain, non-muscle isoform X3
11		A0A6P7TBS7	myosin heavy chain, non-muscle isoform X4
12		A0A6P7TDQ3	myosin heavy chain, non-muscle isoform X5
13		A0A6P7TER7	myosin heavy chain, non-muscle isoform X6
14	LOC115225111	A0A6P7TRC4	myosin heavy chain, striated muscle
1	LOC115214760	A0A6P7SMW9	myosin regulatory light chain 12B isoform X1 isoform X2
		A0A7E6F3I7	myosin regulatory light polypeptide 9
2	LOC115219731	A0A6P7T4N8	myosin regulatory light chain LC-2, mantle muscle isoform X1
3	LOC115219731	A0A6P7T4W5	myosin regulatory light chain LC-2, mantle muscle isoform X2
4	LOC115230703	A0A6P7TWC2	myosin regulatory light chain 12A
5	LOC115219767	A0A6P7T6I9	myosin essential light chain, striated adductor muscle
6	LOC115216469	A0A6P7STT8	myosin-2 essential light chain isoform X1
		A0A6P7SU30	myosin-2 essential light chain isoform X2
7	LOC115219710	A0A6P7T5S9	myosin catalytic light chain LC-1, mantle muscle isoform X1 (myosin catalytic light chain LC-1, mantle muscle isoform X2)
8	LOC115229261	A0A6P7U3N5	myosin light chain kinase, smooth muscle isoform X6

Table 3. Octopus myosin genes identified through proteomic analysis, red fields indicate the genes significantly modulated between T and L muscles

for similarities. We found that octopus muscle MHC and sepia ISO A bare a 89.54% of identity.

The octopus isoform is 1875 aa long compared to 1937 aa of sepia ISO A. Interestingly the octopus MHC covers the entire aa sequence found collectively in the five sepia MHC isoforms.

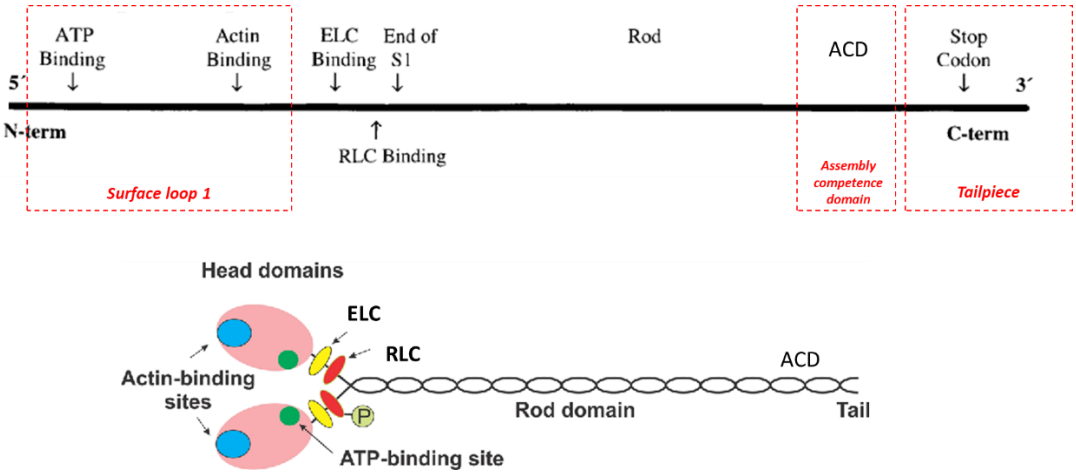

Figure 35 Schematic of the myosin protein structure*. The myosin heavy chan (MHC) is composed by a globular domain in the N-terminal and tail domain on the C-terminal. Two MHCs interact with each other through the tail domain and with two essential and two regulatory myosin light chains (ELC and RLC respectively) through the head domain. Actine binding sites, ATP binding sites, as well as ELC and RLC positions on the MHC are indicated.*

We further analyzed the sequences of three main MHC functional compartments: the motor domain 'Surface loop 1' at the N-term, the 'Assembly competence domain' (ACD) and the 'Tailpiece' at the C-term (see red dashed boxes in Fig. 35).

We found that the octopus MHC surface loop 1 domain, important for the protein function, have a 93.3% similarity with that reported in sepia ISO A (Fig. 36 and table 4).

```
Surface_loop1_sepiaISOA     AGKTENTKKVIQYFALVAASLAGKDKKKDEEKKKDEKKGTLEDQIVQCNPVLEAYGNAKT
Surface_loop1_octopus       AGKTENTKKVIQYFALVAATLDGKKKKDDEEKKKDEKKGTLEDQIVQCNPVLEAYGNAKT
                            ********************:** **.**.********************************
```

Figure 36*. Comparison between surface loop domain of octopus and sepia ISO A myosins*

Moving towards the C-terminus of the rod region, the ACD region have 96.67% similarity to that of the sepia ISO A (Fig. 37 and table 4).

```
ADC_sepiaISOA       DKLQNKIKTYKRQVEEAEEIAAINLAKFRK
ADC_octopus         DKLQNKIKTYKRQVEEAEEIAAVNLAKFRK
                    **********************:*******
```

Figure 37. *Comparison between ACD region of octopus and sepia ISO A myosins*

Last, the C-term tailpiece of octopus MHC is particularly long and show a 97.96% identity with that of ISO E (Fig. 38 and Table 4).

```
tailpiece_sepiaISOE      VSAARASPLSLTSSSSSHQVTTMQGRGPGYSATFSRSVHMSNGGEDDHF
tailpiece_octopus        VSAARASPLSLTSSSSSHQVTTMQGRGSGYSATFSRSVHMSNGGEDDHF
                         ************************.*********************
```

Figure 38. *Comparison between tail region of octopus and sepia ISO E myosins*

Table 4. Sequence identity between sepia and octopus MHCs.

SITE	*O. vulgaris* MHC Isoform	*S. officinalis* MHC Isoform	% similarity
Surface loop 1	A0A6P7TRC4	ISO A	93.30%
ACD	A0A6P7TRC4	ISO A	96.67%
Tail	A0A6P7TRC4	ISO E	97.96%

Comparative proteomic analysis revealed that several myosin-related genes are overexpressed in T muscles (see red dots in the Fig. 39).

Relevant to our biomechanical investigations we observed that while octopus MHC is equally expressed in T and L muscles one myosin essential light chain and three

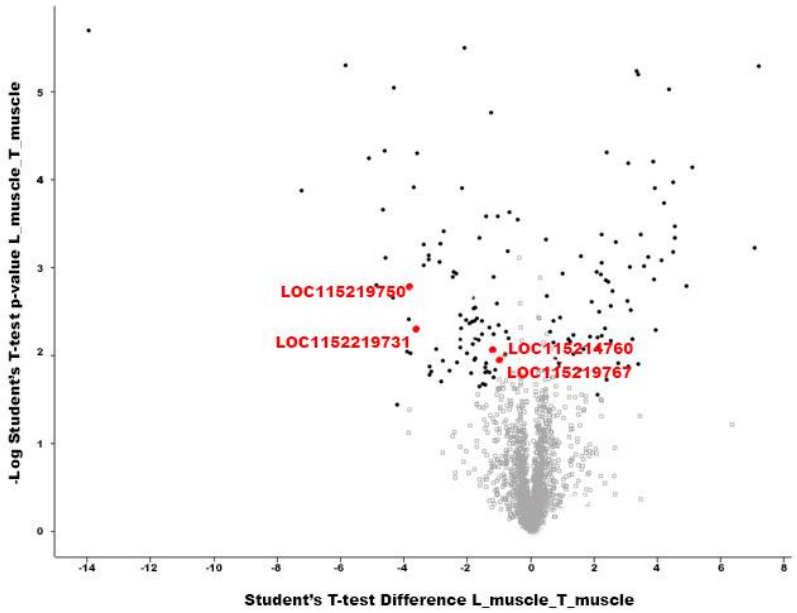

Figure 39*. Vulcan plot of protein expression in T muscles VS L muscles. Black dots indicate proteins significantly modulated in T (P < 0.05, student t-test), red dots indicate myosin related gens significantly modulated in T.*

regulatory light chains are overexpressed in T muscles compared to L (see red fields in the table 3 and heatmap in Fig. 40).

In particular, the expression in T muscles of the unconventional myosin-Va isoforms are about 12 fold higher than L, that of myosin regulatory light chain LC-2 is about 11 fold higher than L, that of the myosin essential light chain is about 5 fold higher than L and

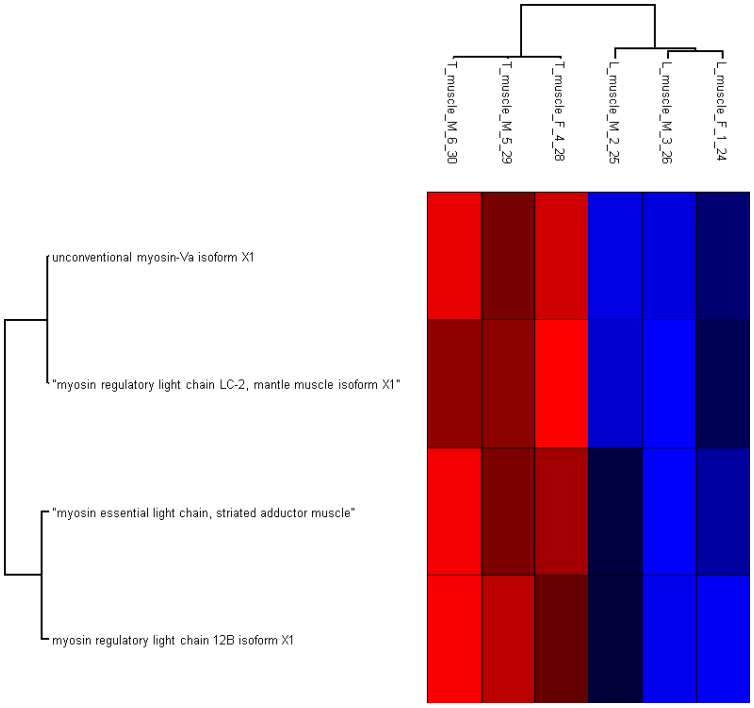

Figure 40. Heatmap of the fold change in expression *of four myosin–related genes between the three T and three L muscles samples. Red indicate overexpression and blue downregulation*

that of the myosin regulatory light chain 12B isoform X1 is about 6 fold higher than L.

Alignment of the myosin essential light chain differently expressed in T and L with that of sepia showed a 81.33% identity (Fig. 41).

```
myosin_ELC_CAE1225290.1_Sepia      MSLKNEVQEVFDLFDFWDGRDGLIDAVKIGDLLRCVGLNPTIELIRRHGGTKKAGEKQLN
myosin_ELC_A0A6P7T6I9_Octopus      FN-SAEVQDVFDLFDFWDGRDGLIDAVKVGDLLRCVGLNPTQELARRHGGTKKAGEKQLT
                                   :. . ***:*******************:*********** ** **************.

myosin_ELC_CAE1225290.1_Sepia      YSEFLACYESITKEKDTGTFKDFMEAFKSFDREGLGFVSAAELYQILTTNGERLADREVN
myosin_ELC_A0A6P7T6I9_Octopus      YAEFLACFESVKKETDTGTFKDFMEAFKSHDREGLGYVSVAELRQILTTSGERLSDREVN
                                   *:*****:**:.**.**************.******:**.*** *****.****:*****

myosin_ELC_CAE1225290.1_Sepia      EILHFTEIRENIDGNLKYEDFINGVLKESQSNF
myosin_ELC_A0A6P7T6I9_Octopus      EIFQFTELRENIDGNVKYEDFINGVLSGGKS--
                                   **::***:*******:**********. .:*
```

Figure 41. *Comparison between ELC of sepia and octopus*

Alignment of the MYL9 Sepia myosin regulatory light chain resulted in 92% similarity with the octopus myosin regulatory light polypeptide 9 isoform X2, 78% similarity with myosin

regulatory light chain 12B and only 50% similarity with myosin regulatory light chain LC-2, mantle muscle isoform X1 (Fig. 42).

Expression of different types of myosin light chain is also found in vertebrate slow and

Figure 42*. Comparison between sepia MYL9 RLC and the three octopus RLCs significantly modulated in T and L muscles*

fast muscles and they are known to affect the kinetics of cross-bridge cycles. Indeed, variation in both V_0 and V_{max} in different fibers, containing the same MHC isoform, have been observed and the relative content of myosin light chain (MLC) isoforms have been found to account for the large variability in shortening velocity (Bottinelli et al., 1994, 1996; Bottinelli & Reggiani, 1995; Greaser et al., 1988; Sweeney & Houdusse, 2010).

Further investigation are needed to uncover the influence of the differential expression of these myosin light chain isoforms on the cross-bridge cycling and contraction velocity of T and L muscles.

Force length

Muscle capability to generate force is highly dependent on its length and this dependence is described by the so-called force-length relationship.

Force-length active and passive components from a total of 5 L (black dots) and 5 T (red dots) muscle preparations are reported in figure 43A and 43B. Passive and active forces

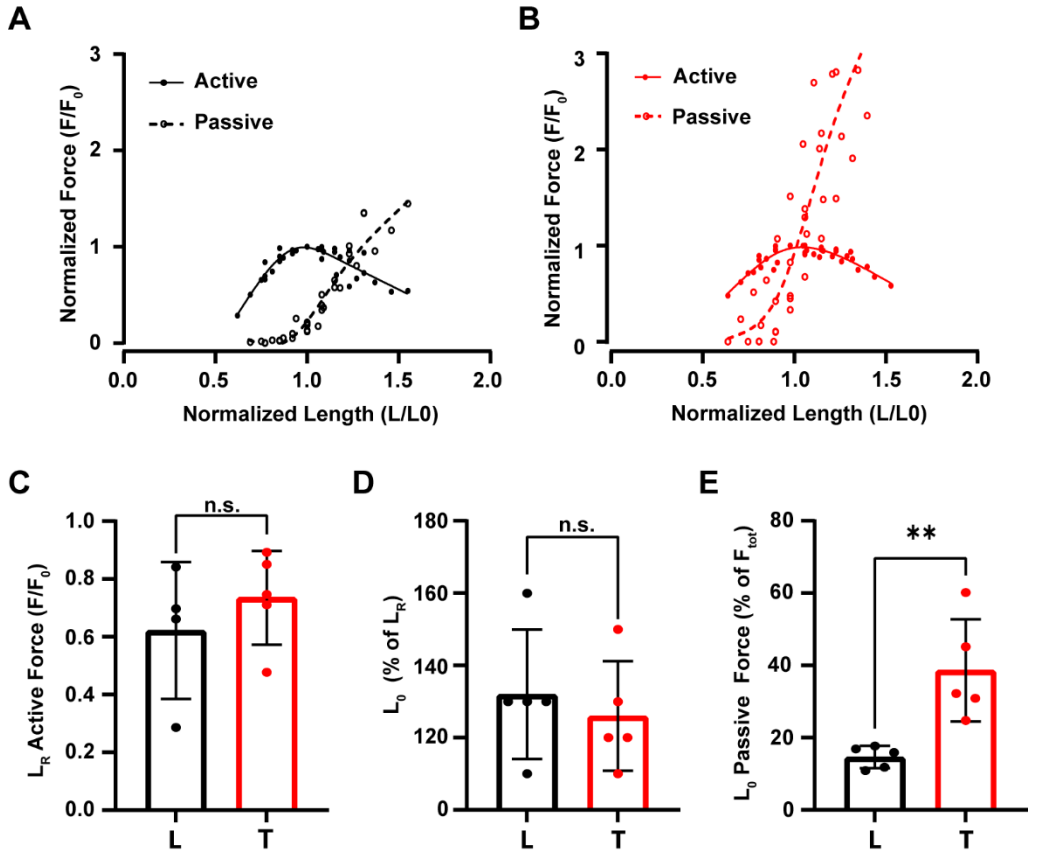

Figure 43. (A) *Passive and active force-length relationship of L muscles. All data points from n = 5 samples are represented. Data were normalized for the sample F_0 and L_0 and fitted with a smoothing spline algorithm (dashed and solid lines in figure). Data fitting is meant to be only descriptive.* ***(B)*** *Passive and active force-length relationship of T muscles. All data points from n = 5 samples are represented. Data were normalized for the sample F_0 and L_0 and fitted with a smoothing spline algorithm (dashed and solid lines in figure). Data fitting is meant to be only descriptive.* ***(C)*** *Relative force of L and T muscles at their L_R (F_R) expressed as fraction of the sample F_0. No significant differences were found between the two muscles (unpaired t-test, P>0.05, n = 4 for L and n = 5 for T). Bars show mean ± SD.* ***(D)*** *L and T muscles strips' L_0 expressed as percentage of their L_R. No significant differences were found between the two muscles (unpaired t-test, P>0.05, n = 5 for both experimental groups). Bars show mean ± SD.* ***(E)*** *Passive contribution to the total force developed by L and T muscle strips at their L_0. T muscles showed a significantly higher contribution of the passive forces (unpaired t-test, **P<0.01, n = 5 for both experimental groups). Bars show mean ± SD*

were normalized for the samples F_0, plotted against their relative lengths (L/L_0) and fitted with a smoothing spline algorithm (dashed and solid lines in Fig. 43A and B). Both muscles were able to produce significant fractions of their F_0 over a relatively wide range of length (the “plateau” region of the force-length relationship in Fig. 43A and B). No significant differences were observed in the relative active force the two muscles are able to exert at their L_R (Fig. 43C, unpaired t-test, $P>0.05$).

Additionally, no difference was found in their L_0 (expressed as percentage of the sample L_R) which was reached around the 30% of stretch (32 ± 18 % in T and 26 ± 15 % in L) in both muscle types (Fig. 43D, unpaired t-test, $P>0.05$).

Conversely, passive forces were remarkably different in the two muscles. T muscle passive forces manifested a higher relative contribution to the total force generated. At L_0, in particular, passive forces in L muscle accounted for the 14.65 ± 3.08% of the total sample force while in T muscles this value was 38.64 ± 14.14 % of the total sample force (Fig. 43E, unpaired t-test, $^{**}P<0.01$).

4.3 Tissue mechanical properties

Muscle resting length in the intact arm

We next investigated the muscle resting length in the intact arm and compared it with that of the isolated muscle strips. To do that we performed a series of morphometric measurements of T and L muscle strips inside the arm and upon dissection analyzing the dimensional changes in the three axes (latero-lateral, LL; oral-aboral, O-A; proximo-distal, P-D, see methods and Fig. 15A). To be consistent with the biomechanical experiments, muscle resting length (L_R) was considered that of the isolated muscle strip. T and L dimensions within the arm (L_{in}) and upon dissection (L_R) were compared and L_{in} was represented as % of L_R. Results showed that L and T muscles change their dimensions upon dissection from the arm (Fig. 44B, number of samples: $n = 11$ (L), $n = 10$ (T) from four different specimens). In particular, in the whole arm configuration, L muscles are

compressed along their main force axis of about 20% of L_R while T muscles, are stretched of about 30% of their L_R (see dashed ellipses in Fig. 44B).

These findings suggest the presence of intrinsic tensional stress inside the arm, resulting in a different level of strain imposed to T and L muscles in the resting arm.

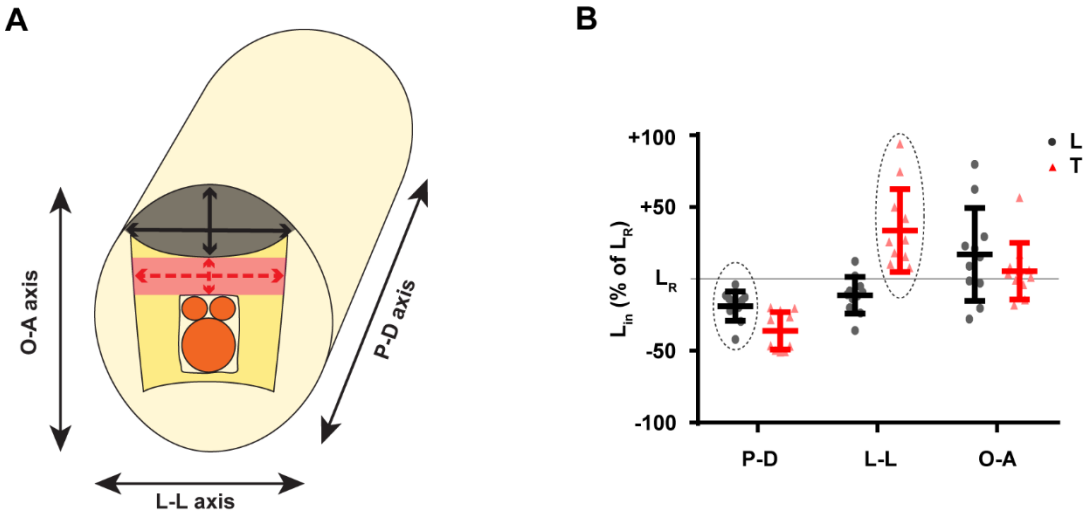

Figure 44. Muscle length inside the arm. (A) *Schematic representation of T and L muscle samples dissection and measurement methodology employed for ex-vivo measurements. Oral-Aboral (O-A), Latero-Lateral (L-L) and Proximal-Distal (P-D) axis are indicated. In the whole arm configuration, the length along the P-D axis was obtained measuring the length of the whole segment cut out from the arm. Red, dashed arrows in figure indicate how was measured the length of T muscles along O-A and L-L axes. Black solid arrows indicate how was measured the length of L muscles along O-A and L-L axes. Grey and red shadings indicate, respectively, the cross sectional area of L and T muscle dissected from the arm to measure the change in their dimension once isolated.* ***(B)*** *Length of T (n = 10) and L (n = 11) muscles inside the arm (L_{in}). L_{in} is expressed as % of L_R, where L_R is the resting length of the muscle once dissected from the arm. Measurements were taken in the three axes: Proximal-Distal (P-D), Latero-Lateral (L-L) and Oral-Aboral (O-A). Bars show mean ± SD. Dashed ellipses highlights, for T and L, the axis along which the muscles fibers are oriented (i.e. the main force axis). Note that, L muscles are compressed along their main force axis, with a length inside the arm of ~ -20% of their L_R outside the arm. Conversely, T muscles are stretched, with a length inside the arm of ~ +30% of their L_R outside the arm.*

Stress-strain relationship

Muscle resistance to mechanical deformation is a key determinant of their function. This is especially true for antagonistic muscles systems, where the active shortening of one muscle needs to be coupled with the passive elongation of the antagonistic one. To

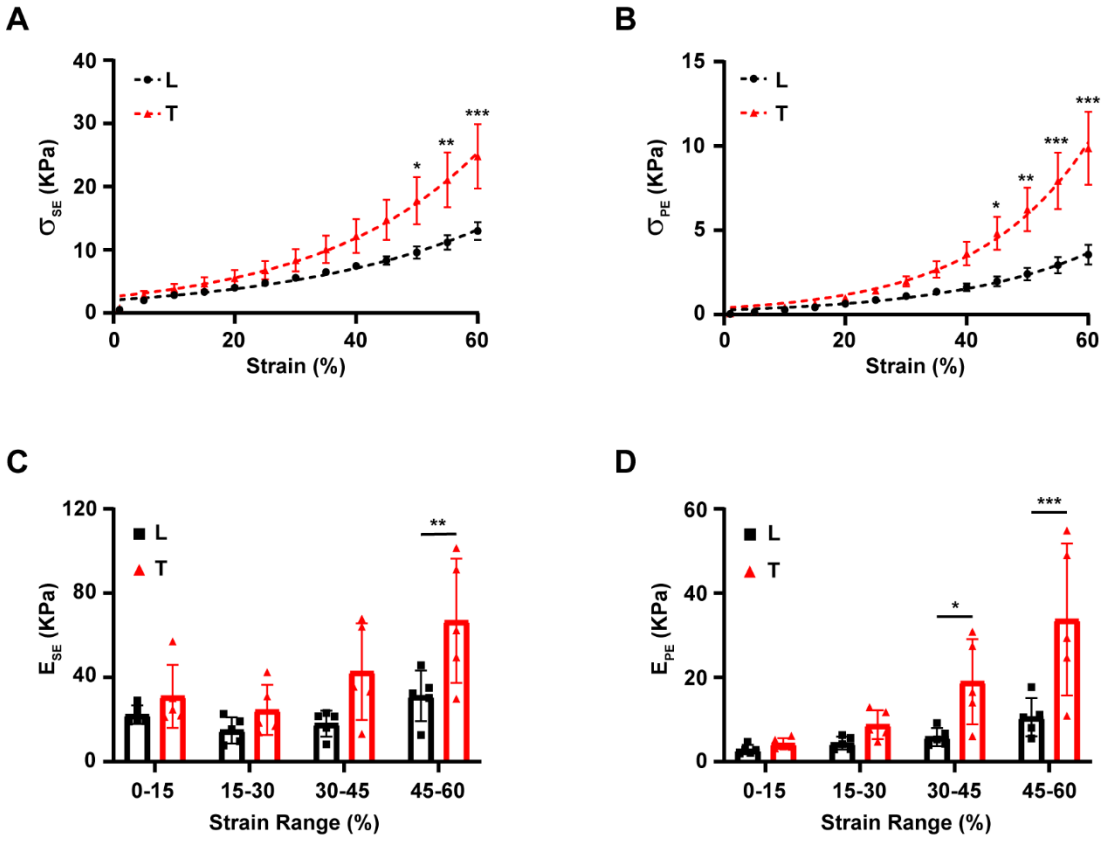

Figure 45. Muscle stress-strain relationship. (A) *Longitudinal and transverse muscle stress-strain relationship for SE components. Data are expressed as mean ± SEM. A significant difference was found between the two muscle types for strains equal to or higher than 50% of strain (RM two way ANOVA with Sidak's multiple comparisons test, *P<0.05, **P<0.01, ***P<0.001, n = 5 for both experimental groups).* ***(B)*** *Longitudinal and transverse stress-strain relationship for PE components. Data are expressed as mean ± SEM. A significant difference was found between the two muscle types for strains equal to or higher than 45% of strain (RM two way ANOVA with Sidak's multiple comparisons test, *P<0.05, **P<0.01, ***P<0.001, n = 5 for both experimental groups).* ***(C)*** *Longitudinal and transverse muscles Young's Modulus for SE components (ESE). ESE was significantly higher in T muscles at high level of strain (45-60%)(RM two way ANOVA with Sidak's multiple comparisons test, **P<0.01, n = 5 for both experimental groups).* ***(D)*** *Longitudinal and transverse muscles Young's Modulus for PE components (EPE). EPE was significantly higher in T muscles at medium-high (30-45%) and high (45-60%) levels of strain (RM two way ANOVA with Sidak's multiple comparisons test, *P<0.05, ***P<0.001, n = 5 for both experimental groups).*

investigate this property in T and L muscles, we analyzed their stress-strain relationship and then we derived their Young's Module (E) for different strain ranges.

Stress-Strain relationship was obtained measuring the passive tension developed by the muscle at different levels of strain. Following Hill model, muscle response to mechanical strain was then subdivided in an early peak force, mainly dependent upon series (SE) elastic components, and a steady-state force generated mainly by parallel (PE) elastic components (F_{SE} and F_{PE}) (see methods for details). These two forces were used to calculate the stress-strain relationship for SE and PE components (Fig. 45A and B respectively). From this relationship we also calculated the Young's Modulus at low (0-15%), medium-low (15-30%), medium-high (30-45%) and high (45-60%) levels of strain (Fig. 45C and D)

For SE components, T muscles showed higher levels of stress at strain equal to or higher than 50%. For PE components, T muscles showed higher levels of stress already at 45% of strain (RM two way ANOVA with Sidak multiple comparisons, *P<0.05, **P<0.01, ***P<0.001, N = 5 for each experimental group). Accordingly, the Young's Modulus for SE components (E_{SE}) was higher in T muscles at high level of strain (45-60%) while Young's Modulus for PE components (E_{PE}) was already higher in T muscles at medium-high (30-45%) level of strain (RM two way ANOVA with Sidak multiple comparisons, *P<0.05, **P<0.01, ***P<0.001, N = 5 for each experimental group).

We can conclude that the T muscles are overall stiffer than L muscles and, interestingly, this difference is more pronounced under static condition.

5 Discussion

According to the most accepted models, the integration of sensory information into motor outputs is achieved by interfacing the neural representations of the sensory and motor systems. This representation is reflected, in vertebrates, in the topographical organization that can be found at various levels of the control pathway. Motor and sensory neurons in the spinal cord are topographically arranged and project to specific areas of the brain organized in somatotopic maps (Kandel et al., 2013; Penfield & Rasmussen, 1950).

Sensory feedback areas tend to be topographically organized also in the higher centers of most invertebrates nervous systems. Central ganglia receive projections from various body parts and show a general somatotopy (Vitzthum et al., 2002; Walters et al., 2004; Wong et al., 2002).

Exceptions appear among the cephalopods. Sensory-motor somatotopic representation is absent at the level of the higher brain centers of the octopus, where an organization of overlapping circuits is possibly employed to represent motor functions (Zullo et al., 2009), and a topographic organization has only partially been shown at intermediate stations of the control hierarchy (Budelmann & Young, 1985; Dubas et al., 1986; Gaston & Tublitz, 2004, 2006; Saidel, 1981). Thus, the modern cephalopod nervous system shows an organization different from the somatotopy of other mollusks, other invertebrates and vertebrates. The special features of their nervous system most likely co-evolved with their highly dynamic embodiment allowing complex behaviors to emerge (Zullo & Hochner, 2011). The completely unrestrained body and arms of the octopus would indeed pose major problems for the computation of movement in terms of precise body coordinates. One possibility that has been suggested is that this animal evolved a unique “embodied” motor control strategy, based on local sensorimotor processing, that would not require a central neural representation of the body (Hochner, 2012, 2013) enabling a kind of ‘intelligence without representation’ (Brooks, 1991).

Nevertheless, the existence of a topographical organization has never been investigated at the peripheral level. The axial nerve cord of each arm hosts roughly 3 million motor neurons and is considered to be functionally comparable to the vertebrates’ spinal cord

(Hochner, 2012; Shigeno et al., 2018; Young, 1971). However, it is not known whether these motor neurons are topographically organized, similarly to what happens in vertebrate spinal cord, or sparsely distributed. Here, we provide the first evidence regarding the identification of motor neurons and their organization in the octopus ANC ganglia and we show that motor neurons are clustered in the dorsal part of the arm ganglia Interestingly, motor neurons show a certain degree of topographical organization. This suggests that a neural representation of the different arm portions may be retained in the NS, although at the peripheral level.

One consequence of this is that motor command neurons, sparsely arranged within the higher motor centers, send their efferent commands to motor neurons topographically arranged within the arm PNS, which innervates specific portions of the arm and thus contributes to the specification of the arm (and possibly also muscle type) activated during different types of motion. Next, we asked what is the mechanical output of T and L muscles activation.

The mechanical output of muscle contraction is not linearly defined by the intensity of the stimulation but is rather influenced by the biomechanical and architectural features of the muscle fibers and the tissue in which they are embedded. These features are usually shaped by evolution to meet muscles use in motion, allowing different muscles to efficiently work as motors, brakes, springs, struts or stabilizers (for a comprehensive review see (Full & Meijer, 2010).

In this work, we show that the two main muscles making up the arm bulk manifest important differences in their biomechanical properties, possibly underlying their differential use in motion. In particular, T muscles have slower twitch contraction kinetics, exert higher fractions of their maximal force at lower frequencies of stimulation, have higher twitch to tetanus ratio and lower shortening velocities.

Interestingly, contraction kinetics and activation properties of T muscles were comparable to those of typical vertebrate slow-twitching muscles, like the soleus whereas contraction kinetics and activation properties of L muscles were comparable to those of typical vertebrate fast-twitching muscles like the extensor *digitorum lungus* (Hessel et al., 2019).

In vertebrates, regulation of contraction kinetics in fast- and slow-twitching muscles involves many actors including myosin heavy chain (MHC) and myosin light chain (MLC) isoforms and their functional changes (Schiaffino & Reggiani, 2011).

The shortening velocity of a muscle fiber is directly proportional to the ATPase activity of the myosin isoform expressed in that fiber; higher ATPase activity means higher cross-bridge cycling rate and thus faster reciprocal sliding of thick and thin filaments, with a consequent direct effect on muscle fiber shortening velocity (Bárány, 1967).

Many animals tune muscle fiber contractile velocity largely through the expression of tissue-specific MHC isoforms that vary in ATPase activity. This is due to differences in amino acid composition in two major regions of MHC S1 heads: surface loop 1, which binds ATP (Murphy & Spudich, 1999), and surface loop 2, which binds actin (Uyeda et al., 1994). Even small differences in the sequence of orthologous MHCs can result in significant functional differences (Canepari et al., 2000). The surface loops of the myosin heavy chain are the least conserved regions and are likely to be of functional importance, as indicated by their locations in the crystal structure of chicken striated muscle myosin S1 (Rayment et al., 1993), possibly accounting for the diversity of ATPase activity and motility (Finer et al., 1994).

For example, rat fast skeletal muscle fibers shorten two to three times faster than rat slow skeletal muscle fibers (Bottinelli et al., 1991), primarily due to the higher ATPase activity of the rat fast skeletal myosin isoform.

Shaffer and Kier investigated the expression of myosin heavy chain isoforms in four different muscular tissues of *Octopus bimaculoides* (mantle, arm, funnel retractor and buccal mass). They identified six different isoforms generated through alternative RNA splicing of a single gene and differing in a small number of nucleotides at the level of the surface loop 1 region and tail (Shaffer & Kier, 2016). Nevertheless, they didn’t check for the differential expression of these MHC in T and L muscles.

The differences in shortening velocity of T and L octopus muscles might well be due to variable ATPase activities of the myosins linked to myosin heavy chain sequence variations within the flexible surface loop 1 that forms part of the ATP binding pocket of the motor domain. Here, we addressed this issue with a proteomic approach.

In both, T and L muscles, we identified a single octopus gene for MHC with more than 90% identity with that of sepia and other cephalopods. All the important functional sites were highly conserved and the single protein transcript covered all the isoforms identified in the other cephalopods.

We did not observe a different expression of this gene in the two muscles; thus we cannot conclude that different MHC isoforms underlie the observed differences in activation and contraction properties. However, as a difference of only 5 aa at the surface loop 1 was expected, further proteomic detailed investigations are currently ongoing to identify possible small nested differences in these isoforms expression.

Interestingly, we found a significant difference in the expression of one essential MLC that may contribute to the observed biomechanical differences. Indeed, expression of different types of myosin light chains is found also in vertebrate slow and fast muscles where alteration of the shortening velocity of striated muscle correlates with the specific MLC isoforms composition (Bottinelli et al., 1994, 1996; Bottinelli & Reggiani, 1995; Greaser et al., 1988; Sweeney & Houdusse, 2010).

Our current knowledge about the molecular players of the muscle contraction kinetics in octopus ends here; further investigations are required to understand the fine regulation of the molecular machinery underlying cross-bridge cycling and filament sliding in octopus muscles. Altogether, our results suggest that T muscles behave as slow muscles and may be more adapted to sustain strong and prolonged period of activity and to work as “postural” muscles. Conversely, L muscles behave as fast muscles and may be involved in finely tuned movements, like bending and manipulation, typical of cephalopod arms.

This is also in accordance with the reported passive properties of T muscles manifesting a higher passive stiffness. Passive stiffness plays a crucial role in motor control and several studies have shown that it is involved in posture maintenance and load-bearing functions (Amiri & Kearney, 2020; Moorhouse & Granata, 2007; Morasso & Schieppati, 1999; Shadmehr & Wise, 2005; Winter et al., 2022). The higher passive stiffness of T was also confirmed by characterization of the force-length relationship. The active, contractile component of this relationship was not significantly different between T and L; both muscles showed a wide bell-shaped curve typical of hydrostatic muscles (Full & Meijer,

2010). However, the contribution of the passive component to the total force was significantly higher in T muscles.

This difference is possibly driven by the organization of elastic fibers in the extracellular matrix arranged along the main muscle force vector in the L muscles and more chaotically in the T muscles. This matrix organization is functional in several arm deformations and may allow for a reduction in energy consumption during motion (Di Clemente et al., 2021).

The difference in the passive stiffness of T and L muscles is also amplified by the hydrostatic pressure present in the arms at rest and imposing a different resting condition on the muscles. Indeed, we showed that hydrostatic pressures are inherently present within the octopus arm, and that they have a different effect on the strain of T and L muscles, allowing T to be stretched and L to be compressed. Hence, the contribution of the passive stiffness will be even more relevant in T. Furthermore, the different resting conditions imposed on T and L muscles means that, in the arm at rest, they will operate in different regions of their force-length relationship, with T muscles closer to their optimal length and L muscles farther away from it. Consequently, they will produce different amounts of force when activated and, thus, the same type of motor neuronal input reaching T or L can induce different responses based on the strain level. This allows the same muscle to become functionally different, thereby providing an intelligent mechanism to increase its flexibility in use.

Muscles in hydrostatic structures can be subjected to different levels of pressure based on their position and function within the animal body. This aspect is extremely important as it allows unconstrained muscles to quinckly and efficiently adapt to large length excursion and to modulate their biomechanical response in a length-dependent manner (Kier, 2020; Sleboda & Roberts, 2017, 2020). In the octopus, given the cylindrical shape of the arm and the constant-volume constraint, T muscle fibers undergo a mechanical deformation equal to the arm diameter's reduction and proportional to the square root of the imposed length change. Conversely, L muscle fibers will be subject to a deformation equal to that of the entire arm. Interestingly, the initial strain conditions of L and T matches also their need to accommodate a higher or lower magnitude of deformation respectively.

One of the main roles proposed for T muscle during arm motion is to counteract longitudinal compression, thereby enabling arm bending and stiffening (Kier, 2016a). Our

results support this hypothesis, providing arm-embedded solutions to resist arm diameter increase in an energetic cost-effective way.

To illustrate this concept, we will dissect point-by-point one typical octopus arm motion: the arm extension.

Arm extension starts with the formation of a bending point along the first 2/3 of the arm, preferentially in the lateral and aboral-up directions (Kennedy et al., 2020). Bend production is due to the contraction of L muscles on one side of the arm with concomitant contraction of T muscles on the same size and elongation of L muscles on the opposite side. The initial configuration of the arm, with T muscles stretched and L muscles compressed, will favor this causing elastic energy in T (on the bending site) and L (on the side opposite to bending) to be 'released', hence reducing the energetic cost for bending. Upon bend formation, arm extension is generated through gradual stiffening of the arm, which propels the bend towards the arm tip (Gutfreund et al., 1996; German Sumbre et al., 2001). Arm stiffening is achieved through the co-contraction of the T and L muscles. During this process we can expect T muscles to be 'favored' by their higher stiffness further reducing the energetic cost of motion. Finally, and perhaps not least important, arm reconfiguration after extension (arm returning to its resting state) might be reached, at reduced cost, simply by stopping muscle contraction, thus allowing for passive redistribution of strain along the arm (Di Clemente et al., 2021).

Notably, the possibility of generating stiffening in selective muscle layers of hydrostatic muscles, have also profound implications in motor control strategies as stiffened muscles can be used as artificial 'skeletons' against which other muscles can act through contraction (Hooper, 2006; Kier, 2012).

The presence of intrinsic hydrostatic forces within the arm, together with the muscle-specific biomechanical properties, represents an arm-embedded readily accessible system for a neural motor code to reconfigure the limb without the need for a complex feed-forward process. Thus, it may be an additional simplification strategy developed to further reduce the complexity of controlling highly flexible structures.

5.1 Conclusions

Cephalopods are distinguishable animals that have developed simplification strategies based on multifunctional design constraints to control hyperredundant limbs and bodies in a large variety of environmental niches (Hanlon & Messenger, 2018). The ability to control this wide range of complex motor performance have to be seen in light of the topographical arrangement of motor neurons within the peripheral nervous system, the physiology of the muscles and, most importantly, their embedding and anatomical organization within the arm. The presence of intrinsic tensional stresses in the arm embedding affects the muscle ability to produce force and its response to passive deformation. Hence, arm muscle physiological properties are only part of a scenario in which muscle embedding and regionalization play an important role in the determination of muscle use during specific tasks.

Octopus motor system can be considered as an ensemble of well-coordinated effectors, from neural organization to body constraints. This consideration is particularly relevant in the field of bio-robotics (Guglielmino et al., 2012; Kang et al., 2016; C. Laschi et al., 2009), as it may provide important insights into both the construction and activation of artificial soft elements while leveraging their control architecture.

6 References

AL-Khayat, H. A. (2013). Three-dimensional structure of the human myosin thick filament: Clinical implications. *Global Cardiology Science and Practice*, *2013*(3), 36. https://doi.org/10.5339/gcsp.2013.36

Alexander, R. M., & Ker, R. F. (1990). The Architecture of Leg Muscles. In *Multiple Muscle Systems* (pp. 568–577). Springer New York. https://doi.org/10.1007/978-1-4613-9030-5_36

Aljure, E. F., & Borrero, L. M. (1968). The influence of muscle length on the development of fatigue in toad sartorius. *The Journal of Physiology*, *199*(2), 241–252. https://doi.org/10.1113/jphysiol.1968.sp008651

Amiri, P., & Kearney, R. E. (2020). Patterns of muscle activation and modulation of ankle intrinsic stiffness in different postural operating conditions. *Journal of Neurophysiology*, *123*(2), 743–754. https://doi.org/10.1152/jn.00558.2019

Anderson, R. C., & Mather, J. A. (1996). It ' s All in the Cues : Octopuses (Enteroctopus do- fleini) Learn to Open Jars Materials & Methods. *Ferrantia*.

Bárány, M. (1967). ATPase activity of myosin correlated with speed of muscle shortening. *The Journal of General Physiology*, *50*(6). https://doi.org/10.1085/jgp.50.6.197

Batth, T. S., Tollenaere, M. A. X., Rüther, P., Gonzalez-Franquesa, A., Prabhakar, B. S., Bekker-Jensen, S., Deshmukh, A. S., & Olsen, J. V. (2019). Protein aggregation capture on microparticles enables multipurpose proteomics sample preparation. *Molecular and Cellular Proteomics*, *18*(5), 1027–1035. https://doi.org/10.1074/mcp.TIR118.001270

Bizzi, E., Cheung, V. C. K., d'Avella, A., Saltiel, P., & Tresch, M. (2008). Combining modules for movement. *Brain Research Reviews*, *57*(1), 125–133. https://doi.org/10.1016/j.brainresrev.2007.08.004

Botterman, B. R., Iwamoto, G. A., & Gonyea, W. J. (1986). Gradation of isometric tension by different activation rates in motor units of cat flexor carpi radialis muscle. *Journal*

of Neurophysiology, *56*(2), 494–506. https://doi.org/10.1152/jn.1986.56.2.494

Bottinelli, R., Betto, R., Schiaffino, S., & Reggiani, C. (1994). Unloaded shortening velocity and myosin heavy chain and alkali light chain isoform composition in rat skeletal muscle fibres. *The Journal of Physiology*, *478*(2), 341–349. https://doi.org/10.1113/jphysiol.1994.sp020254

Bottinelli, R., Canepari, M., Pellegrino, M. A., & Reggiani, C. (1996). Force-velocity properties of human skeletal muscle fibres: Myosin heavy chain isoform and temperature dependence. *Journal of Physiology*, *495*(2), 573–586. https://doi.org/10.1113/jphysiol.1996.sp021617

Bottinelli, R., & Reggiani, C. (1995). Force-velocity properties and myosin light chain isoform composition of an identified type of skinned fibres from rat skeletal muscle. *Pflügers Archiv European Journal of Physiology*, *429*(4), 592–594. https://doi.org/10.1007/BF00704166

Bottinelli, R., Schiaffino, S., & Reggiani, C. (1991). Force-velocity relations and myosin heavy. *Journal of Physiology*, 655–672.

BOYLE, P. R. (1986). Neural Control of Cephalopod Behavior. In *The Mollusca* (Vol. 9, pp. 1–99). Elsevier. https://doi.org/10.1016/B978-0-12-751409-3.50006-1

Brooks, R. A. (1991). Intelligence without representation. *Artificial Intelligence*, *47*(1–3), 139–159. https://doi.org/10.1016/0004-3702(91)90053-M

Budelmann, B. U., & Young, J. Z. (1985). *Central Pathways of the Nerves of the Arms and Mantle of Octopus*. *August*. https://doi.org/10.1098/rstb.1985.0101

Burkholder, T. J., & Lieber, R. L. (2001). Sarcomere length operating range of vertebrate muscles during movement. *Journal of Experimental Biology*, *204*(9), 1529–1536. https://doi.org/10.1242/jeb.204.9.1529

Canepari, M., Rossi, R., Pellegrino, M. A., Bottinelli, R., Schiaffino, S., & Reggiani, C. (2000). Functional diversity between orthologous myosins with minimal sequence diversity. *Journal of Muscle Research and Cell Motility*, *21*(4), 375–382. https://doi.org/10.1023/a:1005640004495

Chandar, K., Medical, C., & Western, C. (2014). *Spinal Cord Anatomy*. *4*, 339–348. https://doi.org/10.1016/B978-0-12-385157-4.01176-3

Cooke, D. F., Taylor, C. S. R., Moore, T., & Graziano, M. S. A. (2003). Complex movements evoked by microstimulation of the ventral intraparietal area. *Proceedings of the National Academy of Sciences of the United States of America*, *100*(10), 6163–6168. https://doi.org/10.1073/pnas.1031751100

Cox, J., & Mann, M. (2008). MaxQuant enables high peptide identification rates, individualized p.p.b.-range mass accuracies and proteome-wide protein quantification. *Nature Biotechnology*, *26*(12), 1367–1372. https://doi.org/10.1038/nbt.1511

Crocini, C., & Gotthardt, M. (2021). Cardiac sarcomere mechanics in health and disease. *Biophysical Reviews*, *13*(5), 637–652. https://doi.org/10.1007/s12551-021-00840-7

Deprá, P. P., Amado, A., & van Emmerik, R. E. A. (2019). Postural Control Underlying Head Movements While Tracking Visual Targets. *Motor Control*, *23*(3), 365–383. https://doi.org/10.1123/mc.2018-0064

Di Clemente, A., Maiole, F., Bornia, I., & Zullo, L. (2021). Beyond muscles: role of intramuscular connective tissue elasticity and passive stiffness in octopus arm muscle function. *Journal of Experimental Biology*, *224*(22). https://doi.org/10.1242/jeb.242644

Dubas, F., Hanlon, R., Ferguson, G., & Pinsker, H. (1986). Localization and stimulation of chromatophore motoneurones in the brain of the squid. *Journal of Experimental Biology*, *0182*(86), 1–18.

Enoka, R. (2008). *Neuromechanics of Human Movement*.

Evarts, E. V., Fromm, C., Kroller, J., & Jennings, V. A. (1983). Motor cortex control of finely graded forces. *Journal of Neurophysiology*, *49*(5), 1199–1215. https://doi.org/10.1152/jn.1983.49.5.1199

Feinstein, N., Nesher, N., & Hochner, B. (2011). Functional morphology of the neuromuscular system of the Octopus vulgaris arm. *Vie et Milieu*, *61*(4), 219–229.

Ferrantini, C., Coppini, R., Sacconi, L., Tosi, B., Zhang, M. L., Wang, G. L., Vries, E. De, Hoppenbrouwers, E., Pavone, F., Cerbai, E., Tesi, C., Poggesi, C., & Ter Keurs, H. E. D. J. (2014). Impact of detubulation on force and kinetics of cardiac muscle contraction. *Journal of General Physiology*, *143*(6), 783–797.

https://doi.org/10.1085/jgp.201311125

Finer, J. T., Simmons, R. M., & Spudich, J. A. (1994). Single myosin molecule mechanics: Piconewton forces and nanometre steps. *Nature*, *368*(6467), 113–119. https://doi.org/10.1038/368113a0

Finn, J. K., Tregenza, T., & Norman, M. D. (2009). Defensive tool use in a coconut-carrying octopus. *Current Biology*, *19*(23), 1069–1070.

Fiorito, G., & Gherardi, F. (1999). Prey-handling behaviour of Octopus vulgaris (Mollusca, Cephalopoda) on Bivalve preys. *Behavioural Processes*, *46*(1), 75–88. https://doi.org/10.1016/S0376-6357(99)00020-0

Fiorito, Graziano, Affuso, A., Anderson, D. B., Basil, J., Bonnaud, L., Botta, G., Cole, A., D'Angelo, L., De Girolamo, P., Dennison, N., Dickel, L., Di Cosmo, A., Di Cristo, C., Gestal, C., Fonseca, R., Grasso, F., Kristiansen, T., Kuba, M., Maffucci, F., … Andrews, P. (2014). Cephalopods in neuroscience: Regulations, research and the 3Rs. *Invertebrate Neuroscience*, *14*(1), 13–36. https://doi.org/10.1007/s10158-013-0165-x

Fiorito, Graziano, Affuso, A., Basil, J., Cole, A., de Girolamo, P., D'angelo, L., Dickel, L., Gestal, C., Grasso, F., Kuba, M., Mark, F., Melillo, D., Osorio, D., Perkins, K., Ponte, G., Shashar, N., Smith, D., Smith, J., & Andrews, P. lr. (2015). Guidelines for the Care and Welfare of Cephalopods in Research –A consensus based on an initiative by CephRes, FELASA and the Boyd Group. *Laboratory Animals*, *49*, 1–90. https://doi.org/10.1177/0023677215580006

Fitts, R. H., McDonald, K. S., & Schluter, J. M. (1991). The determinants of skeletal muscle force and power: Their adaptability with changes in activity pattern. *Journal of Biomechanics*, *24*(SUPPL. 1), 111–122. https://doi.org/10.1016/0021-9290(91)90382-W

Flash, T., & Hochner, B. (2005). Motor primitives in vertebrates and invertebrates. In *Current Opinion in Neurobiology* (Vol. 15, Issue 6, pp. 660–666). https://doi.org/10.1016/j.conb.2005.10.011

Forget, R., & Lamarre, Y. (1990). Anticipatory postural adjustment in the absence of normal peripheral feedback. *Brain Research*, *508*(1), 176–179.

https://doi.org/10.1016/0006-8993(90)91135-4

Franklin, D. W., So, U., Kawato, M., Milner, T. E., David, W., & Theodore, E. (2004). Impedance Control Balances Stability With Metabolically Costly Muscle Activation. *Journal of Neurophysiology*, 3097–3105. https://doi.org/10.1152/jn.00364.2004

Fritzsch. (1993). *Fast axonal diffusion of 3000 molecular weight dextran amines*. *50*, 95–103.

Fuglevand, A. J., Macefield, V. G., & Bigland-Ritchie, B. (1999). Force-frequency and fatigue properties of motor units in muscles that control digits of the human hand. *Journal of Neurophysiology*, *81*(4), 1718–1729. https://doi.org/10.1152/jn.1999.81.4.1718

Full, R., & Meijer, K. (2010). Metrics of Natural Muscle Function. *Electroactive Polymer (EAP) Actuators as Artificial Muscles: Reality, Potential, and Challenges, Second Edition*, 73–89. https://doi.org/10.1117/3.547465.ch3

Gaston, M. R., & Tublitz, N. J. (2004). Peripheral innervation patterns and central distribution of fin chromatophore motoneurons in the cuttlefish Sepia officinalis. *Journal of Experimental Biology*, *207*(17), 3089–3098. https://doi.org/10.1242/jeb.01145

Gaston, M. R., & Tublitz, N. J. (2006). Central distribution and three-dimensional arrangement of fin chromatophore motoneurons in the cuttlefish Sepia officinalis. *Invertebrate Neuroscience*, *6*(2), 81–93. https://doi.org/10.1007/s10158-006-0021-3

Georgopoulos, A. P., Caminiti, R., Kalaska, J. F., & Massey, J. T. (1983). Spatial coding of movement: A hypothesis concerning the coding of movement direction by motor cortical populations. *Experimental Brain Research*, *49*(Suppl. 7), 327–336. https://doi.org/10.1007/978-3-642-68915-4_34

Georgopoulos, Apostolos P. (1988). Spatial coding of visually guided arm movements in primate motor cortex. *Canadian Journal of Physiology and Pharmacology*, *66*(4), 518–526. https://doi.org/10.1139/y88-081

Giszter, S. F. (2015). Motor primitives-new data and future questions. In *Current Opinion in Neurobiology* (Vol. 33, pp. 156–165). Elsevier Ltd. https://doi.org/10.1016/j.conb.2015.04.004

Greaser, B. M. L., Moss, R. L., & Reisert, P. J. (1988). *MYOSIN LIGHT CHAINS By MlARION L. GREASER*, RICHARD*. 85–98.

Grilliner, S., & El Manira, A. (2020). *Current principles of motor control, with special refernce to vertebrate locomotion*. 271–320. https://doi.org/10.1152/physrev.00015.2019

Guertin, P. A. (2013). *Central pattern generator for locomotion : anatomical , physiological , and pathophysiological considerations*. *3*(February), 1–15. https://doi.org/10.3389/fneur.2012.00183

Guglielmino, E., Zullo, L., Cianchetti, M., Follador, M., Branson, D., & Caldwell, D. G. (2012). The application of embodiment theory to the design and control of an octopus-like robotic arm. *Proceedings - IEEE International Conference on Robotics and Automation*, 5277–5282. https://doi.org/10.1109/ICRA.2012.6224907

Gutfreund, Y., Flash, T., Yarom, Y., Fiorito, G., Segev, I., & Hochner, B. (1996). Organization of octopus arm movements: A model system for studying the control of flexible arms. *Journal of Neuroscience*, *16*(22), 7297–7307. https://doi.org/10.1523/jneurosci.16-22-07297.1996

Gutfreund, Y., Matzner, H., Flash, T., & Hochner, B. (2006). Patterns of motor activity in the isolated nerve cord of the octopus arm. *Biological Bulletin*, *211*(3), 212–222. https://doi.org/10.2307/4134544

Hanlon, R. T., & Messenger, J. B. (2018). *Cephalopod Behaviour*. Cambridge University Press. https://doi.org/10.1017/9780511843600

Hessel, A. L., Joumaa, V., Eck, S., Herzog, W., & Nishikawa, K. C. (2019). Optimal length, calcium sensitivity and twitch characteristics of skeletal muscles from mdm mice with a deletion in N2A titin. *Journal of Experimental Biology*, *222*(12). https://doi.org/10.1242/jeb.200840

Hill, A. (1938). The heat of shortening and the dynamic constants of muscle. *Proceedings of the Royal Society of London. Series B - Biological Sciences*, *126*(843), 136–195. https://doi.org/10.1098/rspb.1938.0050

Hochner, B. (2012). An embodied view of octopus neurobiology. *Current Biology*, *22*(20), R887–R892. https://doi.org/10.1016/j.cub.2012.09.001

Hochner, B. (2013). How nervous systems evolve in relation to their embodiment: What we can learn from octopuses and other molluscs. *Brain, Behavior and Evolution*, *82*(1), 19–30. https://doi.org/10.1159/000353419

Hooper, S. L. (2006). Motor Control: The Importance of Stiffness. *Current Biology*, *16*(8), R283–R285. https://doi.org/10.1016/j.cub.2006.03.045

Hsu, L., Zelenin, P. V, Orlovsky, G. N., & Deliagina, T. G. (2017). *Supraspinal control of spinal reflex responses to body bending during different behaviours in lampreys*. *3*, 883–900. https://doi.org/10.1113/JP272714

Huffard, C. L., Boneka, F., & Full1, R. J. (2005). Underwater Bipedal Locomotion by Octopuses in Disguise. *Science*, *1*(4), 1927–1927. https://doi.org/10.1126/science.1109616

Kandel, E. R., Schwartz, J. H., Jessel, T. M., Siegelbaum, S. A., & Hudspeth, A. J. (2013). *Principles of Neural Science*. McGraw Hill.

Kang, R., Guglielmino, E., Zullo, L., Branson, D. T., Godage, I., & Caldwell, D. G. (2016). Embodiment design of soft continuum robots. *Advances in Mechanical Engineering*, *8*(4), 168781401664330. https://doi.org/10.1177/1687814016643302

Kennedy, E. B. L., Buresch, K. C., Boinapally, P., & Hanlon, R. T. (2020). Octopus arms exhibit exceptional flexibility. *Scientific Reports*, *10*(1), 20872. https://doi.org/10.1038/s41598-020-77873-7

Kier, W. M. (1982). The functional morphology of the musculature of squid (Loliginidae) arms and tentacles. *Journal of Morphology*, *172*(2), 179–192. https://doi.org/10.1002/jmor.1051720205

Kier, W. M. (1985). The musculature of squid arms and tentacles: Ultrastructural evidence for functional differences. *Journal of Morphology*, *185*(2), 223–239. https://doi.org/10.1002/jmor.1051850208

Kier, W. M. (2012). The diversity of hydrostatic skeletons. *Journal of Experimental Biology*, *215*(8), 1247–1257. https://doi.org/10.1242/jeb.056549

Kier, W. M. (2016a). The musculature of coleoid cephalopod arms and tentacles. *Frontiers in Cell and Developmental Biology*, *4*(FEB), 1–16. https://doi.org/10.3389/fcell.2016.00010

Kier, W. M. (2016b). The Musculature of Coleoid Cephalopod Arms and Tentacles. *Frontiers in Cell and Developmental Biology*, *4*(February), 1–16. https://doi.org/10.3389/fcell.2016.00010

Kier, W. M. (2020). Muscle force is modulated by internal pressure. *Proceedings of the National Academy of Sciences of the United States of America*, *117*(5), 2245–2247. https://doi.org/10.1073/pnas.1921726117

KIER, W. M., & SMITH, K. K. (1985). Tongues, tentacles and trunks: the biomechanics of movement in muscular-hydrostats. *Zoological Journal of the Linnean Society*, *83*(4), 307–324. https://doi.org/10.1111/j.1096-3642.1985.tb01178.x

Kier, W. M., & Stella, M. P. (2007). The arrangement and function of octopus arm musculature and connective tissue. *Journal of Morphology*, *268*(10), 831–843. https://doi.org/10.1002/jmor.10548

Kim, S., Laschi, C., & Trimmer, B. (2013). Soft robotics: A bioinspired evolution in robotics. *Trends in Biotechnology*, *31*(5), 287–294. https://doi.org/10.1016/j.tibtech.2013.03.002

Lanciego, J. L., & Wouterlood, F. G. (2020). Neuroanatomical tract-tracing techniques that did go viral. In *Brain Structure and Function* (Vol. 225, Issue 4). Springer Berlin Heidelberg. https://doi.org/10.1007/s00429-020-02041-6

Laschi, C., Mazzolai, B., Mattoli, V., Cianchetti, M., & Dario, P. (2009). Design of a biomimetic robotic octopus arm. *Bioinspiration and Biomimetics*, *4*(1). https://doi.org/10.1088/1748-3182/4/1/015006

Laschi, Cecilia, & Cianchetti, M. (2014). Soft robotics: New perspectives for robot bodyware and control. *Frontiers in Bioengineering and Biotechnology*, *2*(JAN), 1–5. https://doi.org/10.3389/fbioe.2014.00003

Levy, G., Nesher, N., Zullo, L., & Binyamin, H. (2017). Motor Control in Soft-Bodied Animals: The Octopus. *The Oxford Handbook of Invertebrate Neurobiology*, *February*, 1–28. https://doi.org/10.1093/oxfordhb/9780190456757.013.36

Marder E., & Bucher D. (2001). Central pattern generators and the control of rhythmic movements. *Current Biology*, *11*(23), R986–R996.

Massion, J. (2017). Postural control system_thesis. *Elseiver*, *4*(6), 877–887.

Matzner, H., Gutfreund, Y., & Hochner, B. (2000). Neuromuscular system of the flexible arm of the octopus: physiological characterization. *Journal of Neurophysiology*, *83*(3), 1315–1328. https://doi.org/10.1152/jn.2000.83.3.1315

Mazzolai, B., & Laschi, C. (2015). Octopus-inspired robotics. *Bioinspiration and Biomimetics*, *10*(3), 1–2. https://doi.org/10.1088/1748-3190/10/3/030301

Messenger, J. B. (1983). Multimodal convergence and the regulation of motor programs in cephalopods. *Fortschritte Der Zoologie*, *28*, 77–98.

Mijailovich, S. M., Prodanovic, M., Poggesi, C., Geeves, M. A., & Regnier, M. (2021). Multiscale modeling of twitch contractions in cardiac trabeculae. *Journal of General Physiology*, *153*(3). https://doi.org/10.1085/JGP.202012604

Moorhouse, K. M., & Granata, K. P. (2007). Role of reflex dynamics in spinal stability: Intrinsic muscle stiffness alone is insufficient for stability. *Journal of Biomechanics*, *40*(5), 1058–1065. https://doi.org/10.1016/j.jbiomech.2006.04.018

Morasso, P. G., & Schieppati, M. (1999). Can muscle stiffness alone stabilize upright standing? *Journal of Neurophysiology*, *82*(3), 1622–1626. https://doi.org/10.1152/jn.1999.82.3.1622

Motoyama, K., Ishizaki, S., Nagashima, Y., & Shiomi, K. (2006). Cephalopod tropomyosins: Identification as major allergens and molecular cloning. *Food and Chemical Toxicology*, *44*(12), 1997–2002. https://doi.org/10.1016/j.fct.2006.06.018

Murphy, C. T., & Spudich, J. A. (1999). The sequence of the myosin 50-20K loop affects myosin's affinity for actin throughout the actin-myosin ATPase cycle and its maximum ATPase activity. *Biochemistry*, *38*(12), 3785–3792. https://doi.org/10.1021/bi9826815

Narayan, J., Kalita, B., & Dwivedy, S. K. (2021). Development of Robot-Based Upper Limb Devices for Rehabilitation Purposes: a Systematic Review. In *Augmented Human Research* (Vol. 6, Issue 1). Springer Singapore. https://doi.org/10.1007/s41133-020-00043-x

Nesher, N., Maiole, F., Shomrat, T., Hochner, B., & Zullo, L. (2019). From synaptic input to muscle contraction: Arm muscle cells of Octopus vulgaris show unique neuromuscular junction and excitation-contraction coupling properties. *Proceedings*

of the Royal Society B: Biological Sciences, *286*(1909). https://doi.org/10.1098/rspb.2019.1278

Nödl, M. T., Kerbl, A., Walzl, M. G., Müller, G. B., & de Couet, H. G. (2016). The cephalopod arm crown: Appendage formation and differentiation in the Hawaiian bobtail squid Euprymna scolopes. *Frontiers in Zoology*, *13*(1), 1–16. https://doi.org/10.1186/s12983-016-0175-8

Norman, M. D., Finn, J., & Tregenza, T. (2001). Dynamic mimicry in an Indo-Malayan octopus. *Proceedings of the Royal Society B: Biological Sciences*, *268*(1478), 1755–1758. https://doi.org/10.1098/rspb.2001.1708

Novojilova, A. P., & Babmindra, V. P. (1978). Intracortical horizontal connections of neurons in cat and monkey motor cortex. *Journal of Neuroscience Research*, *3*(5–6), 389–396. https://doi.org/10.1002/jnr.490030510

Park, M. C., Belhaj-Saïf, A., Gordon, M., & Cheney, P. D. (2001). Consistent features in the forelimb representation of primary motor cortex in rhesus macaques. *Journal of Neuroscience*, *21*(8), 2784–2792. https://doi.org/10.1523/jneurosci.21-08-02784.2001

Paul Shannon, 1, Andrew Markiel, 1, Owen Ozier, 2 Nitin S. Baliga, 1 Jonathan T. Wang, 2 Daniel Ramage, 2, Nada Amin, 2, Benno Schwikowski, 1, 5 and Trey Ideker2, 3, 4, 5, 山本隆久, 豊田直平, 深瀬吉邦, & 大森敏行. (1971). Cytoscape: A Software Environment for Integrated Models. *Genome Research*, *13*(22), 426. https://doi.org/10.1101/gr.1239303.metabolite

Pearson, K. G. (1993). *COMMON PRINCIPLES OF INVERTEBRATES*.

Penfield, W., & Rasmussen, T. (1950). *The cerebral cortex of man : a clinical study of localization of function*. MacMillan.

Pfeifer, R., Lungarella, M., & Iida, F. (2007). Self-Organization, Embodiment, and Biologically Inspired Robotics. *Science*, *318*(5853), 1088–1093. https://doi.org/10.1126/science.1145803

Polit, A., & Bizzi, E. (1979). Characteristics of motor programs underlying arm movements in monkeys. *Journal of Neurophysiology*, *42*(1), 183–194. https://doi.org/10.1152/jn.1979.42.1.183

Prochazka, A., Gosgnach, S., Capaday, C., & Geyer, H. (2017). Neuromuscular Models for Locomotion. In *Bioinspired Legged Locomotion: Models, Concepts, Control and Applications* (Issue May 2018). https://doi.org/10.1016/B978-0-12-803766-9.00008-7

Puhl, J. G., Bigelow, A. W., Rue, M. C. P., & Mesce, K. A. (2018). *Functional Recovery of a Locomotor Network after Injury : Plasticity beyond the Central Nervous System*. *5*(August), 1–16.

Rathelot, J., & Strick, P. L. (2006). *Muscle representation in the macaque motor cortex : An anatomical perspective*. *103*(21), 8257–8262.

Rayment, I., Rypniewski, W., Schmidt-Base, K., Smith, R., Tomchick, D., Benning, M., Winkelmann, D., Wesenberg, G., & Holden, H. (1993). Three-dimensional structure of myosin subfragment-1: a molecular motor. *Science*, *261*(5117), 50–58. https://doi.org/10.1126/science.8316857

Robertson, J. D., Schwartz, O. M., & Lee, P. (1993). Carbocyanine dye labeling reveals a new motor nucleus in octopus brain. *Journal of Comparative Neurology*, *328*(4), 485–500. https://doi.org/10.1002/cne.903280404

Rowell, B. Y. C. H. F. (1963). Excitatory and Inhibitory Pathways in the Arm of Octopus. *Journal of Experimental Biology*, *40*(2), 257–270.

Saidel, W. M. (1981). Evidence for visual mapping in the peduncle lobe of octopus. *Neuroscience Letters*, *24*(1), 7–11. https://doi.org/10.1016/0304-3940(81)90350-5

Schiaffino, S., & Reggiani, C. (2011). Fiber types in Mammalian skeletal muscles. *Physiological Reviews*, *91*(4), 1447–1531. https://doi.org/10.1152/physrev.00031.2010

Shadmehr, R., & Wise, S. P. (2005). The computational neurobiology of reaching and pointing: A foundation for motor learning. In *The computational neurobiology of reaching and pointing: A foundation for motor learning.*

Shaffer, J. F., & Kier, W. M. (2016). Tuning of shortening speed in coleoid cephalopod muscle: no evidence for tissue-specific muscle myosin heavy chain isoforms. *Invertebrate Biology*, *135*(1), 3–12. https://doi.org/10.1111/ivb.12111

Shigeno, S., Andrews, P. L. R., Ponte, G., & Fiorito, G. (2018). Cephalopod brains: An

overview of current knowledge to facilitate comparison with vertebrates. *Frontiers in Physiology*, *9*(JUL), 1–16. https://doi.org/10.3389/fphys.2018.00952

Shomrat, T., Zarrella, I., Fiorito, G., & Hochner, B. (2008). The Octopus Vertical Lobe Modulates Short-Term Learning Rate and Uses LTP to Acquire Long-Term Memory. *Current Biology*, *18*(5), 337–342. https://doi.org/10.1016/j.cub.2008.01.056

Sleboda, D. A., & Roberts, T. J. (2017). Incompressible fluid plays a mechanical role in the development of passive muscle tension. *Biology Letters*, *13*(1). https://doi.org/10.1098/rsbl.2016.0630

Sleboda, D. A., & Roberts, T. J. (2020). Internal fluid pressure influences muscle contractile force. *Proceedings of the National Academy of Sciences of the United States of America*, *117*(3), 1772–1778. https://doi.org/10.1073/pnas.1914433117

Sumbre, Germán, Fiorito, G., Flash, T., & Hochner, B. (2006). Octopuses Use a Human-like Strategy to Control Precise Point-to-Point Arm Movements. *Current Biology*, *16*(8), 767–772. https://doi.org/10.1016/j.cub.2006.02.069

Sumbre, German, Gutfreund, Y., Fiorito, G., Flash, T., & Hochner, B. (2001). Control of Octopus Arm Extension by a Peripheral Motor Program. *Science*, *293*(5536), 1845–1848. https://doi.org/10.1126/science.1060976

Sweeney, H. L., & Houdusse, A. (2010). Structural and functional insights into the myosin motor mechanism. *Annual Review of Biophysics*, *39*(1), 539–557. https://doi.org/10.1146/annurev.biophys.050708.133751

Thompson, J. T., Shelton, R. M., & Kier, W. M. (2014). The length-force behavior and operating length range of squid muscle varies as a function of position in the mantle wall. *Journal of Experimental Biology*, *217*(12), 2181–2192. https://doi.org/10.1242/jeb.083907

Turchetti-Maia, A., Shomrat, T., & Hochner, B. (2019). The Vertical Lobe of Cephalopods. In *The Oxford Handbook of Invertebrate Neurobiology* (Issue October, pp. 558–574). https://doi.org/10.1093/oxfordhb/9780190456757.013.29

Tyanova, S., Temu, T., Sinitcyn, P., Carlson, A., Hein, M. Y., Geiger, T., Mann, M., & Cox, J. (2016). The Perseus computational platform for comprehensive analysis of (prote)omics data. *Nature Methods*, *13*(9), 731–740.

https://doi.org/10.1038/nmeth.3901

Uyeda, T. Q. P., Ruppel, K. M., & Spudich, J. A. (1994). Enzymatic activities correlate with chimaeric substitutions at the actin-binding face of myosin. *Nature*, *368*(6471), 567–569. https://doi.org/10.1038/368567a0

Vercelli, A., Repici, M., Garbossa, D., & Grimaldi, A. (2000). Recent techniques for tracing pathways in the central nervous system of developing and adult mammals. *Brain Research Bulletin*, *51*(1), 11–28. https://doi.org/10.1016/S0361-9230(99)00229-4

Vitzthum, H., Müller, M., & Homberg, U. (2002). Neurons of the central complex of the locust Schistocerca gregaria are sensitive to polarized light. *Journal of Neuroscience*, *22*(3), 1114–1125. https://doi.org/10.1523/jneurosci.22-03-01114.2002

Walters, E. T., Bodnarova, M., Billy, A. J., Dulin, M. F., Díaz-Ríos, M., Miller, M. W., & Moroz, L. L. (2004). Somatotopic Organization and Functional Properties of Mechanosensory Neurons Expressing Sensoring-A mRNA in Aplysia californica. *Journal of Comparative Neurology*, *471*(2), 219–240. https://doi.org/10.1002/cne.20042

Wells, M. (1978). *Octopus. Physiology and Behaviour of an Advanced Invertebrate*. London: Chapman and Hall. https://doi.org/10.1086/411059

Winter, D. A., Patla, A. E., Prince, F., Ishac, M., Gielo-perczak, K., Jc, Q., David, A., Patla, A. E., Prince, F., & Ishac, M. (2022). *Stiffness Control of Balance in Quiet Standing*.

Wong, A. M., Wang, J. W., & Axel, R. (2002). Spatial representation of the glomerular map in the Drosophila protocerebrum. *Cell*, *109*(2), 229–241. https://doi.org/10.1016/S0092-8674(02)00707-9

Yekutieli, Y., Sagiv-Zohar, R., Aharonov, R., Engel, Y., Hochner, B., & Flash, T. (2005). Dynamic model of the octopus arm. I. Biomechanics of the octopus reaching movement. *Journal of Neurophysiology*, *94*(2), 1443–1458. https://doi.org/10.1152/jn.00684.2004

Young, J. Z. (1971). *The Anatomy of the Nervous System of Octopus Vulgaris*. Oxford, Clarendon Press.

Zullo, L. (2004). FUNCTIONAL ORGANISATION OF THE SENSORY-MOTOR AREAS IN THE SNC OF Octopus vulgaris. *PhD Dissertation Thesis*.

Zullo, L., Eichenstein, H., Maiole, F., & Hochner, B. (2019a). Motor control pathways in the nervous system of Octopus vulgaris arm. *Journal of Comparative Physiology A: Neuroethology, Sensory, Neural, and Behavioral Physiology*, *205*(2), 271–279. https://doi.org/10.1007/s00359-019-01332-6

Zullo, L., Eichenstein, H., Maiole, F., & Hochner, B. (2019b). Motor control pathways in the nervous system of Octopus vulgaris arm. *Journal of Comparative Physiology A*, *0*(0), 0. https://doi.org/10.1007/s00359-019-01332-6

Zullo, L., Fossati, S. M., Imperadore, P., & Nödl, M. T. (2017). Molecular determinants of cephalopod muscles and their implication in muscle regeneration. *Frontiers in Cell and Developmental Biology*, *5*(MAY), 1–11. https://doi.org/10.3389/fcell.2017.00053

Zullo, L., & Hochner, B. (2011). A new perspective on the organization of an invertebrate brain. *Communicative and Integrative Biology*, *4*(1), 1–4. https://doi.org/10.4161/cib.13804

Zullo, L., Sumbre, G., Agnisola, C., Flash, T., & Hochner, B. (2009). Nonsomatotopic Organization of the Higher Motor Centers in Octopus. *Current Biology*, *19*(19), 1632–1636. https://doi.org/10.1016/j.cub.2009.07.067

7 Appendix

The Diversity of Muscles and Their Regenerative Potential across Animals

Letizia Zullo, Matteo Bozzo, Alon Daya, Alessio Di Clemente, Francesco Paolo Mancini, Aram Megighian, Nir Nesher, Eric Röttinger, Tal Shomrat, Stefano Tiozzo, Alberto Zullo, Simona Candiani.

Cells. 2020 Aug 19;9(9):1925. doi: 10.3390/cells9091925.

Abstract

Cells with contractile functions are present in almost all metazoans, and so are the related processes of muscle homeostasis and regeneration. Regeneration itself is a complex process unevenly spread across metazoans that ranges from full-body regeneration to partial reconstruction of damaged organs or body tissues, including muscles. The cellular and molecular mechanisms involved in regenerative processes can be homologous, co-opted, and/or evolved independently. By comparing the mechanisms of muscle homeostasis and regeneration throughout the diversity of animal body-plans and life cycles, it is possible to identify conserved and divergent cellular and molecular mechanisms underlying muscle plasticity. In this review we aim at providing an overview of muscle regeneration studies in metazoans, highlighting the major regenerative strategies and molecular pathways involved. By gathering these findings, we wish to advocate a comparative and evolutionary approach to prompt a wider use of "non-canonical" animal models for molecular and even pharmacological studies in the field of muscle regeneration.

In this review, I wrote the chapter on the cephalopod muscles types

Beyond muscles: role of intramuscular connective tissue elasticity and passive stiffness in octopus arm muscle function

Alessio Di Clemente, Federica Maiole, Irene Bornia, Letizia Zullo

J Exp Biol. 2021 Nov 15;224(22):jeb242644. doi: 10.1242/jeb.242644

Abstract

The octopus arm is a 'one of a kind' muscular hydrostat, as demonstrated by its high maneuverability and complexity of motions. It is composed of a complex array of muscles and intramuscular connective tissue, allowing force and shape production. In this study, we investigated the organization of the intramuscular elastic fibers in two main muscles composing the arm bulk: the longitudinal (L) and the transverse (T) muscles. We assessed their contribution to the muscles' passive elasticity and stiffness and inferred their possible roles in limb deformation. First, we performed confocal imaging of whole-arm samples and provided evidence of a muscle-specific organization of elastic fibers (more chaotic and less coiled in T than in L). We next showed that in an arm at rest, L muscles are maintained under 20% compression and T muscles under 30% stretching. Hence, tensional stresses are inherently present in the arm and affect the strain of elastic fibers. Because connective tissue in muscles is used to transmit stress and store elastic energy, we investigated the contribution of elastic fibers to passive forces using step-stretch and sinusoidal length-change protocols. We observed a higher viscoelasticity of L and a higher stiffness of T muscles, in line with their elastic fiber configurations. This suggests that L might be involved in energy storage and damping, whereas T is involved in posture maintenance and resistance to deformation. The elastic fiber configuration thus supports the specific role of muscles during movement and may contribute to the mechanics, energetics and control of arm motion.

In this paper, I performed the biomechanical experiments and the morphometric measurements. I also collaborated with Federica Maiole and Irene Bornia to carry out the histological measurements and with Letizia Zullo to write the manuscript and prepare the figures

How octopus arm muscle contractile properties and anatomical organization contribute to the arm functional specialization

Letizia Zullo*, Alessio Di Clemente*, Federica Maiole

*equal contribution

J Exp Biol. (*under review*)

Abstract

Octopus arms are highly flexible structures capable of complex motions used in a wide repertoire of behaviors. Movements are generated by the coordinated summation of innervation signals to packed arrays of muscles oriented in different directions and moving based on their anatomical relationships. In this study, we investigated the interplay between muscle biomechanics and anatomical organization in the Octopus vulgaris arm to elucidate their role in different arm movements. We performed isometric and isotonic force measurements on isolated longitudinal (L) and transverse (T) arm muscles and showed that L has a higher rate of activation and relaxation, lower twitch-to-tetanus ratio, and lower passive tension than T muscles, thus prompting their use as faster and slower muscles, respectively. This points to the use of L in more graded responses, such as those involved in precise actions, and T in intense and sustained actions, such as motion stabilization and posture maintenance. Once activated, the arm muscles undergo volumetric deformations transmitted to neighboring muscles based on their morphology and within-limb organization. Here, we show that, although continuous, the arm manifests a certain degree of morphological specialization, where arm muscles have a different aspect ratio along the arm. This possibly supports the functional specialization of arm portion observed in various motions, such as fetching and crawling. Hence, the octopus arm as a whole can be seen as a ‘reservoir’ of possibilities where different types of motion may emerge at the limb level through the co-option of the muscle contractile properties and structural arrangement.

In this paper I performed all the biomechanical experiments and I wrote the manuscript and prepared the figures together with Letizia Zullo.

Neuronal tract tracing in the octopus arm nervous system

Alessio Di Clemente and Letizia Zullo

(*In preparation)*

8 Acknowledgements

First of all, I would like to thank my supervisor, Letizia Zullo, because none of this work would have been possible without her. But more than that, I would like to thank her for the insightful advices, which guided me through this project and through my professional growth, and for always helping me to keep an open mind and to pursue any chance to learn new things.

I am also really thankful to Fabio Benfenati for allowing me to join the NSYN group and for its leadership, which made possible to establish and sustain, the stimulating environment of the NSYN group.

Last, but definitely not the least, I would like to thank all the members of the NSYN group. They say that the first requirement for the knowledge to advance is a stimulating environment where different ideas and expertize can be put together and exchanged among different peoples. In the NSYN I certainly found all that. There are simply too many people that helped me, one way or another, maybe just with a new idea or a clever solution to a technical problem or just by supporting me. Saying thank you to every one of them would require much more space than these few lines, so I am forced to thank them all in here, wishing that this will be enough.